EFFECT OF SEEDING ON THE PROPERTIES OF MFI TYPE ZEOLITE MEMBRANES

A THESIS SUBMITTED TO
THE GRADUATE SCHOOL OF NATURAL AND APPLIED SCIENCES
OF
MIDDLE EAST TECHNICAL UNIVERSITY

BY

ESER DİNÇER

IN PARTIAL FULFILLMENT OF THE REQUIREMENTS
FOR
THE DEGREE OF MASTER OF SCIENCE
IN
CHEMICAL ENGINEERING

AUGUST 2005

Approval of the Graduate School of Natural and Applied Sciences

Prof. Dr. Canan Özgen
Director

I certify that this thesis satisfies all the requirements as a thesis for the degree of Master of Science.

Prof. Dr. Nurcan Baç
Head of Department

This is to certify that we have read this thesis and that in our opinion it is fully adequate, in scope and quality, as a thesis for the degree of Master of Science.

Prof. Dr. Ali Çulfaz
Co-Supervisor

Asst. Prof. Dr. Halil Kalıpçılar
Supervisor

Examining Committee Members

Prof. Dr. Müjgan Çulfaz (Gazi Univ., ChE) _____

Asst. Prof. Dr. Halil Kalıpçılar (METU,ChE) _____

Prof. Dr. Ali Çulfaz (METU,ChE) _____

Prof. Dr. Hayrettin Yücel (METU,ChE) _____

Prof. Dr. Levent Yılmaz (METU,ChE) _____

I hereby declare that all information in this document has been obtained and presented in accordance with academic rules and ethical conduct. I also declare that, as required by these rules and conduct, I have fully cited and referenced all material and results that are not original to this work.

Name, Last name: Eser Dinçer

Signature:

ABSTRACT

EFFECT OF SEEDING ON THE PROPERTIES OF MFI TYPE ZEOLITE MEMBRANES

Dinçer, Eser
M.Sc., Department of Chemical Engineering
Supervisor: Assist. Prof. Dr. Halil KALIPÇILAR
Co-supervisor: Prof. Dr. Ali ÇULFAZ

August 2005, 131 pages

The effect of seeding on the properties of alumina supported MFI membranes was investigated in this study. Membranes were synthesized from clear solutions with a molar batch composition of $TPAOH:9.80SiO_2:0.025NaOH:0.019Al_2O_3:602.27H_2O:39.16C_2H_5OH$ on bare and seeded alumina supports at 130°C in autoclaves. The amount of seed on the support surface was changed between 0.6 mg/cm^2 and 6.9 mg/cm^2 by vacuum seeding method, which provided uniform and closely packed seed layers.

Membranes were characterized by XRD and SEM, and by measuring single gas permeances of N_2, SF_6, n-C_4H_{10} and i-C_4H_{10}. The quality of membranes was evaluated on the basis of N_2/SF_6 ideal selectivity. Membranes, which showed N_2/SF_6 ideal selectivity higher than 40, were considered to be good quality, comprising few defects. Good quality membranes were also used to separate butane isomers.

Membranes synthesized on seeded supports had compact and uniform MFI layer if the seed amount is less than 1.0 mg/cm^2 on the support surface. Membranes that were synthesized on the supports coated with higher amount of seed

crystals showed an asymmetric structure with a dense and uniform MFI layer at the top, the support at the bottom and a seed layer between.

Half of the membranes synthesized on seeded supports had N_2/SF_6 ideal selectivity higher than 40. These membranes exhibited n-C_4H_{10}/i-C_4H_{10} separation selectivities between 5 and 27 and 8 and 21 at room temperature and at 200^oC, respectively. High ideal and separation selectivities showed that membranes did not include non-zeolitic pores.

Membranes synthesized on bare support had non-uniform MFI layer. Those membranes showed N_2/SF_6 ideal selectivities below Knudsen selectivity, indicating the existence of large non-zeolitic pores in the MFI layer.

Keywords: Seeding, MFI membranes, Vacuum seeding, Gas permeation, Reproducibility

ÖZ

TOHUMLAMANIN MFI TİPİ ZEOLİT MEMBRANLARIN ÖZELLİKLERİ ÜZERİNE ETKİSİ

Dinçer, Eser

Yüksek Lisans, Kimya Mühendisliği

Tez Yöneticisi: Yrd. Doç. Dr. Halil KALIPÇILAR

Ortak Tez Yöneticisi: Prof. Dr. Ali ÇULFAZ

Ağustos 2005, 131 sayfa

Bu çalışmada, tohumlamanın alumina destekli MFI membranların özellikleri üzerine etkisi incelenmiştir. Membranlar boş ve tohumlanmış destekler üzerine $9.80SiO_2$:TPAOH:$0.025NaOH$:$0.019Al_2O_3$:$602.27H_2O$:$39.16C_2H_5OH$ başlangıç bileşimindeki berrak çözeltilerden 130^oC'de ve otoklavlarda sentez edilmiştir. Destek yüzeyi üzerindeki tohum miktarı, sıkı dolgulu ve tekdüze tohum tabakaları veren vakumla kaplama yöntemi ile 0.6 mg/cm^2 ve 6.9 mg/cm^2 arasında değiştirilmiştir.

Membranlar XRD ve SEM ve N_2, SF_6, n-C_4H_{10} ve i-C_4H_{10} tek gaz geçirgenlik ölçümleri ile nitelendirilmiştir. Membran kalitesi N_2/SF_6 ideal seçiciliği temelinde değerlendirilmiştir. N_2/SF_6 ideal seçiciliği 40'ın üzerinde olan membranların az delik içerdiği ve iyi kalitede olduğu kabul edilmiştir. İyi kalite membranlar bütan izomerlerinin ayırımında da kullanılmıştır.

Tohumlanmış destek üzerinde sentez edilmiş membranlar, destek yüzeyi üzerindeki tohum miktarı 1.0 mg/cm^2'dan az olduğu durumda sıkı ve tekdüze MFI tabakalara sahiptir. Daha fazla miktarda tohumla kaplanmış destekler üzerine sentez edilmiş membranlar, üstte sıkı ve tekdüze MFI tabaka, altta destek ve arada tohum tabakasından oluşan asimetrik bir yapı göstermiştir.

Tohumlanmış destekler üzerinde sentez edilen membranların yarısının N_2/SF_6 ideal seçiciliği 40'ın üzerindedir. Bu membranlar oda sıcaklığı ve 200^oC'de sırasıyla 5 ile 27 ve 8 ile 21 arasında n-C_4H_{10}/i-C_4H_{10} ayırma seçiciliği göstermiştir. Yüksek ideal ve ayırma seçicilikleri, membranların zeolit dışı gözenek içermediğini göstermiştir.

Boş destek üzerinde sentez edilen membranlar tekdüze olmayan MFI tabakalarına sahiptir. Bu membranların Knudsen seçiciliğinden küçük N_2/SF_6 ideal seçiciliği göstermeleri MFI tabaka içinde büyük zeolit dışı gözeneklerin varlığını göstermektedir.

Anahtar sözcükler: Tohumlama, MFI membranlar, Vakumla tohumlama, Gaz geçirgenliği, Tekraredilebilirlik

To my mother Şükran Dinçer and
my father İsmail Dinçer

ACKNOWLEDGMENTS

I wish to express my deepest gratitude to my supervisor Assist. Prof. Dr. Halil Kalıpçılar for his guidance, advice, encouragement and insight throughout the research. I would also like to thank to my co-supervisor Prof. Dr. Ali Çulfaz for his suggestions, criticism and interest.

I would like to thank Özge Güvenir for her company at home, in the lab and everywhere in between. I would also thank my labmates Belma Soydaş, Zeynep Çulfaz and Ayşenur Özcan for their sincere friendship and helps.

I would thank to the technicians of Chemical Engineering Department of Middle East Technical University for their helps throughout this study.

I am indebted to my parents for their continuous encouragement, understanding and endless support.

TABLE OF CONTENTS

LIST OF TABLES

TABLES

LIST OF FIGURES

FIGURES

NOMENCLATURE

A	: Membrane area
$\underline{P}$	: Permeance
T	: Temperature
t	: Time
P	: Pressure
P^F	: Partial pressure of feed
P^R	: Partial pressure of retentate
P^P	: Partial pressure of permeate
$\Delta V/\Delta t$	: Volumetric flow rate
R	: Ideal gas constant

Greek Letters

ϕ	: Porosity
δ	: Thickness
α_{ij}	: Selectivity
ρ	: Density
ΔP	: Transmembrane pressure difference

Abbreviations

SEM	: Scanning electron microscopy
XRD	: X-ray diffractometer
BPV	: Back pressure valve
GC	: Gas chromatograph
MFC	: Mass flow controller
TPA	: Tetrapropylammonium

CHAPTER 1

INTRODUCTION

A membrane is a semipermeable barrier between two phases. It allows the passage of some molecules, called permeate, and reject the others, called retentate, with the aid of a driving force such as pressure or concentration difference [1]. Selectivity and permeance are the two key parameters to determine the performance of a membrane.

Zeolites are microporous crystalline materials with uniform-sized pores between 0.3 nm and 1.3 nm. Molecular sieving and selective adsorption properties of zeolites make these materials appropriate for membrane preparation. They also exhibit high chemical, thermal and mechanical stability.

Zeolite membranes have usually an asymmetric composite structure. They consist of a continuous and thin zeolite layer on top of a thick macroporous support. Zeolite layer achieves the separation and the support provides the mechanical strength to the zeolite layer with a little effect on the separation [2,3]. Porous alumina [4-7] and stainless-steel [8-11] are usually used as support. The zeolite layer should be as thin as possible to obtain high permeance and defect-free for high selectivity.

Generally zeolite membranes are hydrothermally synthesized from a gel [10,12] or clear solution [5,13] that contains SiO_2, Al_2O_3, Na_2O, H_2O and a template molecule. The support is put into the synthesis solution and the zeolite layer forms on the support surface during hydrothermal treatment. Synthesis is usually performed at temperatures between 100^{o}C and 200^{o}C at autogeneous pressure [5-7,14]. In order to obtain a continuous zeolite layer frequently thick films are produced and sometimes multiple synthesis steps are required [10,15,16].

The most critical problem faced with the synthesis of zeolite membranes is the reproducibility. Although there are a great number of studies on zeolite membranes, few of them has reported data on the reproducible synthesis of membranes [5,9,17-19].

Seeding the support surface has often been applied to promote the formation of zeolite layer and to improve the membrane quality. Seeding may offer several advantages over the synthesis on the bare supports such as controlling the orientation [20-22] and forming membranes with higher reproducibility [20,21,24]. As well as those advantages seeding shortens the crystallization time by reducing the induction time for nucleation since the seed crystals acts as nuclei for the secondary growth [25,26]. Nevertheless this method introduces additional parameters such as size of seed, thickness of seed layer and makes the synthesis procedure more complicated.

The method applied for seeding is therefore expected to be practical and adequate to prepare seed layers with high coverage. Dip-coating [21], rubbing [13], pulsed laser ablation [8] and vacuum seeding [27] are some of the seeding methods that have been used in membrane synthesis. Among them, vacuum seeding is a simple and efficient method to prepare seed layers. Huang et al. [27] applied this seeding method on tubular supports. The thickness of seed layer was non-uniform through the support because of the gravitational force in addition to vacuum force. Therefore this method can be more suitable for flat supports where negative effect of gravitational force is eliminated.

In this study, the effect of amount of seed on the morphology and quality of MFI (ZSM-5 and silicalite-1) membranes was investigated. MFI type zeolites are appropriate membrane materials because of their pore size that is comparable with the kinetic diameter of industrially important gases [28].

To prepare membranes, disc-shaped alumina supports were coated with seed crystals by vacuum-seeding method. Amount of seed on the support was adjusted by changing the quantity of seed suspension whilst the concentration of suspension was kept constant.

The synthesized membranes were characterized by X-ray diffraction (XRD) for phase identification. Scanning electron microscopy (SEM) was used to determine the morphology of the MFI layer. Membrane quality was evaluated by measuring N_2 permeances through uncalcined membranes and by measuring N_2 and SF_6 permeances through the calcined membranes. Good-quality membranes were also used to separate n-C_4H_{10} and i-C_4H_{10} mixtures. The reproducibility of the membrane syntheses was determined with both gas permeances and SEM images.

CHAPTER 2

LITERATURE SURVEY

2.1 Classification of membranes

A membrane is a semipermeable barrier between two phases which hinders the passage of some components called retentate and permits the passage of the others called permeate. Membranes can separate gas and liquid mixtures under the effect of a driving force, such as pressure or concentration difference [1]. The performance of a membrane is determined by two parameters, namely permeance and selectivity. Permeance is defined as the flux per unit transmembrane driving force. Ideal selectivity (permselectivity) is usually used to describe the performance of a membrane. Ideal selectivity is the ratio of single gas permeances. Separation selectivity is also used in the case of mixture separation and it can be defined as the ratio of compositions of components A and B in the permeate relative to the composition ratio of these components in retentate side [29].

Synthetic membranes can be divided into two sub-groups; polymeric and inorganic membranes. Polymeric membranes show high selectivities in gas separation and can be easily processed to prepare membranes with large surface areas. However they are not resistant to high temperatures and chemically harsh conditions. Operating limitations of polymeric membranes can be overcome by inorganic membranes. Inorganic materials are chemically inert, stable at high temperatures and high pressures [28]. Carbon membranes, sol-gel based membranes (silica, alumina, zirconia etc.) and zeolite membranes are the types of inorganic membranes.

2.2 Structure of MFI type zeolites

Zeolites are crystalline hydrated aluminasilicalites of alkali or alkali earth metal elements. The zeolite framework is built up by $[AlO_4]^{-5}$ and $[SiO_4]^{-4}$ tetrahedra. The tetrahedra are connected by sharing oxygen atoms and construct the three-dimensional framework [30]. The negative charge of framework is compensated by alkali or alkaline earth cations, which can be reversibly and totally exchanged by other cations. Zeolites exhibit high thermal, mechanical and chemical resistance. Zeolites are known as molecular sieving materials because of their uniform and molecular-sized pores (0.3-1.3 nm). The pore size of some zeolites can be tuned by ion exhange, for example the pore size of Na-A type zeolite is 0.42 nm, where as K-form of zeolite A has pores with 0.30 nm.

Several types of zeolites are applied for membrane preparation such as; MFI-type (silicalite-1 and ZSM-5) [4-7,9-21], LTA-type [22,27], mordenite [31] and faujasite [32]. Among them MFI type is the one that is frequently used in membrane preparation. Because the pore size of MFI type zeolites is comparable with the kinetic diameter of industrially important gases [28].

MFI is a group name given to 10-membered zeolites. ZSM-5 and silicalite-1 are the group members of this family. ZSM-5 and silicalite-1 differ from each other by Si/Al ratio which ranges between 20 and 4000 in ZSM-5 while silicalite-1 is alumina free form of ZSM-5.

MFI type zeolites have intersecting channel system (Figure 2.1). The channels in the b-direction are straight with a pore diameter of 0.51x0.55 nm and they are connected to zig-zag channels in the a-direction. The pore diameter of zig-zag channels is 0.51x0.57 nm. No channels are present in c-direction [33].

Zeolites are synthesized hydrothermally either at autogeneous or at atmospheric pressures from synthesis solutions that usually contain SiO_2, Na_2O, Al_2O_3, H_2O and sometimes template molecule as structure directing agent [34]. For example tetrapropylammonium ion (TPA^+) is frequently used as template for MFI type zeolite. During the synthesis of MFI type zeolite template molecules

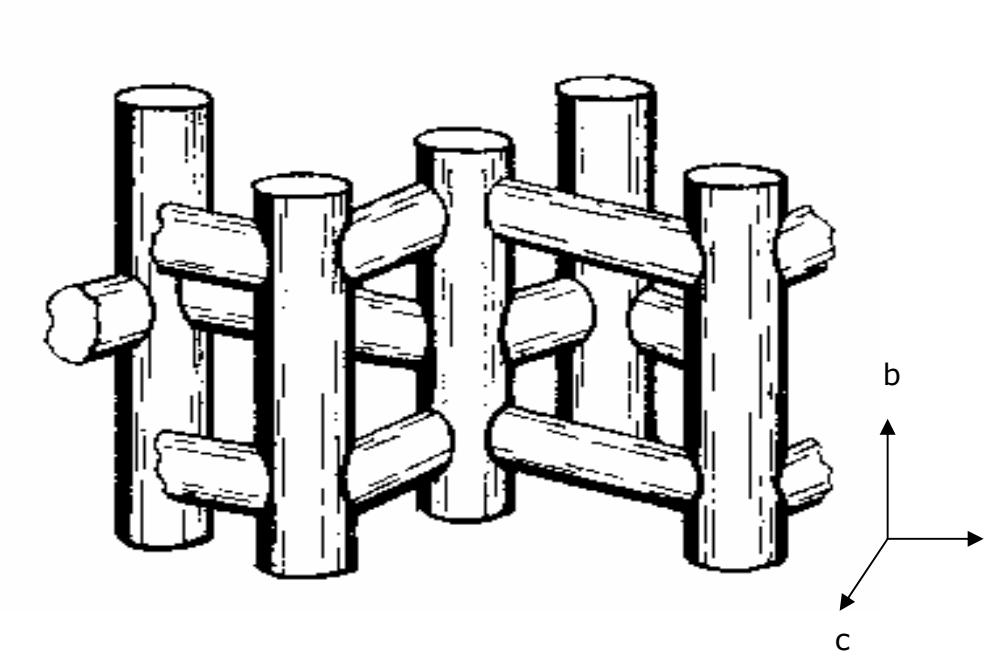

Figure 2.1 Pore structure of MFI type zeolite

are located at the intersection of zig-zag and straight channels and blocks the MFI pores. For this reason calcination step is required to open the MFI pores. Temperatures higher than 400^{o}C are usually required for the complete removal of the template molecule [35].

2.3 Synthesis of zeolite membranes

Zeolite membranes can be prepared as self-supported zeolite films or zeolite layer on a support. Self-supported zeolites films are usually prepared as thick films (30-250 μm) to gain mechanical strength yet this reduces the permeance through the membrane [36-38]. In order to produce thin zeolite layers with sufficient mechanical strength, zeolite membranes are prepared on porous support materials such as α- and γ-alumina [4-7] or stainless-steel supports [8-11]. Zeolite membranes on a support can be synthesized by two different methods, in-situ hydrothermal synthesis and vapor phase transport method.

In vapor phase transport (VPT) method, the support material is immersed into aluminasilicate gel and coated with a gel layer. Then amorphous dry-gel is crystallized in vapor mixture of water and organics such as triethylamine and

ethylendiamine at autogenous pressure [39]. VPT method is utilized to control the thickness of the zeolite membrane and to minimize the consumption of chemicals used for membrane synthesis. However, it is difficult to prepare uniform precursor gel layers which in turn affect the membrane quality.

In in-situ hydrothermal synthesis method, the support material is immersed into the synthesis solution, which includes the chemical reagents for zeolite synthesis. Crystallization of zeolite layer takes place on the support surface at temperatures between 100^{o}C and 200^{o}C [5-7,14]. Synthesis is performed either at autogenous [5-7] or at atmospheric pressure [14].

Several different mechanisms for zeolite layer growth under in-situ hydrothermal conditions have been proposed. Koegler et al. [40] suggested that at the early stages of crystallization primary gel particles that form in the synthesis solution accumulate on the support surface and form a silica gel layer with low (TPA) template content. Nucleation and crystal growth take place at the interface of the gel layer and synthesis solution. Similarly Lai et al. [41] prepared ZSM-5 membranes on bare porous alumina supports. They proposed that a gel layer formed on the support surface and crystallization occurred in the amorphous gel layer. On the other hand Vilaseca et al. [42] suggested a four step mechanism for zeolite layer growth. At the beginning of the synthesis nuclei with a size of 50 nm forms on the support surface. As the synthesis proceeds, those nuclei are transformed to zeolite crystals and at the same time nuclei forms continuously both on the support and on the zeolite crystals. Then crystals cover the support and a new generation of nuclei forms on those crystals so that nucleation and crystal growth take place simultaneously. Finally nuclei formation stops and crystal growth continues to form a continuous zeolite layer.

In order to obtain thin and continuous zeolite layers without defects by in-situ synthesis on bare supports several synthesis procedures have been investigated. For example Vroon et al. [16] prepared MFI membranes by consecutive synthesis on α-alumina supports from clear synthesis solutions at temperatures between 371 K and 459 K. They obtained good quality membranes with a thickness of 2 μm and 7 μm after two consecutive hydrothermal syntheses. When they repeated synthesis more than twice they obtained thick membranes

with poor quality and they concluded that membranes became too thick and cracked during calcination step.

Coronas et al. [10] synthesized ZSM-5 membranes on tubular α- and γ-alumina supports and investigated the synthesis procedure on membrane quality. They filled alumina tubes with synthesis gel and wrapped the ends of the tube with Teflon tape. They repeated synthesis until uncalcined membranes became impermeable to N_2. With this method, ZSM-5 membranes having N_2/SF_6 ideal selectivities between 138 and 299 at room temperature were obtained. However when the outer surface of tube was covered with Teflon tape and the autoclave was rotated at horizontal position, they could not obtain continuous ZSM-5 layers even after two consecutive synthesis steps. They concluded that quality of ZSM-5 membranes depended on the synthesis procedure.

A number of studies have shown that good quality membranes can be obtained by in-situ synthesis on bare supports but synthesis of thick membranes or consecutive synthesis is needed to obtain a continuous zeolite layers. This may result in decrease in membrane quality by leading to crack formation or decreasing the permeance through the membrane. To increase the quality and reproducibility of zeolite membranes seeding method is to be used.

In this method, the support material is coated with previously synthesized zeolite crystals and then seed coated support is subjected to hydrothermal synthesis to obtain continuous zeolite layers. Hydrothermal synthesis on seeded support is usually called as *secondary growth* [20-24].

Table 2.1 shows the thicknesses of MFI membranes and films prepared by secondary growth. Particle size of the seed crystals and the thickness of the seed layer affect morphology of the resulting zeolite layer. For example Lai and Gavalas [43] prepared zeolite membranes about 5 μm and 10 μm thick with the use of 0.4 μm and 2 μm seed crystals, respectively. They have concluded that the membrane thickness increases with the size of seed crystals under the same synthesis conditions. Similarly Hedlund et al. [23] investigated the effect of seed layer thickness on the film morphology. Synthesis on silicon wafers coated with a monolayer (about 160 nm thick) resulted in thinner MFI films than those coated

with bilayer (about 240 nm thick) of seed crystals. Huang et al. [27], who examined the effect of seed size and seed layer thickness on the thickness of zeolite A membranes, concluded that increase of either seed size or seed layer thickness increases the membrane thickness.

Table 2.1 Morphology of MFI films and membranes reported in literature

Reference	Seed size	Seed layer thickness	MFI layer thickness	Pattern
Hedlund et al. [14]	50 nm	Nearly a monolayer	500 nm	Random orientation
Gavalas et al. [43]	0.4 μm	No information	5 μm	Random orientation
	2 μm		10 μm	
Tsapatsis et al. [21]	100 nm	Nearly a monolayer	1 μm	Preferred orientation
Au et al. [44]	120 nm	1.5 μm	2.5 μm	Preferred orientation
Hedlund et al. [45]	60 nm	monolayer	1.5 μm	Random orientation
Lin et al. [13]	4 μm	No information	10 μm	Random orientation
Hedlund et al. [23]	160 nm	160 nm (monolayer)	240 nm	Preferred orientation
		240 nm (bilayer)	500 nm	

Seeding also influences the orientation of the zeolite crystals forming the zeolite layer (Table 2.1). Tsapatsis and co-workers [20-24] synthesized membranes with columnar structure by secondary growth on seeded alumina supports. They stated that seeding leads to the formation of oriented layers. With the alignment of MFI crystals in the same direction, the permeance through the membrane can be increased and membrane quality can be improved.

Crystalline phase in the synthesized zeolite layer can be controlled by seeding [31,46]. Li et al. [31] observed that MFI and mordenite membranes can be

synthesized under the same synthesis conditions by changing the type of the zeolite that is used as seed crystals.

Seeding also shortens the synthesis time of membranes. Lin et al. [25] synthesized silicalite membranes on seeded and bare porous mullite supports. They obtained well-intergrown membrane on seeded supports for 8 h of synthesis but a continuous zeolite layer was not obtained after 16 h of crystallization on bare support. They concluded that seed crystals provide nucleation sites and by the way increase the growth rate of compact zeolite layers. Similarly, Xomeritakis et al. [26] synthesized MFI films on bare and seeded glass supports. They observed that synthesis on seeded support resulted in formation of zeolite film after 4 h of synthesis while on bare support amorphous gel around the zeolite crystals was observed. They stated that increasing the crystallization time to 20 h resulted in intergrown and polycrystalline films on seeded supports on the other hand, continuous zeolite films were not obtained in unseeded systems. They concluded that existence of seed layer led to formation of intergrown zeolite layer and shortened the synthesis time. When seed crystals are used they serve as nucleus and thus required time to obtain continuous zeolite layer is reduced.

Xomeritakis et al. [26] and Lin et al. [13] observed hemispherical dome like defects in the zeolite layer synthesized on non-uniform seed layers. They concluded that absence of uniform and close-packed seed layers decrease zeolite film quality by the formation of defects (dome-like defects).

In view of these studies seed layer properties such as uniformity, coverage and packing density are important factors which affect the membrane quality. Different methods have been developed for seeding and the main target is to coat support surface with packed and uniform seed layers.

2.4 Seeding methods

Dip-coating, rubbing, pulsed layer ablation and vacuum seeding are some the seeding methods employed for coating the support surface with seed crystals.

One of the most frequently used method is dip-coating [20-22,24]. In this method, a colloidal seed suspension is prepared with nanosize zeolite crystals. Then the support material is dipped into the colloidal seed suspension to attach seed crystals to the support surface. In order to prevent the loss of seed crystals from the support surface, dipping and withdrawal rates of the support are kept so slow like 1-2 cm/h. For complete coverage, coating process is repeated several times. Although thin and uniform seed layers are obtained with this method [20-22,24] it is a time consuming method because of the requirement for coating steps and it is limited to nanosize seed crystals as larger crystals settle down quickly. In dip-coating sometimes cationic polymers are used to reverse the charge of the support to enhance the attachment of seed crystals to the support surface by electrostatic forces [14,23,45]. But this method also requires an additional pretreatment step which is impractical.

In rubbing, slurry of seed crystals is rubbed on the support surface with a brush [12,13,25]. It is very simple method to obtain seed coated supports and applicable with either micron or submicron size seed crystals. However it is difficult to control the uniformity and thickness of seed layer. Lin et al. [13] prepared silicalite membranes on seeded alumina tubes by a single hydrothermal synthesis. The outer surface of alumina tubes were coated with 4 μm silicalite seed crystals by rubbing method. They stated that tube surface was covered with seed crystals but seed layer included large voids, therefore the seed layer quality was low. They concluded that seed layer quality depends on the seed size and roughness of the surface.

Seeded layers can also be prepared by pulsed ablation method. This method is utilized by Munoz et al. [8] for the preparation of zeolite UTD-1 membranes. They first pressed zeolite UTD-1 crystals to obtain zeolite pellets and seed crystals from this pellet were deposited on a temperature controlled silicon wafer and porous stainless-steel supports by laser ablation. They obtained about 700 nm thick seed layer on silicon supports. However seeded layers were mainly amorphous according to XRD. They obtained oriented UTD-1 layers after secondary growth and concluded that film deposited prior to membrane synthesis serve like a seed layer though it was mainly amorphous. Although uniform seed layers are obtained through pulsed laser ablation technique, it

caused decomposition of seed crystals. Special equipment needed for this method also limits its usage.

Vacuum seeding method is also used for seeding the support surfaces. In this method a seed suspension is prepared and suspension is poured on the support surface. Seed crystals are deposited on the support surface by means of vacuum. The main advantage of this method over the others is that the amount of seed crystals deposited on the support can be controlled by changing the concentration and amount of the suspension. Huang et al. [27] used this method to coat α-alumina tubular supports. They seeded support surfaces with different amounts of zeolite A seed crystals by changing the suspension concentration. They stated that closely packed seed layers can be obtained by vacuum seeding method in a practical way.

2.5 Gas permeation through MFI membranes

Separation through zeolite membranes is accomplished due to difference in diffusion rates and adsorption behavior of the permeating gases. Separation performance indicates the quality of the membrane and is affected by the morphology of the zeolite layer such as thickness, grain boundaries, orientation, size and shape of the crystals forming the zeolite layer [44,47]. Separation is also influenced by the size and shape of the permeating gases and operating conditions such as temperature and pressure [7,9].

Various groups used specific gas pairs to determine the quality of MFI membranes. Mostly n-butane/i-butane and N_2/SF_6 ideal selectivity are taken as a quality criterion [4,5,9,10,16,48,49]. Vroon et al. [16] defined a good quality membrane as a membrane showing ideal selectivity for butane isomers higher than 10 at 473 K. As Knudsen diffusion controls the flow in mesopores separation of isomers cannot be accomplished by a membrane including mesopores. Therefore separation of butane isomers would indicate that the membrane consists of few defects. Noble and co-workers [10] suggested N_2/SF_6 ideal selectivity as quality criterion. A membrane that exhibited N_2/SF_6 ideal selectivity higher than 80 at room temperature was defined as high quality. Since kinetic diameter of N_2 is smaller than MFI pores, it can easily pass through

the MFI layer. On the other hand kinetic diameter of SF_6 is comparable with the size of MFI pores so SF_6 permeance is expected to be low in a defect-free membrane.

Figure 2.2 shows the relationship between N_2 permeances and N_2/SF_6 ideal selectivities for MFI membranes reported in literature (see Appendix I for tabulated form of Figure 2.2). The plot is constructed on a log-log scale. Membranes synthesized with and without seeding are shown on the graph by full and open symbols, respectively. As these membranes were produced with different synthesis conditions, membranes probably showed different morphological behavior which affects the performance of the membrane. For example, membranes obtained on seeded supports exhibit lower selectivities and similar permeances compared to membranes synthesized on bare supports.

It is known that thick membranes usually show higher selectivities and lower permeances than thinner membranes. Membranes produced on seed coated supports usually exhibit thin MFI layers. To obtain defect free membranes without seeding, consecutive synthesis was used yielding thicker membranes. For example Hedlund et al. [14] synthesized MFI membranes by secondary growth with seed crystals of 50 nm. Before the membrane synthesis they plugged the pores of the support therefore crystallization in the support pores was eliminated. They obtained MFI membranes about 500 nm thick and membrane exhibit N_2/SF_6 selectivity of 10. In contrast Coronas et al. [10] synthesized ZSM-5 membranes by two consecutive synthesis steps on bare support and obtained membranes with thicknesses between 25 μm and 30 μm. Those membranes showed N_2/SF_6 ideal selectivities between 138 and 299. Similarly Tuan et al. [50] obtained ZSM-5 membrane on bare support after two synthesis steps. The membrane had a thickness of 40 μm and exhibited N_2/SF_6 ideal selectivity of 56.

The permeance through a membrane depends on the amount of grain boundaries [28]. MFI membranes that are obtained by seeding are usually composed of small crystals. This may increase the amount of grain boundaries which may result in the decrease of permeances even if they had thin MFI layers. For example, Algieri et al. [51] synthesized MFI membranes by secondary

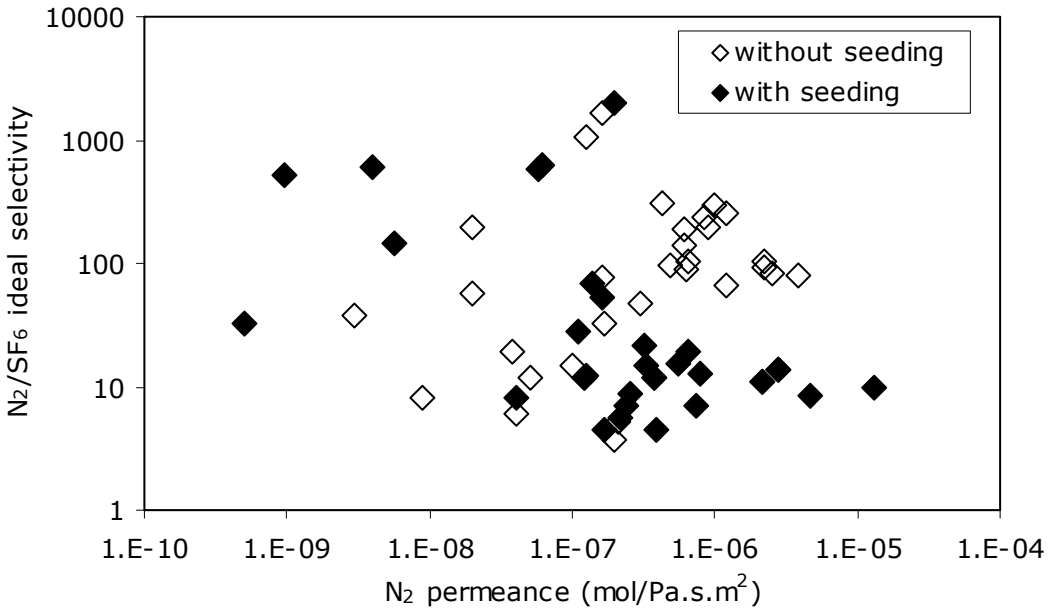

Figure 2.2 N_2 permeances and N_2/SF_6 ideal selectivities for MFI type membranes reported in literature

growth method. MFI membranes synthesized on seed layer composed of 400 nm MFI crystals and had a thickness of 2 μm. The N_2 permeances through those membranes were about $2x10^{-6}$ mol/Pa.s.m^2. On other hand Coronas et al. [10] reported similar N_2 permeances through a membrane composed larger ZSM-5 crystals and 15 times thicker ZSM-5 layer than the previous work as result of grain boundaries.

2.6 Reproducibility of MFI membrane synthesis

Figure 2.2 shows that a reproducibility problem exists in zeolite membrane synthesis. Although all membranes are MFI type, their permeances and ideal selectivities exhibit a wide distribution. In addition to this, reproducibility is reported only in a few articles [5,9,17-19]. To determine the reproducibility of membrane synthesis, researchers define a quality criterion like the ideal selectivity of specific gas pairs and evaluate the membranes according to this quality criterion.

Van de Graaf et al. [9] used n-butane/isobutane ideal selectivity higher than 10 as the quality criterion and they confirmed that 8 of 12 membranes did not satisfy the quality criterion without an obvious cause. They concluded that membranes cracked during calcination step and poor reproducibility can be caused by the surface properties of the support or defects formed during membrane synthesis. Kalıpçılar and Çulfaz [5] utilized N_2/SF_6 ideal selectivity higher than 80 as the quality criterion and they stated that 30% of the membrane synthesis were successful according to their quality criterion although membranes showed similar morphological behavior according to SEM images. They concluded that reproducibility can be influenced by the defects formed during membrane synthesis. Noack et al. [17] used H_2/SF_6 permselectivity higher than 43 as a quality criterion. They observed that reproducibility increased from 10% to about 70% by optimizing the synthesis conditions and composition of MFI membranes. Similarly Gora et al. [18] optimized the synthesis conditions of silicalite-1 membrane by changing the synthesis temperature and time. They evaluated reproducibility of membranes by single gas permeation of n-butane and isobutane and SEM images. They observed that all eight membranes synthesized under the same optimized conditions had similar thicknesses and also exhibited similar n-butane permeances and n-butane/isobutane ideal selectivities. On the other hand Li et al. [19] synthesized ZSM-5 membranes on large area α-alumina supports by repeating the synthesis steps at least three times until the uncalcined membranes became impermeable to N_2. They selected H_2/n-butane ideal selectivity higher than 27 as a quality criterion and they obtained 50% reproducibility according to their criterion.

Reproducibility is a significant problem in zeolite membrane synthesis. This problem should be overcome in order to use zeolite membranes in industry.

CHAPTER 3

EXPERIMENTAL

3.1 Synthesis of MFI type seed crystals

MFI type seed crystals (ZSM-5 and silicalite-1) were synthesized from clear synthesis solutions. Chemicals used to prepare synthesis solution were tetraethylorthosilicate (TEOS, Acros Organics, 98% in water), tetrapropylammoniumhydroxide (TPAOH, Acros Organics, 25% in water) as organic template, sodium aluminate (44% Na_2O, 55% Al_2O_3, 1% H_2O, Riedel de Haen), NaOH pellets (97% NaOH, 1.98% H_2O, Merck) and deionized water (DI water).

The batch with a molar composition of $TPAOH:9.80SiO_2:0.025Na_2O:0.019Al_2O_3:602.27H_2O:39.16C_2H_5OH$ (C1) [52] was used for the synthesis of micron-size seed crystals and that of $TPAOH:8.17SiO_2:0.08Na_2O:162.09H_2O:32.68C_2H_5OH$ (C2) [35] was used for the synthesis of submicron-size crystals. A sample calculation for amounts of reagents to prepare 100 g synthesis solution for a batch composition is given in Appendix A.

The synthesis solution was prepared in polypropylene cups. TPAOH was diluted with DI water and TEOS was added into this solution. Then, sodium aluminate (0.54 wt% in water) or NaOH (1.4 wt% in water) was added. As TEOS is immiscible with water, a two phase mixture was formed. This mixture was stirred vigorously on a magnetic stirrer at room temperature for the hydrolysis of TEOS. The mixture prepared from Composition C1 was stirred for 24 h, and that prepared from Composition C2 was stirred for 45 h. After stirring homogeneous and clear synthesis solutions were obtained.

The synthesis was carried out in stainless steel autoclaves with PTFE inserts having 35 ml capacity. Approximately 80% of the insert was filled with synthesis

solution. The synthesis with Composition C1 was performed at 130°C for 24 h and 46 h, and the synthesis with Composition C2 was carried out at 91°C for 24 h.

The autoclaves taken out of the oven were quenched to room temperature in cold water. The solid product was recovered from the mother liquid by centrifuging the contents of the autoclave at 640 g for 10 min. The solid product was redispersed in DI water for washing and centrifuged again at the same centrifuging conditions. Washing was repeated several times until the pH of the solution above the solid dropped to nearly 8. The solid products were dried in the centrifuging tubes at 80°C overnight, removed from the tubes and pounded in agate mortar.

3.2 Preparation of alumina discs

Home-made α-alumina discs were used as support in membrane preparation. Discs were prepared from α-Al_2O_3 powder (Aldrich, particle size <10 μm) by using polyvinyl alcohol (PVA, average molecular weight: 22000, Acros organics) solution as binder. The PVA solution (5 wt%) was prepared by dissolving 5 g PVA in 95 g of DI water. The solution was stirred on a magnetic stirrer overnight at room temperature for complete dissolution of PVA particles.

The alumina discs were prepared as follows: 10 g of alumina powder was mixed with 1 ml of PVA solution. The mixture was pounded in agate mortar for about 20 min and then dried at room temperature for an hour. For each alumina disc, one gram of dried solid was pressed under the pressure of 258 MPa. The green discs were sintered at 1400°C for 22 h. The heating rate was 6 °C/min.

Discs had a diameter of 21 mm and a thickness of 1 mm after sintering. Both faces of alumina discs were slightly polished using a 800-grit sandpaper to obtain smoother surfaces. The polished discs were washed with DI water and treated with 0.1 M HNO_3 for 1 h to remove the particles coming from the sandpaper. After treatment with HNO_3, discs were ultrasonicated in water for 5 min and washed with DI water. Finally the discs were dried at 100°C for about 2 h.

3.3 Seeding the alumina supports

One side of alumina discs were coated with seed crystals at room temperature by vacuum seeding method using the apparatus shown in Figure 3.1. The seeding apparatus consists of two polyimide tubes that have an outside diameter of 67 mm and a wall thickness of 30 mm.

The alumina disc was fit into a rubber gasket. The inner and outer diameters of the rubber gasket were 21 mm and 32 mm, respectively and the gasket had a thickness of 2.4 mm. Alumina disc surrounded by the rubber gasket was clamped between the polyimide tubes by means of four screws.

A seed suspension with a concentration of 0.05 wt% was prepared by dispersing 0.05 g of MFI seed crystals in 99.95 g DI water. The suspension was stirred on a magnetic stirrer for 30 min and then ultrasonicated for 20 min. A small portion of this suspension was used for coating of the support and the remaining part was kept stirring on a magnetic stirrer to avoid the precipitation of zeolite crystals.

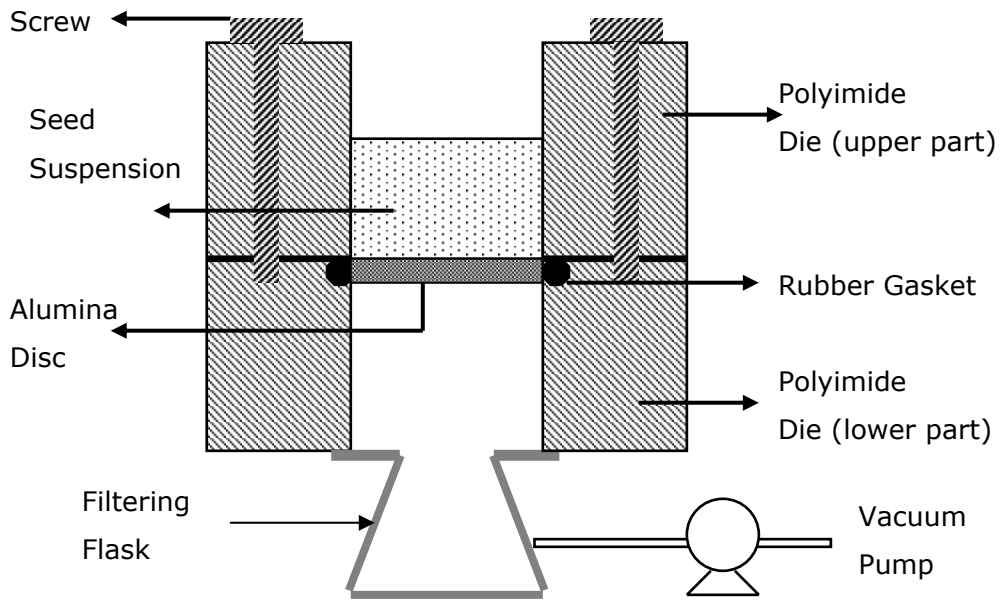

Figure 3.1 Schematic drawing of the seeding apparatus

The amount of seed on the disc surface was adjusted by changing the volume of seed suspension (Table 3.1). As seeding apparatus has a capacity of 8 ml, seeding procedure was repeated several times when the volume of suspension required more than 8 ml.

Table 3.1 The volume of seed suspension and weight of seed crystals and the time for settling of crystals during seeding process

0.05 wt% seed suspension (ml)	Amount of seed (mg)	Settling time* (min)	Amount of seed/surface area of alumina disc (mg/cm^2)
4	2.0	20	0.6
7	3.5	35	1.0
4+8	6.0	20+40	1.7
3x8	12.0	40	3.5
6x8	24.0	40	6.9

* settling time for each step

The seed suspension was poured on to the disc surface with a pipette and waited for a period of time. Meanwhile seed crystals precipitated on the disc surface. The time for precipitation of the seed crystals on the support are shown in Table 3.1. For coating the support with 2 mg of seed, 4 ml suspension was poured on the support surface and waited for 20 min for precipitation. On the other hand for 12 mg of seed, 8 ml of suspension was poured on the support and 40 min was waited for precipitation and this procedure is repeated three times. During precipitation, a small amount of colorless water permeated through the disc indicating that no seed particles passed through the disc. Then the seeding apparatus was put on a filtering flask which was connected to a vacuum pump. The remaining water on the disc surface was sucked, thus the seed crystals were deposited and stuck on the disc surface. The filtrate was again colorless. The seed coated alumina disc was removed from the apparatus and dried at 150^{o}C for 4 h to enhance the attachment of seed crystals on the disc surface [43].

3.4 Hydrothermal synthesis of MFI membranes

Membrane synthesis was carried out with Composition C1, which had also been used for the synthesis of micron-size MFI crystals. The procedure followed to prepare synthesis solution was given in detail in Section 3.1.

The synthesis was performed in stainless steel autoclaves with PTFE inserts. Two alumina discs were placed vertically in an insert by using PTFE holders. One disc was at the bottom and the other was at the top of the insert (Figure 3.2). The insert was then filled with about 33 ml of clear synthesis solution, which corresponds to approximately 80% of the insert's capacity. The synthesis was carried out at 130^{o}C.

To determine the effect of amount of seed on membrane quality, membranes were synthesized on the alumina discs containing 0 mg, 2 mg, 3.5 mg, 12 mg and 24 mg of seed crystals. The crystallization time was 24 h in these experiments. In another set of experiments, the course of crystallization was followed by changing the synthesis time from 3 h to 47 h. In these experiments, the amount of seed on the support was 0 mg, 2 mg or 12 mg.

After crystallization, the autoclaves were removed from the oven and cooled to room temperature. The membranes were taken from the autoclaves and washed with DI water until pH on the membrane surface was equal to 8. The membranes were dried at room temperature overnight.

The membranes were calcined in air at 450^{o}C for 12 h in a muffle furnace to the vacate MFI pores. The heating and cooling rates were 0.5 ^{o}C/s and 0.6 ^{o}C/s, respectively. The calcined membranes were kept in a desiccator containing dried air at room temperature. The air in the desiccator was dried by zeolite A.

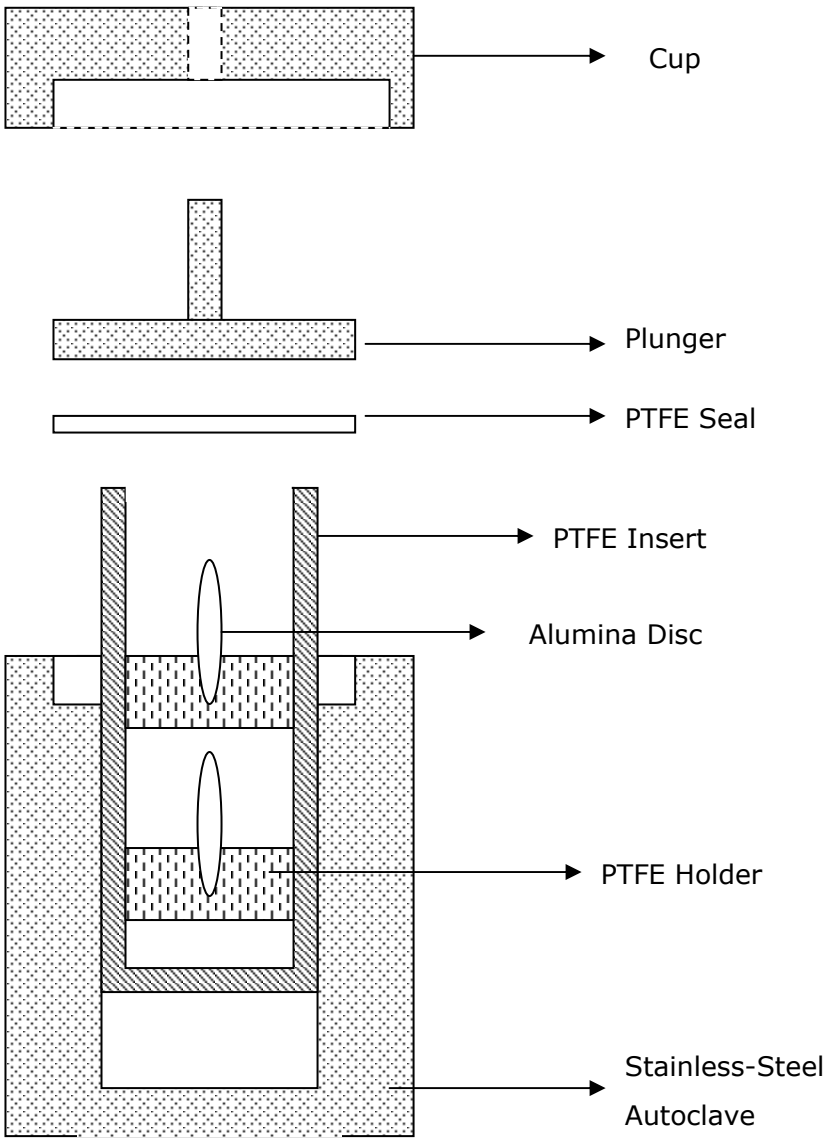

Figure 3.2 A schematic representation of the autoclave and the position of discs in the autoclave

3.5 Characterization

3.5.1 Characterization by XRD

Seed crystals were analyzed by Philips PW1840 X-ray diffractometer using Cu-Kα radiation for phase identification. The XRD patterns were taken between 5^o and 40^o Bragg angles and the samples were prepared in depression mounts.

The crystallinity of products was determined by intensity summation method. For this purpose three characteristic peaks of MFI at Bragg angles of 23^o, 24^o and 24.5^o ($I_{\theta 1}$, $I_{\theta 2}$, $I_{\theta 3}$) were selected. A product having the highest intensity summation for these three characteristic peaks was considered to be 100% crystalline and taken as reference. The crystallinity of the other products was calculated by equation 3.1;

$$\%\,\text{crystallinity} = \frac{(I_{\theta 1} + I_{\theta 2} + I_{\theta 3})_{\text{sample}}}{(I_{\theta 1} + I_{\theta 2} + I_{\theta 3})_{\text{reference}}} \times 100 \qquad 3.1$$

and the % yield of powder synthesis was calculated by equation 3.2;

$$\%\text{yield} = \frac{(m_{MFI})_{\text{sample}}}{(m_{MFI})_{\text{maximum}}} \times 100 \qquad 3.2$$

where m_{MFI} is the weight of MFI obtained and $(m_{MFI})_{max}$ is the maximum amount of MFI that can be synthesized from the initial synthesis solution. The determination of maximum yield is shown in Appendix A.

X-ray diffraction patterns of the membranes were used for identifying the crystalline phases in the membrane and for estimating thickness of membranes. The membranes were analyzed between 20^o and 40^o Bragg angles by mounting them on glass slides.

Alumina supports coated with different amounts of seed crystals were analyzed by XRD. The thickness of seed layer, which was estimated by using the density

of MFI crystals, was correlated to the intensities of MFI and alumina peaks. This correlation was then used to estimate the membrane thickness. Details of this procedure are given in Section 4.3.2.

3.5.2 Characterization by SEM

Morphology of MFI seed crystals and membranes was determined by Scanning Electron Microscopy (SEM) on a JEOL JSM-6400. For SEM analysis MFI seed crystals were pressed into disc shape and broken into small pieces. The membranes were also broken into small pieces. One of these broken pieces was then coated with gold to obtain an electrically conductive layer. SEM images of membranes were taken from both surface and fractured cross-section at magnifications between 750-6000.

3.6 Gas permeation

3.6.1 Description of single gas permeation set-up and membrane module

Single gas permeation set-up is shown in Figure 3.3. The set-up was constructed by using stainless steel tubings and fittings. The system can be divided into three parts as membrane module, feed and permeate side.

The membrane module is connected to feed side by 1/4" tubing and to permeate side by 1/8" tubing. The module has also an exit for retentate, yet this side is kept closed throughout the single gas permeation experiments. Second part of the set-up is the feed side. One end of the feed side is connected to the membrane module and the other end is connected to the regulators through polyurethane tubing. For the permeation experiments above room temperature, membrane module and tubings connected to module are covered with a heating tape. A temperature controller (E5CN-Omron) was used to control the temperature of the membrane. A K-type thermocouple is inserted into the membrane module so that it measures nearly the temperature of the membrane. Permeate side of set-up is connected to the membrane module by 1/8" pipe and to soap bubble flow meter by silicone tubing.

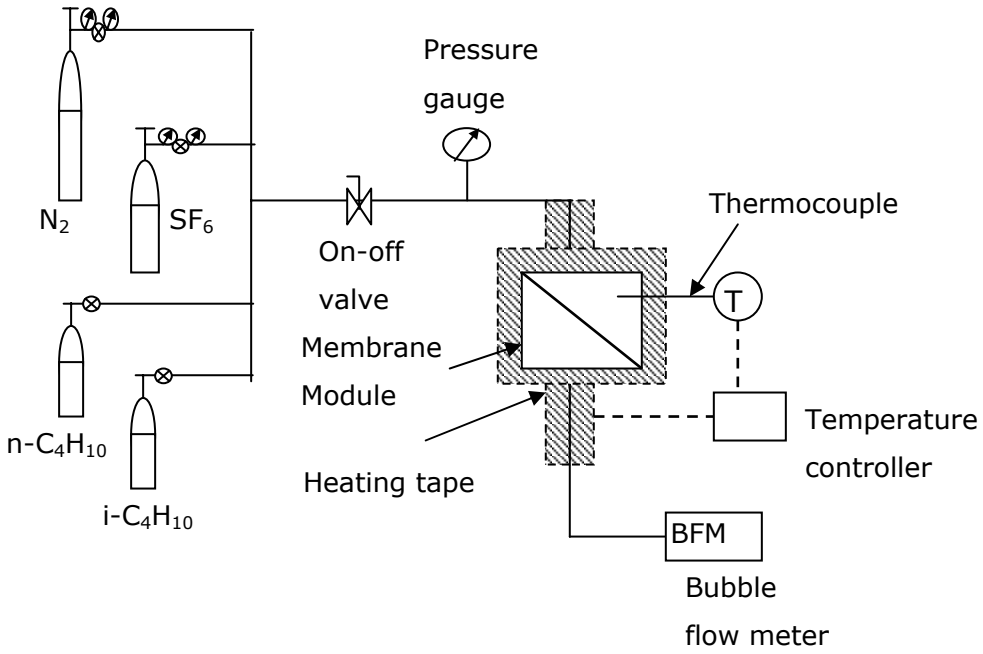

Figure 3.3 Schematic drawing of the single gas permeation set-up

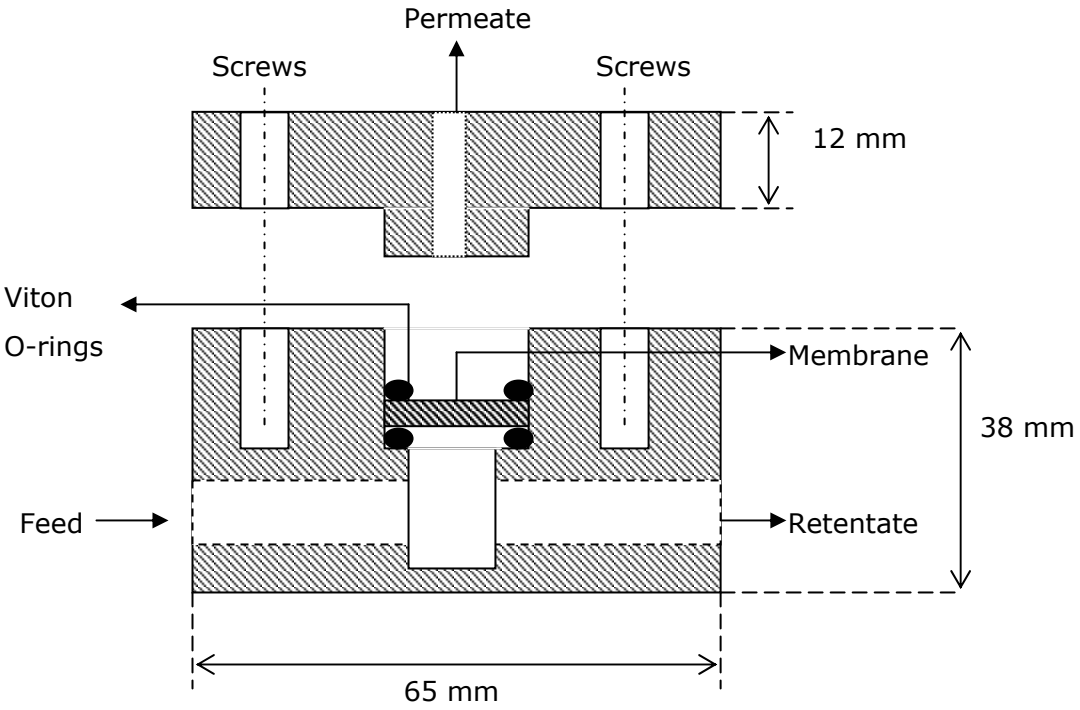

Figure 3.4 Schematic drawing of the membrane module

A stainless-steel membrane module was used in gas permeation tests (Fig. 3.4). The module is appropriate for disc shaped membranes with a diameter of 21 mm and a thickness of 1 mm. Module consists of two cylindrical shaped parts that are 64 mm in diameter. Wall thicknesses of the lower and upper parts are 28 mm and 12 mm, respectively. Membrane was placed in module between two Viton O-rings. Then the lower and upper parts of module were clamped by means of four screws to seal the membrane. O-rings, which have an inner diameter of 17.60 mm and 2.4 mm thickness, ensure sealing between membrane and module. Viton O-rings are stable up to about 200°C.

3.6.2 Single gas permeation measurements

Gas permeation tests were started with N_2 through the uncalcined membranes in order to check if the membrane has defects or not. The pores of the as-synthesized MFI crystals are filled with template so that the membrane without defects is expected to be impermeable [10]. The impermeable membranes (permeance $<10^{-10}$ mol/Pa.s.m^2) were then calcined to open the MFI pores.

Single gas permeances of N_2 (Habaş, high purity) and SF_6 (BOS, 99.9% purity) were measured at room temperature. According to the N_2/SF_6 ideal selectivity, the n-butane and isobutane (Air Products, 99.9% purity) permeances were measured at temperatures 25°C, 50°C, 100°C and 150°C. Before permeation of each gas the membrane was cleaned at room temperature by N_2 flow to remove the adsorbed gas molecules. Cleaning was stopped when the initial N_2 permeance was recovered.

Constant pressure-variable volume method was used through the permeation measurements. The feed was fed to the membrane at a pressure of 1.9 bar, and the permeate side was kept at atmospheric pressure. The permeate flow rate was measured in every 15 min with a soap bubble flow meter until steady state was attained.

Assuming the permeating gas to be ideal, the permeance of a gas was calculated by equation 3.3,

$$\underline{P} = \frac{\frac{P}{R.T}\left(\frac{\Delta V}{\Delta t}\right)}{\Delta P.A} \qquad 3.3$$

where $\underline{P}$ is the permeance (mol/Pa.s.m^2), ΔP is the transmembrane pressure difference (Pa), A is the effective membrane area, which is 2.43 x10^{-4} m^2 (this corresponds to 70% of total membrane area), P is the atmospheric pressure (Pa), R is the ideal gas constant (Pa.m^3/K.mol), T is the room temperature (K) and $\Delta V/\Delta t$ is the volumetric flow rate of the permeate (m^3/s) which is measured by soap bubble flow meter.

Ideal selectivity that is defined as the ratio of the permeances of two single gases can be calculated by equation 3.4.

$$\alpha_{ij} = \underline{P}_i / \underline{P}_j \qquad 3.4$$

A sample calculation for permeance and ideal selectivity are given in Appendix B.

3.6.3 Description of binary gas mixture separation set-up

The set-up for separation of binary gas mixtures is shown in Figure 3.5. The set-up consists of four main parts, namely membrane module, permeate, feed and retentate sides. The membrane module is described in the previous section, although in separation experiments the retentate side was not closed.

The second part of the system is the feed side. The gas cylinders are connected to gas filters (2-5 μm) and the gas filters are connected to mass flow controllers (MFC) by 1/4" stainless steel tubes. Gas filters protect MFC's by filtering impurities in the feed gas. The gases are mixed in a tee-union and fed to the membrane module.

The third part of the system is the permeate side. There exists a by-pass line between feed and permeate sides. Through the by-pass line, the permeate side is filled with the gas mixture and thus air is discharged from the module. A pressure gauge and a back pressure valve (Air Products, 7 bar max. pressure)

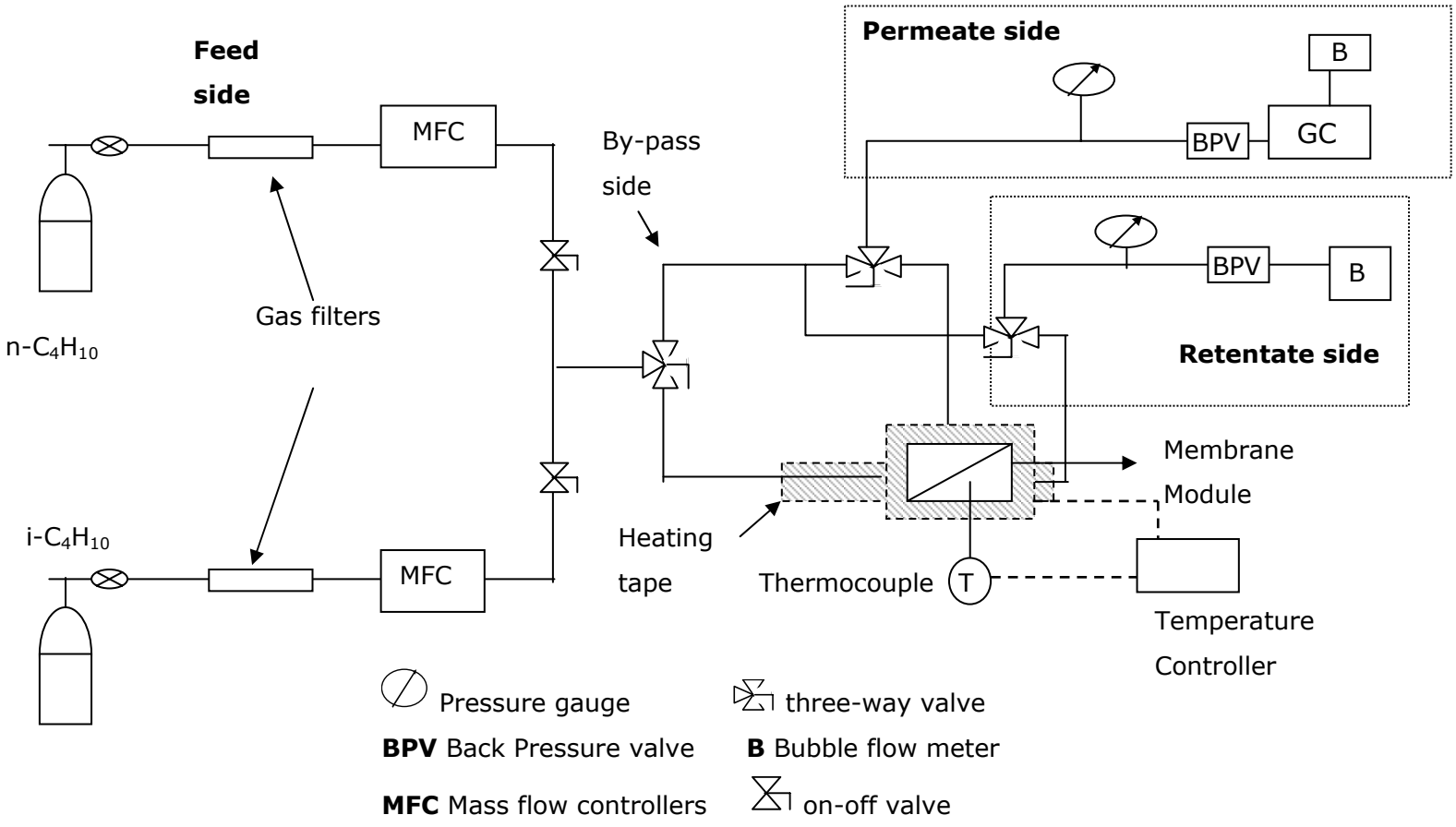

Figure 3.5 Schematic representation of binary gas permeation set-up

are connected to the permeate side by 1/8" pipes. The permeate side is connected to a gas chromatograph (CP-3800 Varian) by a 6-port valve. Outlet of gas chromatograph is hooked up to a soap bubble flow meter by silicone tubing.

The last part of the system is the retentate side. A pressure gauge and a backpressure valve are linked to the system by 1/4" pipes. The feed pressure was kept constant at the desired pressure by backpressure valve and the pressure was measured with a pressure gauge. The retentate flow rate is measured by a soap bubble flow meter.

The temperature was measured by a K-type thermocouple, which is inserted into the membrane module. The system is heated by heating tapes wrapped the module and tubings, and the temperature was controlled by Omron E5CN temperature controller.

3.6.4 Separation of binary gas mixtures

Separation of n-butane and isobutane mixtures was performed at 25^{o}C, 50^{o}C, 100^{o}C, and 150^{o}C. The feed and retentate sides were approximately at 1.9 bar and the permeate side was kept at atmospheric pressure.

Flow rate of feed was adjusted to 40 ml/min. The feed mixture composition was adjusted to 50% n-butane and 50% isobutane by MFC's. The calibration curves for MFC's are given in Appendix C.

The volumetric flow rate of the permeate and the retentate were measured in every 30 min with soap bubble flow meters until steady state was attained (Appendix L). Permeate and feed streams were analyzed online by a gas chromatograph (CP-3800 Varian) with TCD (thermal conductivity detector) and a packed column (chromosorb 80-100 mesh). TCD detector and packed column temperature were adjusted to 100^{o}C and 30^{o}C respectively. The column pressure was 10 psi. For the analysis of gas mixture, gas chromatograph is calibrated for n-butane and isobutane mixtures (see Appendix D).

Log-mean transmembrane pressure difference, equation 3.5, was applied to calculate the permeances;

$$\Delta P_{\log-\text{mean}} = \frac{\left(P_i^F - P_i^P\right) - \left(P_i^R - P_i^P\right)}{\ln\left[\left(P_i^F - P_i^P\right) / \left(P_i^R - P_i^P\right)\right]} \qquad 3.5$$

where $P_i^{F,P,R}$ is the partial pressures of component i in feed, permeate and retentate respectively.

Permeance of each component was calculated by equation 3.6;

$$\underline{P_i} = \left[\left(\frac{\Delta V}{\Delta t}\right)\frac{P_{atm}.y_i}{R.T}\right]\frac{1}{A}\frac{1}{\Delta P_{log-mean}} \qquad 3.6$$

where $\underline{P_i}$ (mol/Pa.s.m^2) is the permeance of i in permeate, y_i is the mol fraction of i in permeate and $\Delta P_{log\text{-}mean}$ (Pa) is the log-mean transmembrane pressure difference.

The separation selectivity is defined as the ratio of gas permeance. Sample calculations of permeance and separation selectivity are given in Appendix D.

CHAPTER 4

RESULTS AND DISCUSSION

4.1 Synthesis of MFI type seed crystals

Seed crystals, micron and submicron in size, are commonly used in the preparation of zeolite films and membranes [20-27,43]. The seed coated supports are subjected to secondary growth to close the voids between seed crystals and to obtain continuous zeolite layers.

In this study, MFI type zeolites for use as seed were synthesized from clear synthesis solutions with two different initial molar batch compositions. These are $TPAOH:9.80SiO_2:0.025NaOH:0.019Al_2O_3:602.27H_2O:39.16C_2H_5OH$ (C1) and $TPAOH:8.17SiO_2:0.08Na_2O:162.09H_2O:32.68C_2H_5OH$ (C2).

ED7 and ED8 were synthesized from composition C1 after 24 h and 46 h of synthesis, respectively. ED6 was synthesized from composition C2 in 24 h (Table 4.1). Figure 4.1 shows the XRD patterns of ED6 and ED7 with the reference pattern of ZSM-5 given in Verified Syntheses of Zeolitic Materials [53]. The peaks in the patterns of samples are in agreement with the reference pattern and no other peaks are present in the patterns. Apparently, MFI is the only crystalline phase in samples. Composition C1 that contains small amount of Al_2O_3 yields ZSM-5 whereas composition C2, no Al_2O_3 in it, yields silicalite-1. As both ZSM-5 and silicalite-1 are members of MFI group and it is difficult to distinguish ZSM-5 from silicalite-1 by XRD, the zeolite crystals (and membranes) synthesized in this study are called with the group name of ZSM-5 and silicalite-1.

The low background and high peak intensities also suggest that the samples are pure. Crystallinity of the samples was also determined quantitatively by equation

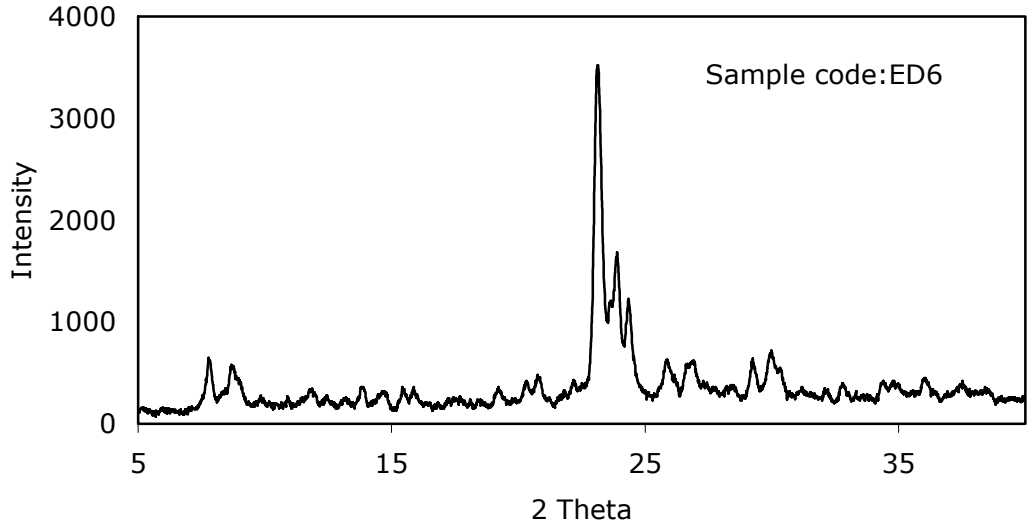

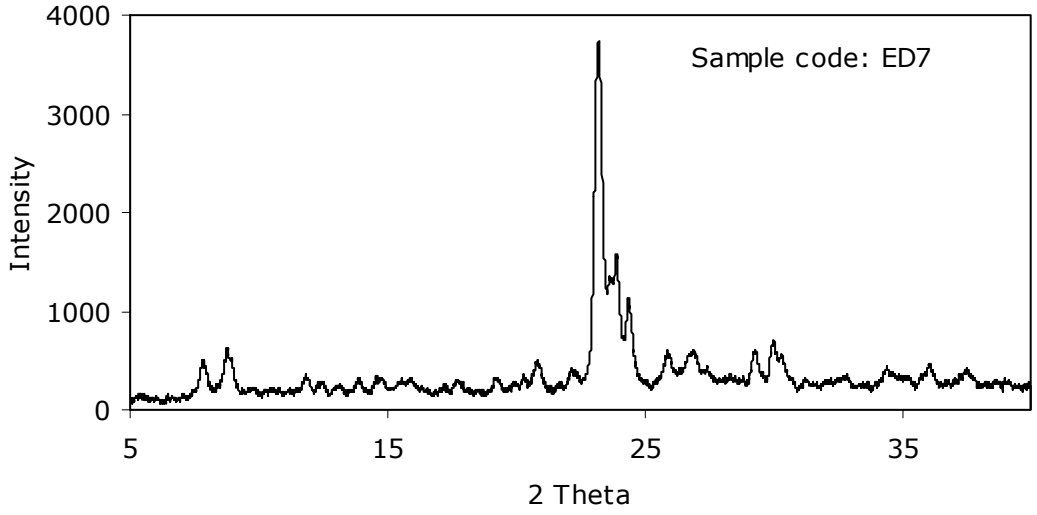

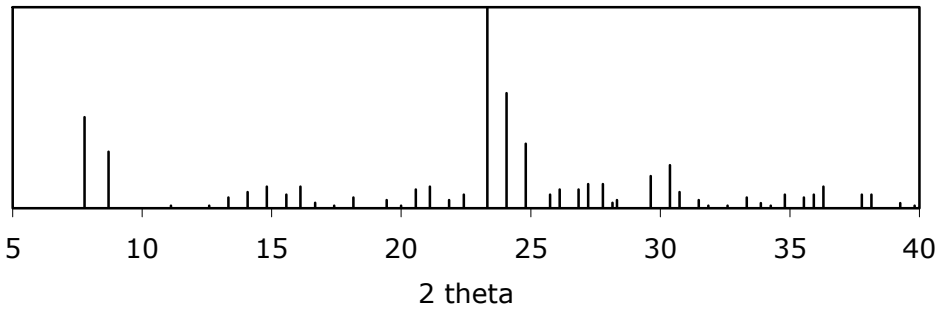

Figure 4.1 XRD patterns of MFI seed crystals (ED6 and ED7) and reference XRD pattern of MFI [53]

3.1. For this purpose, ED8 was chosen as reference and its crystallinity was assumed to be 100%.

Table 4.1 Crystallinity and yield results of MFI seed crystals

Sample code	Molar composition	Temperature (°C)	Crystallization time (h)	% Crystallinity	% Yield
ED6	C2	91	24	84	90
ED7	C1	130	24	89	23
ED8	C1	130	46	100	60

Samples ED6 and ED7 are nearly pure although they have been crystallized in a much shorter time than the reference ED8 (Table 4.1). Yield of the samples were calculated by equation 3.2. The yield was only 23% in 24 h and increased to 60% after 46 h of crystallization for samples crystallized from composition C1. Low yield indicates that most silica remained dissolved in solution, possibly because of low nucleation and crystal growth rates. This could be an advantage in the synthesis of membranes on seeded supports. As crystallization will be slow in the bulk during membrane synthesis, the effect of seed crystals on the membrane properties can be observed more clearly [45]. The product of composition C2 (ED6) had 89% crystallinity and 90% yield. The yield of ED6 is much higher than the yield of ED7 even ED6 was crystallized at a lower temperature. The main difference between composition C1 and C2, which were used to synthesize ED7 and ED6, respectively, is the amount of water in the batch. Composition C2 is much more concentrated than composition C1. It is known that concentrated batches favor crystallization while nucleation and crystal growth is restrained in dilute batches [34].

Figure 4.2 shows the SEM images of ED6 and ED7. Crystals in sample ED7 are greater than 1 μm and has coffin shape, whereas crystals in sample ED6 are smaller than 1 μm and has sphere like shape.

Figure 4.3 shows the particle size distribution of ED6 and ED7. Particle size distribution of ED7 was determined by measuring the length of long edge of the crystals from SEM image. Both samples have narrow particle size distributions.

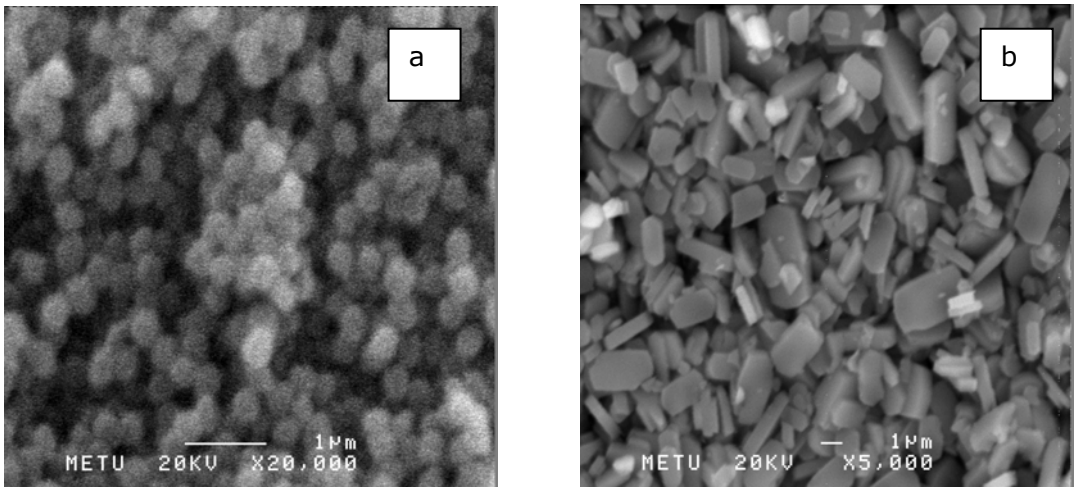

Figure 4.2 SEM images of seed crystals (a) ED6 [submicron size seed crystals] (b) ED7 [micron size seed crystals]

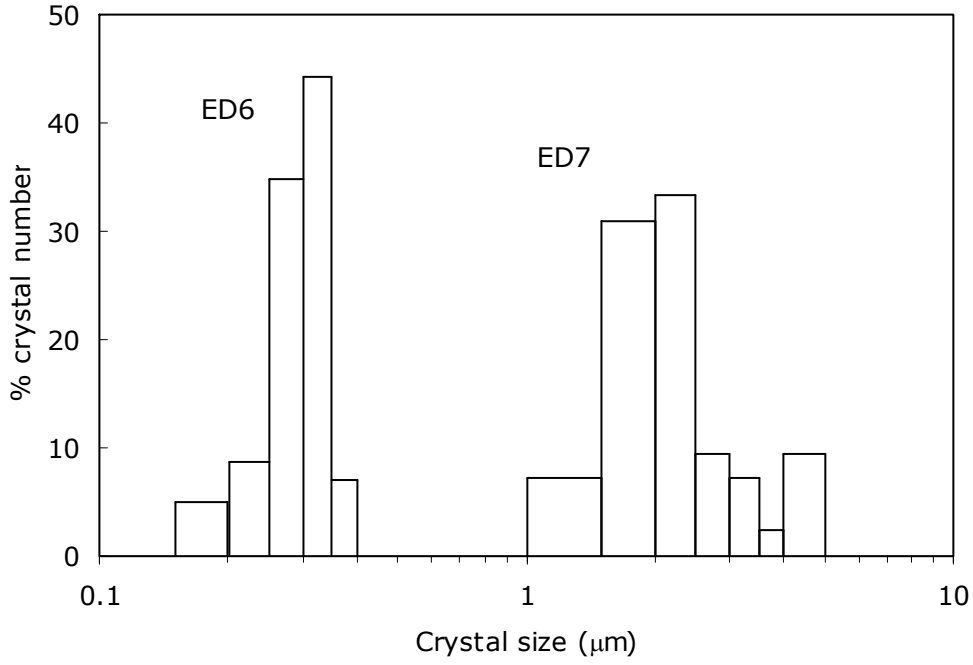

Figure 4.3 Particle size distribution of ED6 and ED7 measured from SEM images

Crystals in ED7 are between 1 μm and 5 μm and those in ED6 are between 0.25 μm and 0.35 μm.

Many researchers have suggested that closely packed seed layers are essential to obtain continuous and defect free membranes with seeding [20-26] although Li et al. [54] prepared continuous membranes on seeded supports having low coverage. Seed crystals with narrow particle size distribution are preferred to be able to prepare closely packed seed layers [24]. Accordingly, MFI type zeolites synthesized in this study which have narrow particle size distribution are appropriate for use as seed in membrane preparation.

Mean particle size of micron size seed crystals is approximately 3 μm in 24 h of synthesis and that is increased to 5 μm after 46 h of synthesis (Table 4.2). Aspect ratio of those crystals is approximately 2. Submicron size seed crystals have a mean particle size of 0.3 μm. Hereafter, the seed with a mean particle size of smaller than 1 μm is called as submicron-size seed and the seed with a mean particle size of greater than 1 μm is called as micron-size seed.

Table 4.2 Particle size and aspect ratio of MFI seed crystals

Sample code	Molar composition	Crystallization time (h)	Mean Particle Size (μm)	Aspect ratio
ED6	C2	24	0.3	-
ED7	C1	24	3	1.6-2.2
ED8	C1	46	5* (3-7)	2*

* results obtained by optical microscope with limits of particle size distribution in parentheses

4.2 Properties of seed coated supports

Quality of seed layer affects the membrane quality since non-uniform seed layers may lead to formation of defects throughout the membrane. Uniform seed layers with intercrystalline distance less than a crystal size are desired [13,26].

Uniformity of the seed layer depends on the seeding technique, particle size distribution of the seed crystals and the properties of the support material.

Several methods have been developed for the preparation of seed layers, such as dip coating, rubbing and vacuum-seeding (Section 2.5). In this study, vacuum seeding method was applied to coat the supports with seed crystals. Vacuum seeding method may provide thin, uniform and closely packed seed layers [27]. In addition amount of seed on the support can be controlled by the concentration and quantity of seed suspension poured on the support surface. Both micron and submicron size seed crystals can be used for coating depending on the pore size of the support.

Membranes were prepared on homemade α-alumina supports, which has an average pore diameter of 1.2 μm. Pore size of the supports was determined with mercury porosimeter (see Appendix E). Both submicron (250-350 nm) and micron (1-5 μm) size seed were used to coat the α-alumina supports.

When submicron size seed crystals were used, cloudy water rather than clear colorless water permeated through the support and the water flux decreased as the suspension was added. This showed that crystals penetrated into the support and blocked the support pores. Seed crystals in support may favor the formation of MFI layer within the support pores which may decrease the permeance through membrane.

When micron size seed crystals were used the water permeated through the support was clear indicating that no seed crystals pass through the support. For this reason micron size seed crystals were used for seeding.

In this study, membranes were synthesized with different amounts of micron size seed crystals. The supports were seeded with 2, 3.5, 6, 12 and 24 mg of seed crystals. In order to determine the weight of seed on the support, both bare and seed coated supports were weighted. The weight of seed on the supports is compared with the amount of seed introduced from the seed suspension in Table 4.3. Seed suspension can be slightly non-uniform as it was prepared with micron-size crystals, those crystals may settle down though the

suspension was stirred continuously. Since a small fraction of this suspension was used to fill the seeding apparatus, a slight non-uniformity in the suspension cause the difference between the measured and presumed weights of seed on the support. The average differences between the measured and presumed weights are quite small, which indicate that vacuum seeding method is reproducible and reliable.

Table 4.3 Amount of seed on the supports coated with different amounts of seed suspension

Number of support	Presumed weight of seed on the support* (mg)	Average of measured weight of seed on the support (mg)	Average difference between presumed and measured weight of seed (mg)	Amount of Seed* / Surface Area of Support (mg/cm^2)
18	2.0	1.7	±0.4	0.6
11	3.5	3.5	±0.2	1.0
10	6.0	5.7	±0.5	1.7
18	12.0	11.8	±0.4	3.5
5	24.0	24.0	±0.4	6.9

* amount of seed in suspension

Figure 4.4 shows the surface images of bare support, 2 mg and 12 mg of seed coated supports. The bare support composed of large alumina particles about 10 μm and the size of voids among those particles is approximately 2 μm. After vacuum seeding the alumina particles and the voids cannot be seen. The support surface is completely covered with randomly oriented coffin shaped MFI crystals.

Figure 4.5 shows the cross-section images of seed coated alumina supports. The seed layers are uniform throughout the whole cross-section. The thickness of the seed layer is nearly 9 μm on the support coated with 2 mg of seed and nearly 25 μm on the support coated with 12 mg of seed. Cross-section images also showed

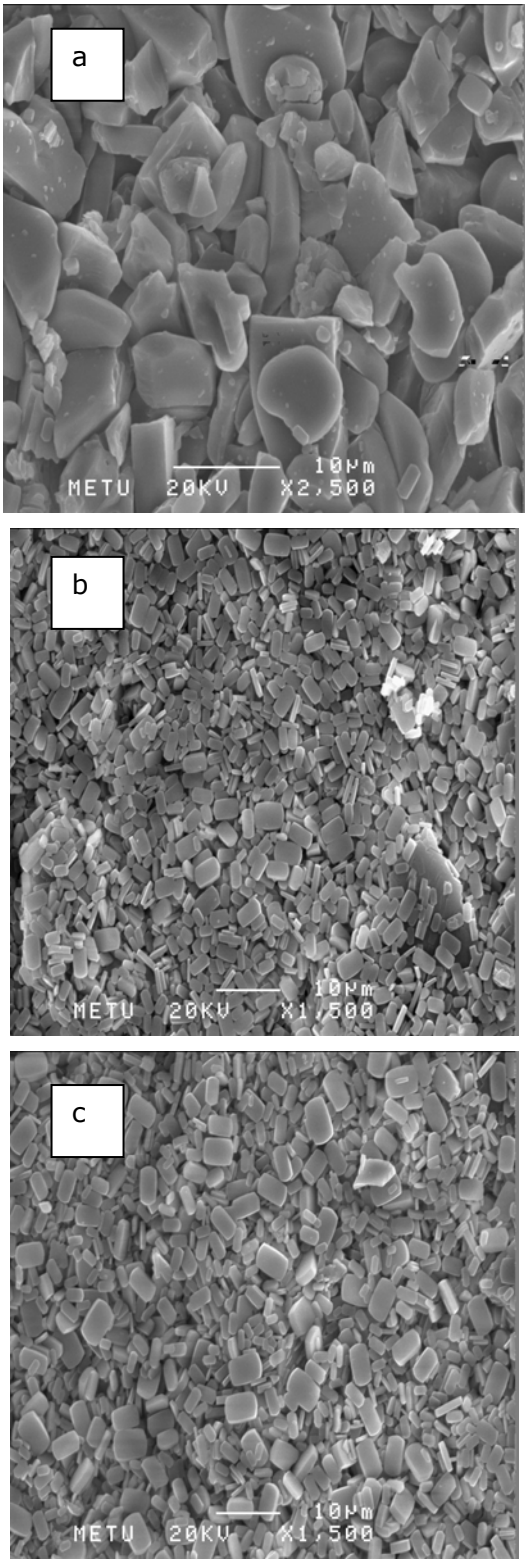

Figure 4.4 Surface image of (a) bare alumina support (b) support coated with 2 mg of seed (c) support coated with 12 mg of seed

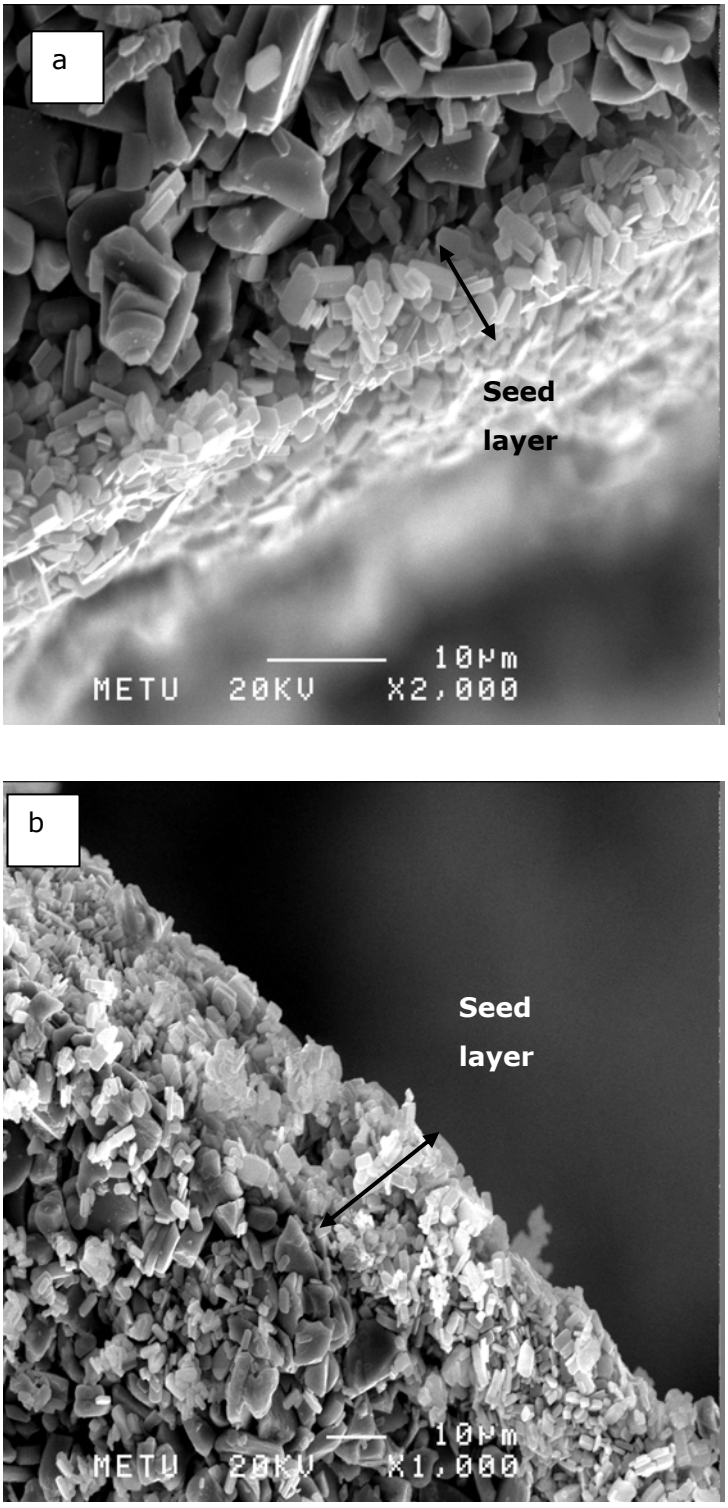

Figure 4.5 Cross-section SEM images of seeded alumina supports (a) support coated with 2 mg of seed (b) support coated with 12 mg of seed

that there are some MFI crystals in the support pores. As the pore size of support ranges between 0.1 μm and 2.2 μm seed crystals which are between 1 μm and 5 μm, inevitably penetrate into the support pores. During seeding, the water passed through the support was clear. This indicates that seed crystals enter but cannot go deeply in the support pores.

Consequently, uniform seed layers with high coverage were obtained reproducibly by vacuum seeding method in a single-step coating process. In addition, as vacuum seeding allows controlling the amount of seed on the support surface it is a suitable method for the investigation of effect the amount of seed on membrane morphology and quality.

4.3 Synthesis of MFI membranes on seed coated alumina supports

4.3.1 Effect of amount of seed on membrane morphology

Membrane synthesis was performed on bare and on supports seeded with different amount of seeds. The synthesis (or secondary growth) was carried out with a molar composition of TPAOH:9.80SiO_2:0.025Na_2O:0.019Al_2O_3:602.27H_2O :39.16C_2H_5OH (C1) at 130^oC for 24 h. Notice that this composition yields small amount of MFI crystals, thus effect of seeding on membrane growth can be seen clearly.

The effect of amount of seed on the membrane morphology and quality was investigated. The reproducibility in membrane morphology was also examined with SEM images.

Figure 4.6 shows the XRD patterns of bare alumina support, 1.0 mg/cm^2 seeded alumina support and a membrane synthesized on 1.0 mg/cm^2 seeded support. The alumina peaks were marked by asterisk on the patterns. MFI seed crystals and synthesized MFI layer decreased the peak intensity of alumina and the intensity ratio ($I_{MFI}/I_{alumina}$) increased, indicating growth of seed crystals, to form continuous layer and possibly formation of new crystals, thus increase of thickness after secondary growth.

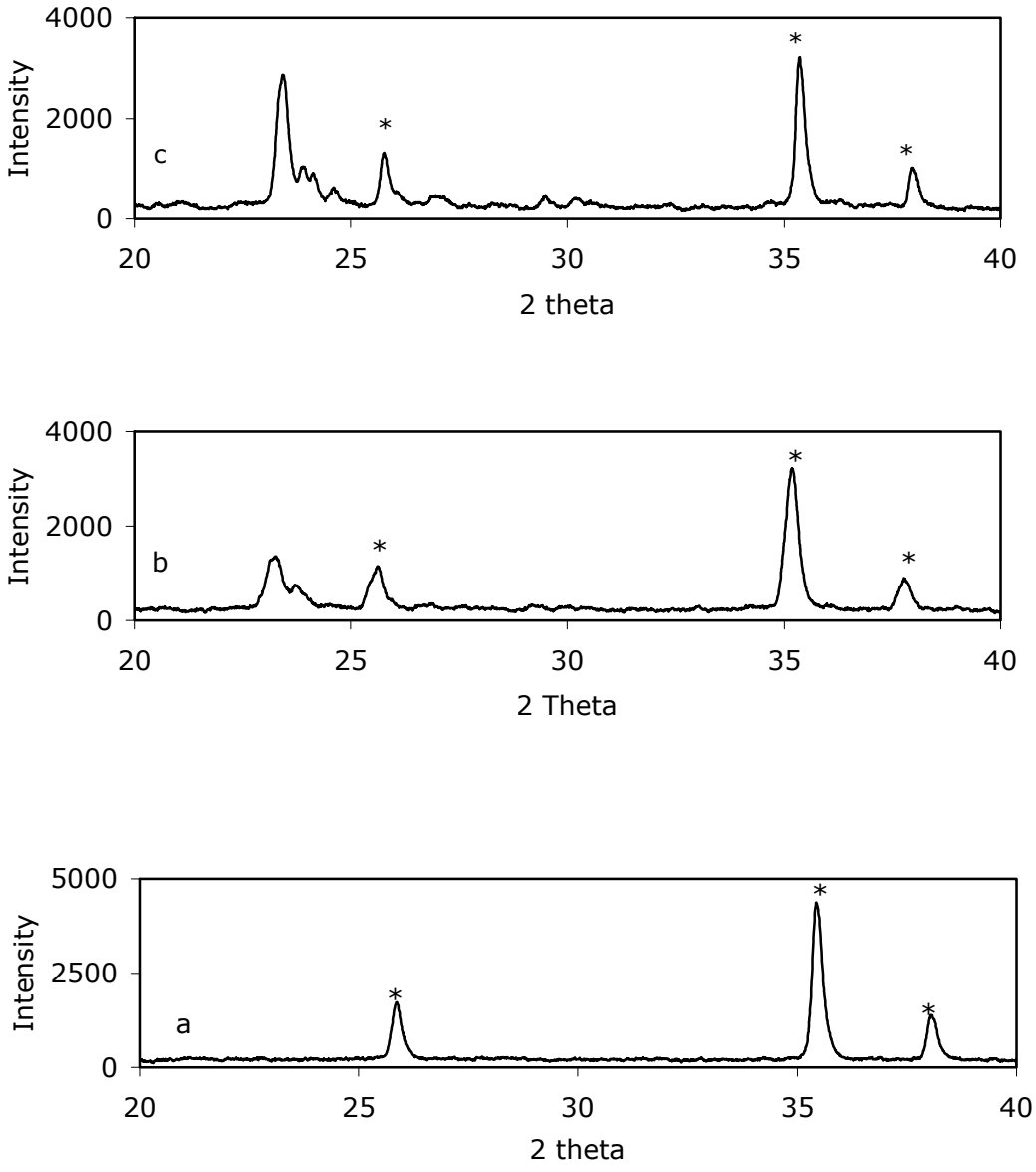

Figure 4.6 XRD pattern of (a) bare support (b) 1.0 mg/cm^2 seeded support (c) membrane synthesized on 1.0 mg/cm^2 seeded support (* alumina peaks)

Figure 4.7 shows the XRD patterns of the membranes synthesized on bare, 0.6, 1.0, 1.7 and 3.5 mg/cm^2 seeded supports. With increasing amount of seed on the support, MFI peaks get stronger while the alumina peaks become weaker, suggesting that thickness of MFI layer depends on the amount (or thickness) of seed layer and membrane thickness increases with the amount of seed on support.

Figure 4.8 shows the surface images of membranes. In all the membranes the support surface is fully covered with highly intergrown MFI crystals after hydrothermal synthesis. The crystals have similar shape and size of crystals range changes 6 μm and 9 μm.

Figure 4.9 shows the cross-section images of those membranes. All the membranes except the membrane synthesized without seed crystals have a continuous MFI layer. The MFI layer is not uniform in the membrane synthesized without seed crystals, its thickness varied between 9 μm and 13 μm. Membranes synthesized on seeded supports, 0.6 and 1.0 mg/cm^2 of seed, have thick, compact and uniform layers. The crystals forming the MFI layer cannot be distinguished from each other because of high intergrowth. Seed crystals that were deposited before membrane synthesis could not be seen in the cross-section images. The layer thickness was 9 μm for the membrane with 0.6 mg/cm^2 of seed and that was 17 μm for the membrane with 1.0 mg/cm^2 of seed.

Membrane synthesized with 1.7 mg/cm^2 of seed was 23 μm thick. This membrane has a loose MFI layer between alumina support and continuous MFI layer, which is at the top (Figure 4.10). The top layer is dense and highly intergrown. Thicknesses of the intermediate and top layer are approximately 18 μm and 5 μm respectively. The membrane synthesized on the support with 3.5 mg/cm^2 seed has also an asymmetric structure. It consisted of two layers with different morphological properties (Figure 4.11). Individual crystals forming the intermediate layer can be clearly seen in Figure 4.11. Apparently seed crystals close to the support have not participated in the secondary growth. Although the whole thickness of membrane is 39 μm, thickness of the intermediate layer is nearly 22 μm. The MFI layer at the top is uniform, continuous and dense. The thickness of the top layer is approximately 17 μm.

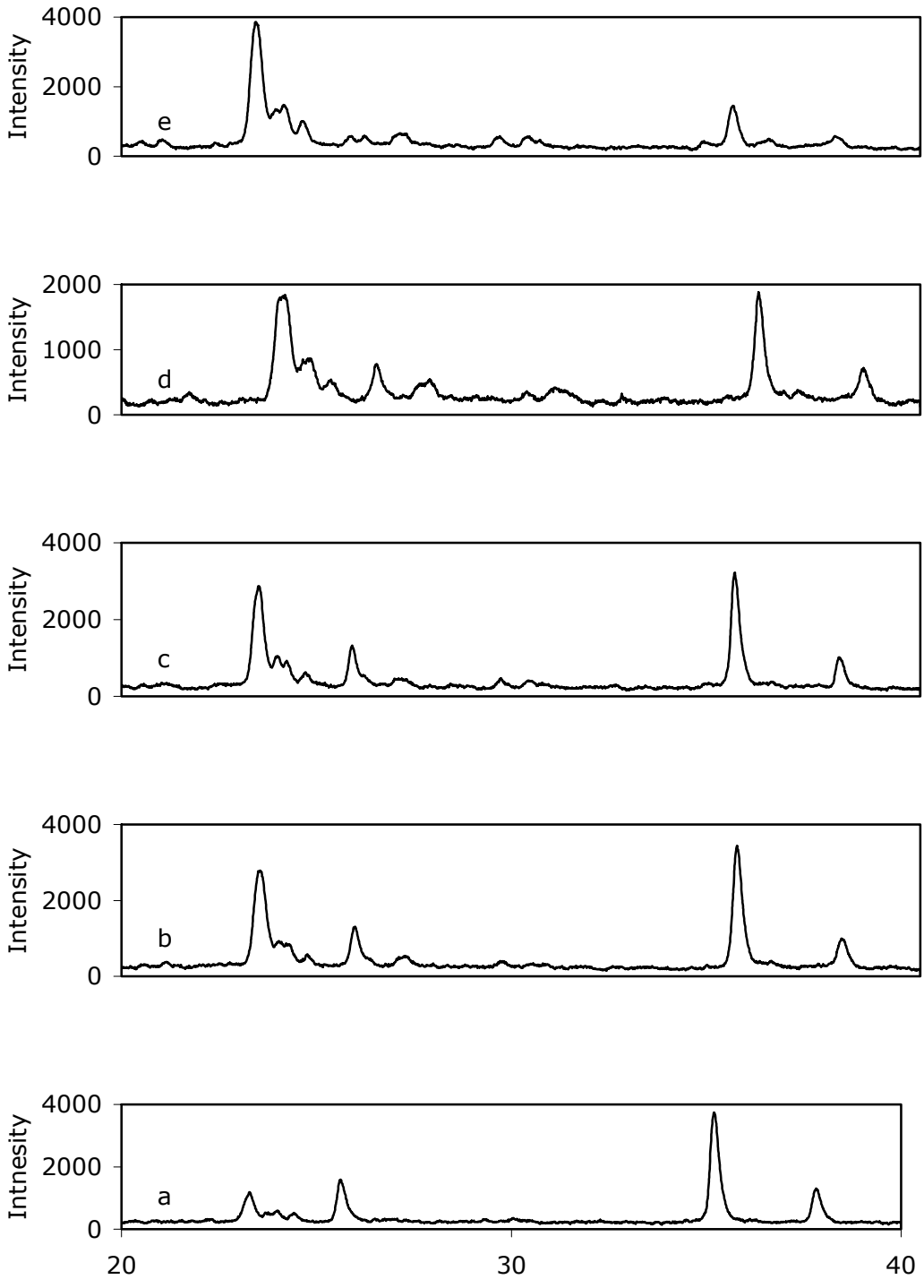

Figure 4.7 XRD patterns of membranes synthesized on supports coated with different amount of seed [mg/cm^2] (a) unseeded (b) 0.6 (c) 1 (d) 1.7 (e) 3.5

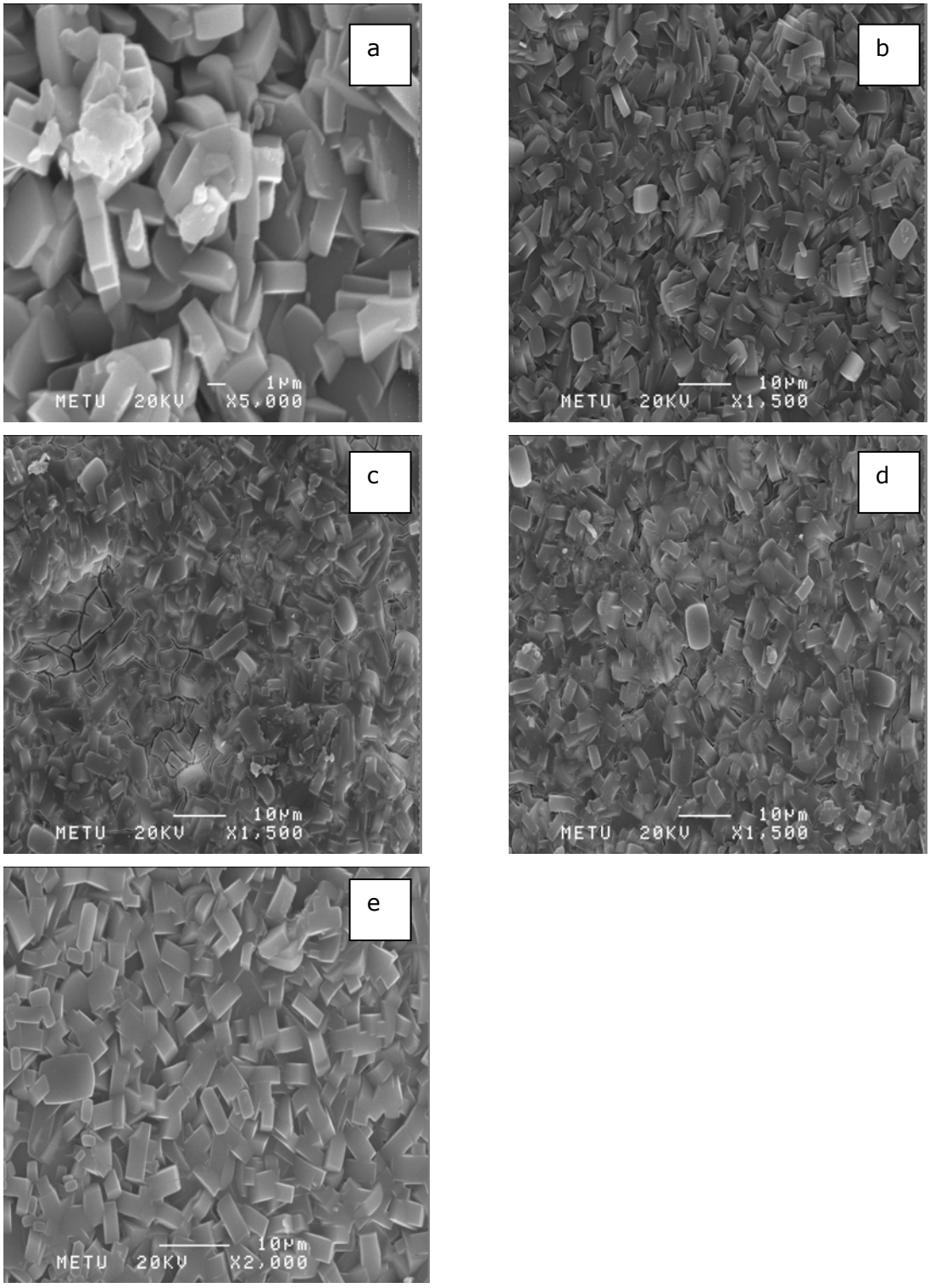

Figure 4.8 Surface SEM images of membranes synthesized on supports coated with different amount of seed [mg/cm^2] (a) unseeded [ED79u] (b) 0.6 [ED74a] (c) 1.0 [ED97u] (d) 1.7 [ED70u] (e) 3.5 [ED50a]

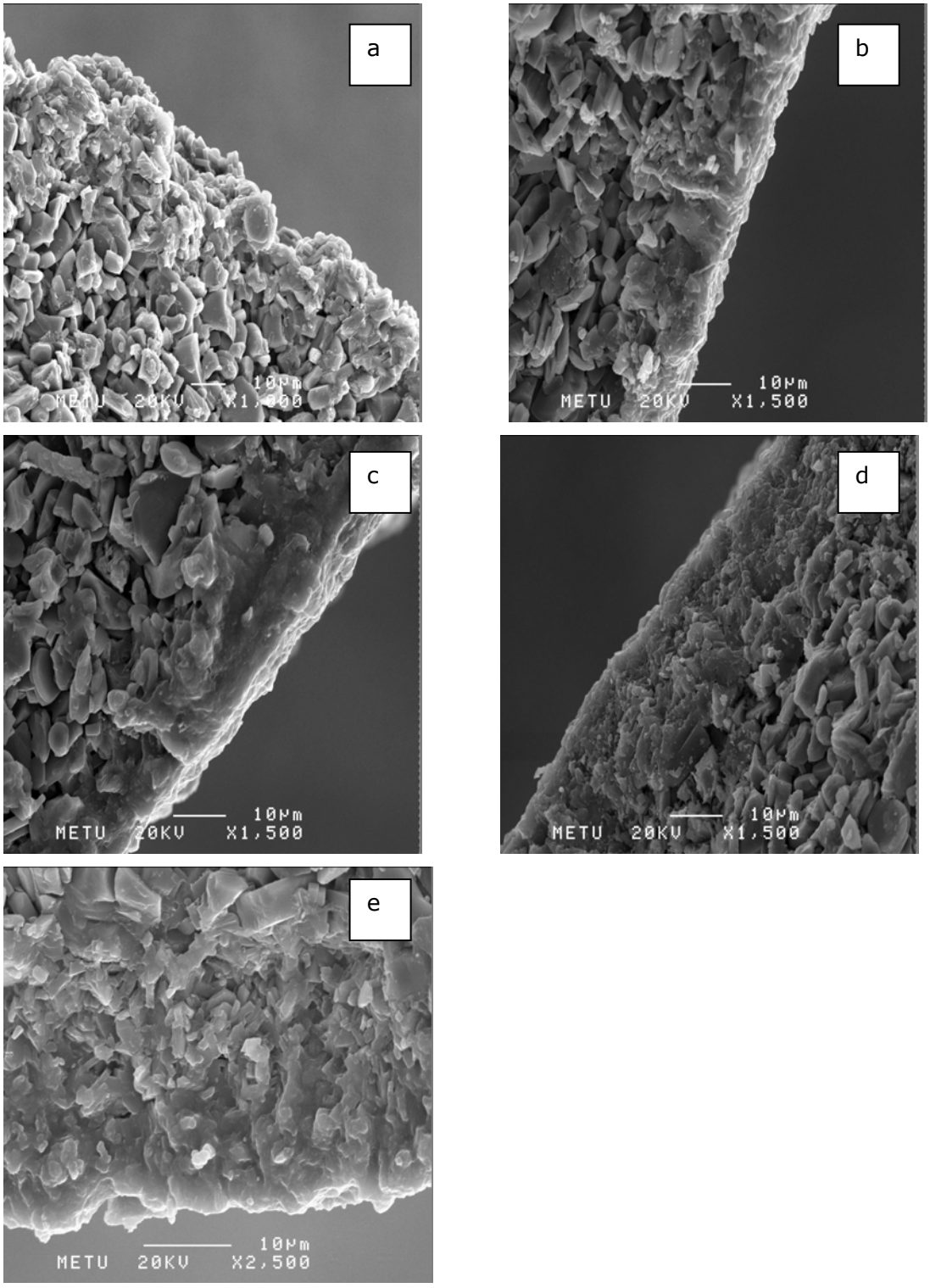

Figure 4.9 Cross-section SEM images of membranes synthesized on supports coated with different amount of seed [mg/cm^2] (a) unseeded [ED79u] (b) 0.6 [ED74a] (c) 1.0 [ED97u] (d) 1.7 [ED70u] (e) 3.5 [ED50a]

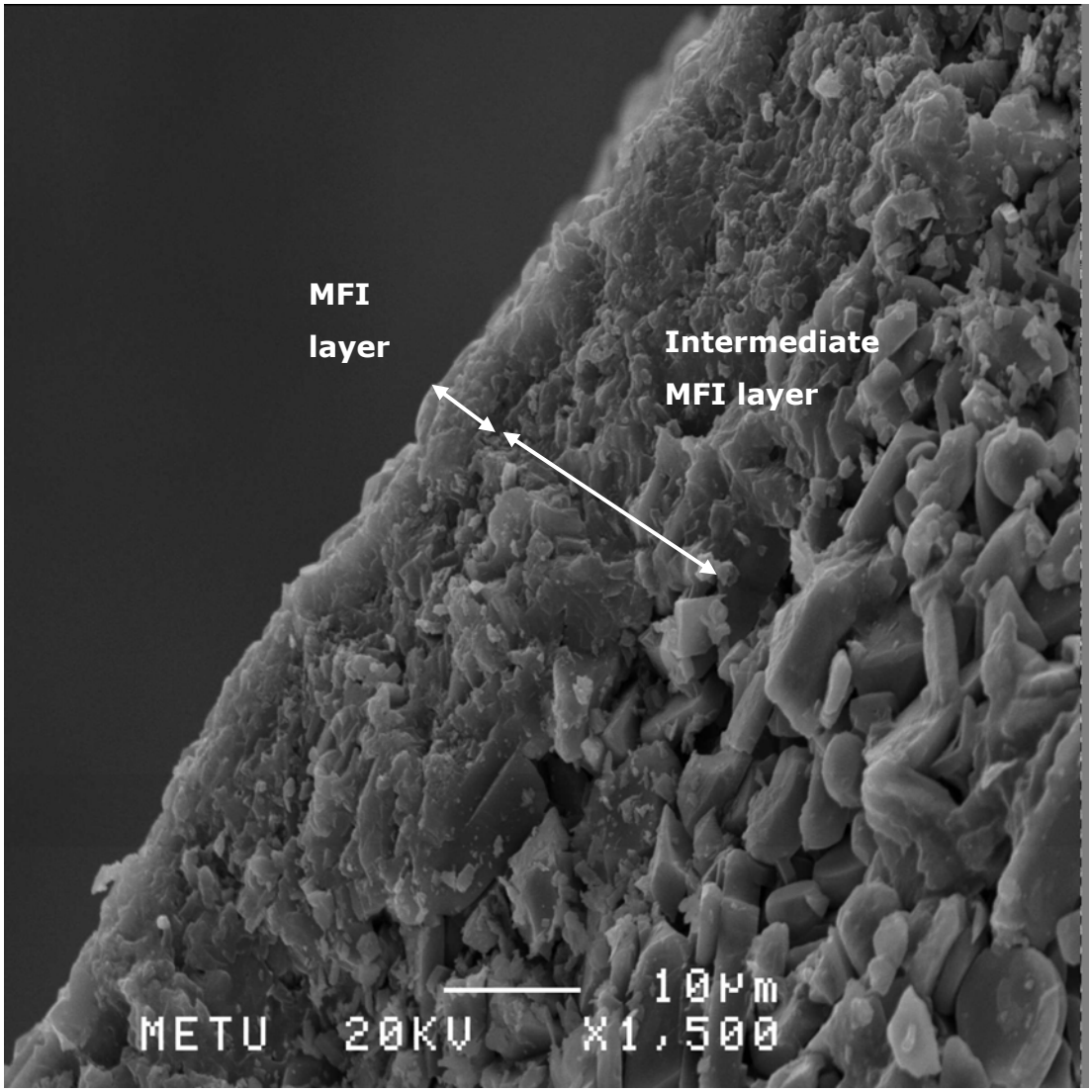

Figure 4.10 Cross-section image of membrane synthesized on support coated with 1.7 mg/cm^2 of seed [ED70u]

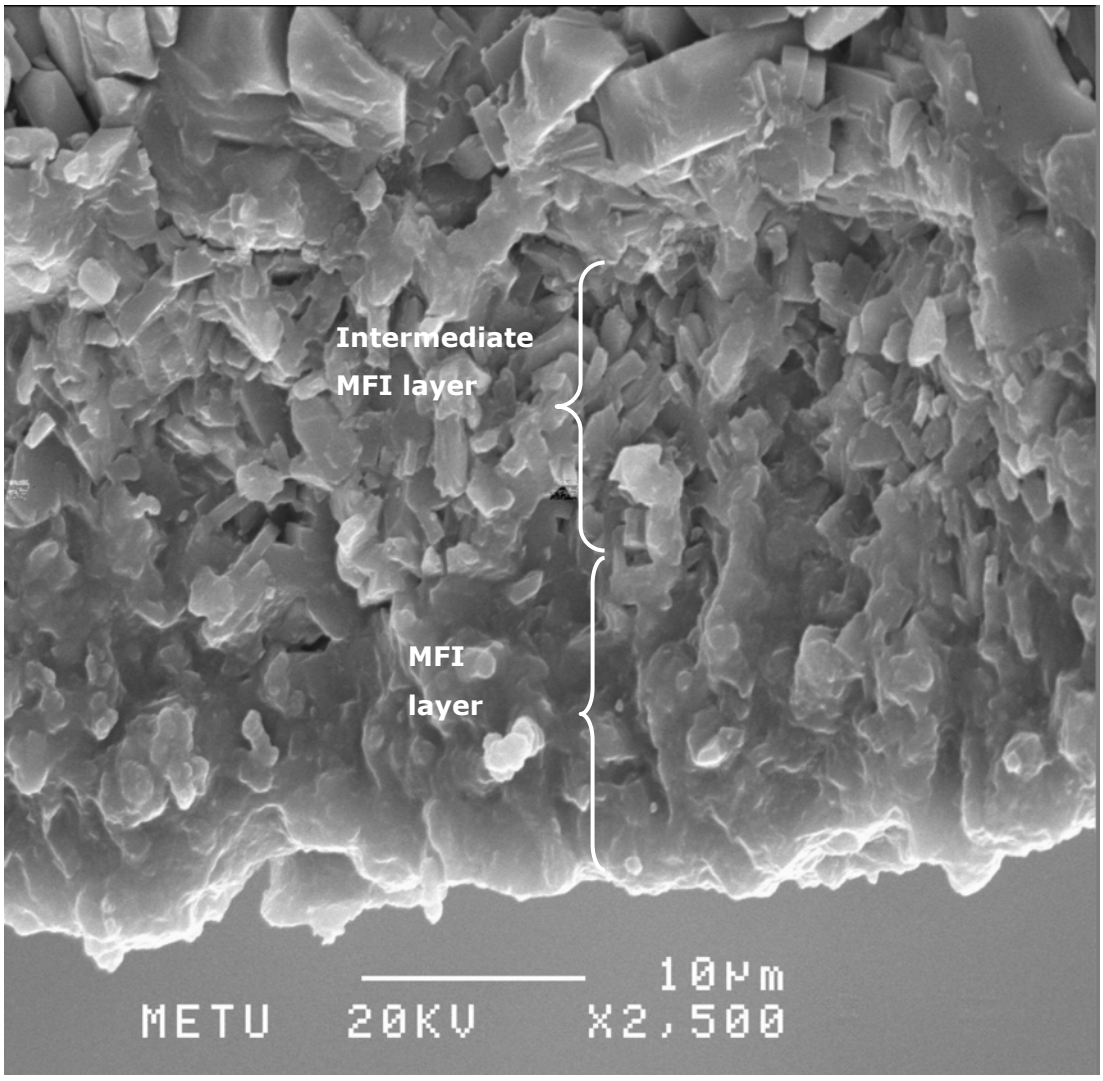

Figure 4.11 Cross-section image of membrane synthesized on support coated with 3.5 mg/cm^2 of seed [ED50a]

Figure 4.12 shows the effect of seed content on the thickness of the resultant membranes. Membrane and seed layer thicknesses shown in this figure were estimated from SEM images. Membrane thickness increased linearly with seed content of support. Membranes had similar thicknesses for the same seed contents. After secondary growth, the thickness of seed layer, 0.6 mg/cm^2 of seed, does not change much, indicating that the crystallization occurs among the seed crystals. On the other hand thickness of seed layer with 3.5 mg/cm^2 of seed increased significantly after hydrothermal synthesis and this indicates that crystallization occurred both among and above the seed crystals.

The reproducibility of membranes was investigated with SEM images. Figure 4.13 shows the cross-section and surface images of two membranes produced on supports coated with 0.6 mg/cm^2 of seed from a molar composition of C1 at 130^{o}C. Those membranes synthesized under the same synthesis conditions but from different batches. SEM images showed that membranes have similar morphology. The support surfaces are completely covered with twinned coffin shaped MFI crystals with particle size between 6 μm and 9 μm. Both membranes have nearly 9 μm thick uniform and dense MFI layers. Figure 4.12 also showed that membranes that were synthesized from different batches had similar thicknesses with the same amount of seed. Consequently, membrane synthesis was reproducible from the morphological point of view.

As observed during the synthesis of seed crystals, yield of the composition (C1) used for membrane synthesis is quite low. This is possibly the result of low nucleation rate [34]. As the number of nuclei formed in the synthesis solution is probably low, sufficient amount of crystals to cover the support surface has not formed from this composition so that continuous MFI layers cannot be obtained without seeding [43]. When synthesis performed on seeded supports, crystallization probably starts directly on the seed crystals which serve as nuclei [13,55]. Therefore voids among the seed crystals are filled during the hydrothermal synthesis and continuous MFI layers are obtained by secondary growth.

In literature zeolite layer growth mechanism is proposed as follows; at early stages of crystallization, an amorphous gel layer form on the support surface by

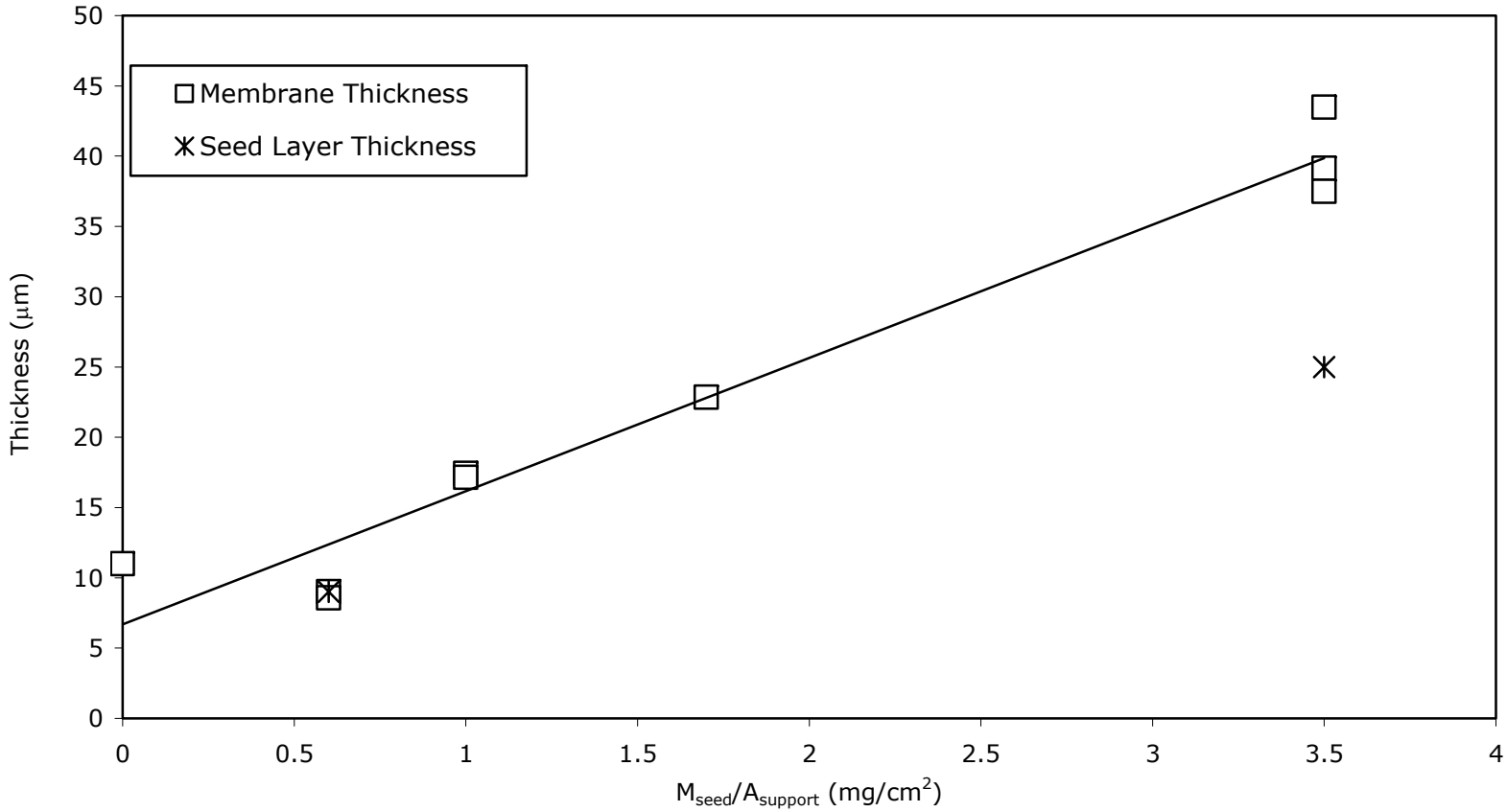

Figure 4.12 Change of membrane thickness with the amount of seed

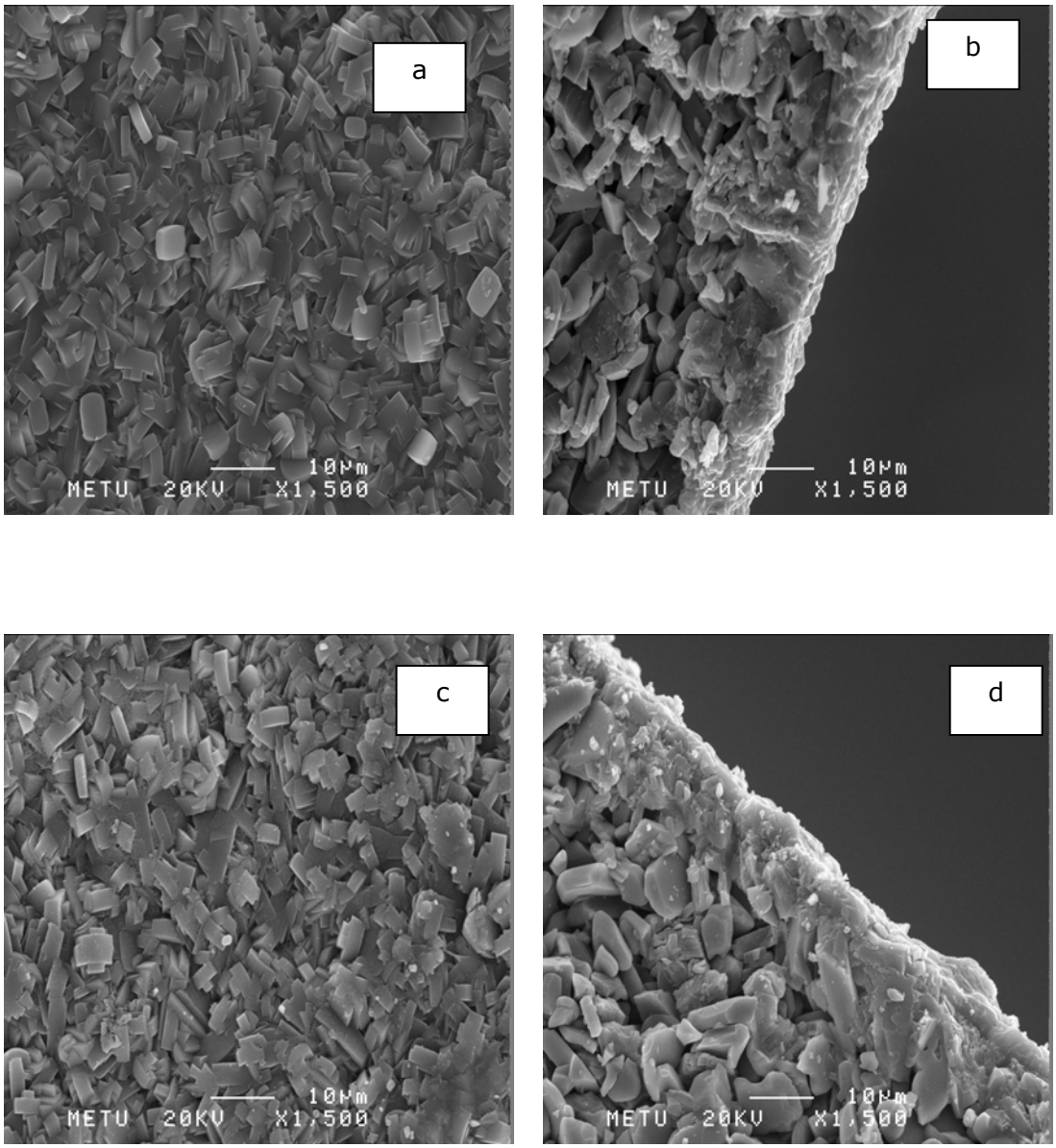

Figure 4.13 Surface and cross-section SEM images of membranes synthesized under the same synthesis conditions (a,b) ED74a (c,d) ED89u

the deposition of the primary gel particles, which are available in the clear synthesis solution [34,35]. Crystallization occurs in this amorphous gel layer and a continuous zeolite layer is obtained [40-42]. Based on this knowledge, one possible explanation for the formation of asymmetric MFI layer in this study is that small gel particles diffuse to the support material. Meanwhile seed layer acts as a filter so that the gel particles accumulate at the solution side of seed layer and form a continuous gel layer among those seed crystals and also above the seed crystals. The further motion of gel particles toward the support is hindered by this continuous gel layer. Therefore two layers were obtained; a top layer at the solution side where amorphous gel layer forms and crystallization occurs in it, an intermediate layer at the support side where gel layer do not form and seed crystals could not incorporate into secondary growth. When synthesis are performed on low amount of seed coated supports (thin seed layer) gel particles can penetrate through the seed layer to form a continuous gel layer among all seed crystals. Therefore continuous and uniform MFI layers can be obtained after secondary growth on the supports coated with low amount of seeds. Accordingly, increasing the seed layer thickness does not necessarily lead to the formation of thicker and uniform MFI layers because significant amount of the seed crystals remain on the support without participating into the secondary growth.

In conclusion using low amount of seed crystals lead to formation of compact and uniform MFI layers whereas continuous MFI layers cannot be obtained without seeding under the same synthesis conditions. Results also showed that increasing the seed amount led to formation of asymmetric MFI layers.

4.3.2 Thickness estimation by XRD patterns

Zeolite membranes usually have an asymmetric structure. Zeolite crystallizes both on the support surface and in the pores of the support [4]. Therefore it is difficult to find out exact thickness of a membrane from SEM images. Alternatively thickness of a membrane can be estimated by XRD patterns [5,16]. In this technique the peak intensities of support and zeolite can be related to the thickness of the zeolite layer. The thinner the zeolite layer is, the weaker the zeolite peak is and the stronger the alumina peak is [6].

Comparing thickness estimation by XRD and SEM, XRD is a non-destructive method, so that membranes can be used later whereas membranes cannot be used after analysis by SEM. XRD gives average thickness of a membrane whereas SEM shows the thickness along a fraction of a membrane. The MFI crystals in the support pores are also taken into account by XRD method. XRD is an indirect method but SEM is a direct method to measure the thickness. Geometry of membranes can be important for XRD analysis because XRD requires flat surfaces (crushed surfaces can also be analyzed by XRD but scattering of X-rays may cause weaker intensities) whereas membrane geometry is not important for SEM. In addition XRD method cannot be applied to very thin and very thick membranes, because zeolite peaks become very weak on thin membranes and support peaks very weak on thick membranes. Despite these disadvantages of XRD, nondestructive analysis by XRD provides a great advantage over SEM.

To estimate average membrane thickness by XRD, a calibration plot was prepared by using the XRD patterns of the seeded alumina discs. The alumina discs were coated with different amounts of seed crystals, between 1.4 mg and 36 mg of seed. The seed coated discs were not subjected to the hydrothermal synthesis. The thickness of seed layer that corresponds to specific amount of seed is calculated by equation 4.1;

$$\delta = \frac{M}{\left(r^2.\pi.\rho\right)\left(1-\phi\right)} \qquad 4.1$$

In this equation r is the radius of the alumina disc, ρ is the density of MFI zeolite (1.76 g/cm^3) [59] and δ is average thickness of the seed layer, ϕ is the void fraction (porosity) and 1-ϕ is the solid fraction throughout the seed layer. The porosity of seed layer is assumed as zero in thickness calculation.

The seed coated discs were then analyzed by XRD. From the XRD patterns, $I_{MFI}/(I_{MFI}+I_{alumina})$ ratio was calculated with MFI peak at 23^o Bragg angle and alumina peak at 35^o Bragg angle after purging the background intensity from the patterns. Those peaks are the strongest MFI and alumina peaks. The reason for

using the strongest peaks only is that when the membrane becomes either too thin or too thick, small peaks would weaken too much or even disappear.

The $I_{MFI}/(I_{MFI}+I_{alumina})$ ratio was related to the thickness of seed layer in Figure 4.14. To improve the accuracy, two discs containing the same amounts of seed were analyzed by XRD. They are shown on the figure with different symbols, namely (1) and (2). In addition, the seed layer thicknesses on two discs were determined by SEM, which are also shown in Figure 4.14.

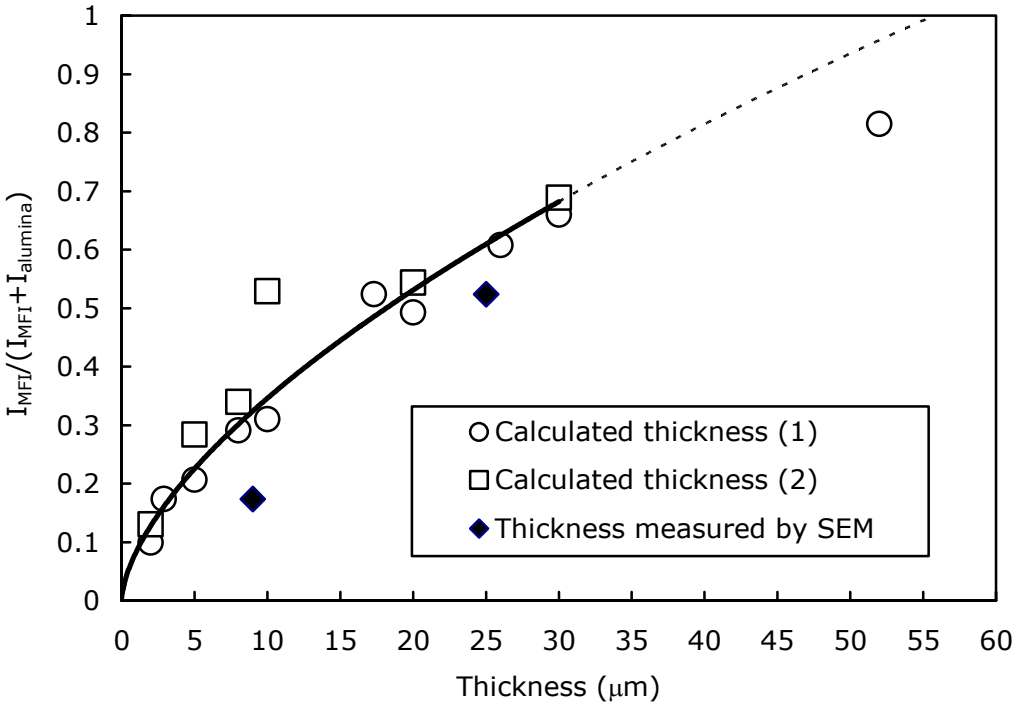

Figure 4.14 Plot for membrane thickness estimation by XRD patterns

The data given in Figure 4.14 shows that the $I_{MFI}/(I_{MFI}+I_{alumina})$ ratio increases with the seed layer thickness, and suggests that the alumina peak can no longer be seen if the thickness of seed layer is greater than about 50 μm. Therefore, this method cannot be applied for membranes thicker than 50 μm.

Seed layer thicknesses measured by SEM images are larger than the calculated thicknesses. The seed layer thicknesses have been calculated assuming that the seed layers are dense, although they are not as shown in Figure 4.5. The thickness calculated by Equation 4.1 would be larger if the porosity of seed layer

were known, so that the difference between measured and calculated thicknesses would be smaller.

The thickness of dense MFI layers (or membranes) can be estimated using Figure 4.14. The $I_{MFI}/(I_{MFI}+I_{alumina})$ ratio is expected to be greater for dense MFI layers than that for loose MFI layers, if both have the same thickness. Therefore, the thickness of dense MFI layers is estimated larger by XRD than the thickness of the layer measured by SEM.

Another reason for the difference between SEM and XRD thicknesses could be the seed crystals which have entered into the pores of alumina disc. XRD counts all the crystals in the disc and on the disc, therefore thickness estimated by XRD would be larger than the thickness measured by SEM if the amount of seed in support is significant.

Figure 4.14 was then used as calibration curve to estimate the MFI membrane thickness from the XRD patterns of the membranes. For this purpose, membranes were analyzed by XRD, and the $I_{MFI}/(I_{MFI}+I_{alumina})$ ratio was calculated. Using Figure 4.14 and the $I_{MFI}/(I_{MFI}+I_{alumina})$ ratio, thickness of the membrane was estimated.

Figure 4.15 shows the thicknesses of the membranes synthesized on alumina supports coated with different amounts of seed. The estimated thicknesses were also compared with the thicknesses measured from SEM images. The thicknesses determined by both methods differ slightly.

Membranes synthesized on bare supports do not have a uniform MFI layer (Figure 4.9), and layer thickness cannot be accurately measured from SEM images. For those membranes, XRD estimates the average thickness of MFI layer on the support assuming that the layer thickness is uniform throughout the surface, therefore XRD thickness cannot be compared with the SEM thickness fairly for the membranes prepared on bare supports.

For the membranes synthesized on the supports coated with low amount of seed, thickness estimated by XRD is greater than the SEM thickness; on the

other hand, at high amounts of seed, thickness estimated by XRD is smaller than the SEM thickness.

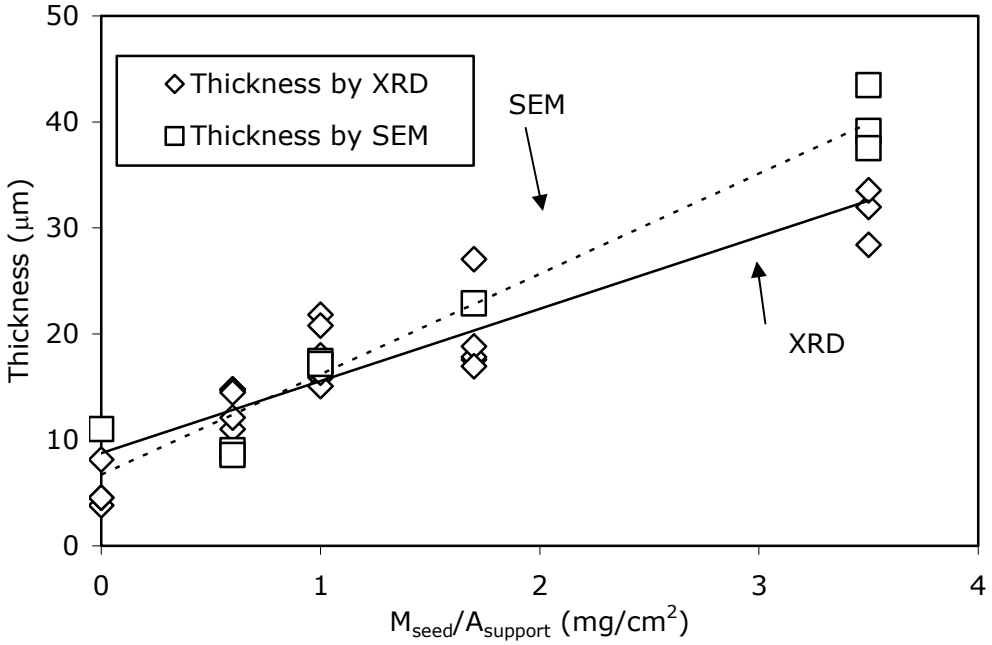

Figure 4.15 Thicknesses of the membranes estimated by XRD patterns and SEM images

At low amounts of seed, the MFI layer on the support is dense, and some MFI crystals may have formed in the support pores. Both dense MFI layers and the crystals in the support pores causes that Figure 4.14 estimates the thickness of dense MFI layers larger than the real thickness is. Therefore, the thickness estimated by XRD could be more than the thickness measured from SEM images for the membranes synthesized on supports coated with low amount of seed.

At very high amounts of seed, on the other hand, MFI membranes consist of a dense top layer and a loose intermediate layer after hydrothermal synthesis, as shown in Figure 4.11. If these two layers could be analyzed separately, Figure 4.14 would estimate dense layer thicker and loose layer thinner. As the membrane contains both types of MFI layers, thickness estimated by XRD depend which layer is dominant. Apparently, as the amount of seed on support increase, the loose MFI layer in the final membrane becomes more dominant,

therefore, the membranes were estimated thinner by XRD than by SEM at very high amounts of seed. Indeed, SEM images (Figure 4.9) showed that the thickness of loose MFI layer in the final membrane increases with the amount of seed on the support.

In conclusion, using XRD patterns is a promising method to estimate the membrane thickness in a non-destructive way, though the method needs further development to increase the accuracy and precision before applying this method to the membranes.

4.3.3 Effect of seeding on the MFI membrane growth

The course of membrane layer growth was followed on bare, 2 mg and 12 mg seeded alumina supports. The batch composition of was TPAOH: $9.80SiO_2$:$0.025Na_2O$:$0.019Al_2O_3$:$602.27H_2O$:$39.16C_2H_5OH$ (C1) and synthesis was carried out at 130^{o}C in autoclaves.

XRD patterns of 0.6 mg/cm^2 of seeded support and membranes synthesized on 0.6 mg/cm^2 of seeded supports at various crystallization times are shown in Figure 4.16. The alumina peak with highest intensity was marked by asterisk on the patterns. Seeded alumina support exhibits weak peak of MFI compared with the alumina peaks and after 4 h of synthesis, MFI peak increases indicating zeolite growth started at the early hours of crystallization. MFI peak increases significantly while alumina peak becomes smaller with synthesis time and after 47 h of synthesis MFI peak becomes stronger than alumina peak. All the XRD patterns exhibit increase in ($I_{MFI}/I_{alumina}$) ratio indicating growth of the MFI layer continued with synthesis time.

Figure 4.17 shows the SEM surface images of membranes synthesized on bare support for 7 h, 10 h, 15 h, 47 h and on 0.6 mg/cm^2 seeded supports for 15 h and 47 h of crystallization.

According to SEM surface images, membranes exhibited different morphological behavior with the presence of seed crystals at the same crystallization time. After 15 h of synthesis on seeded support, continuous MFI layer made up of

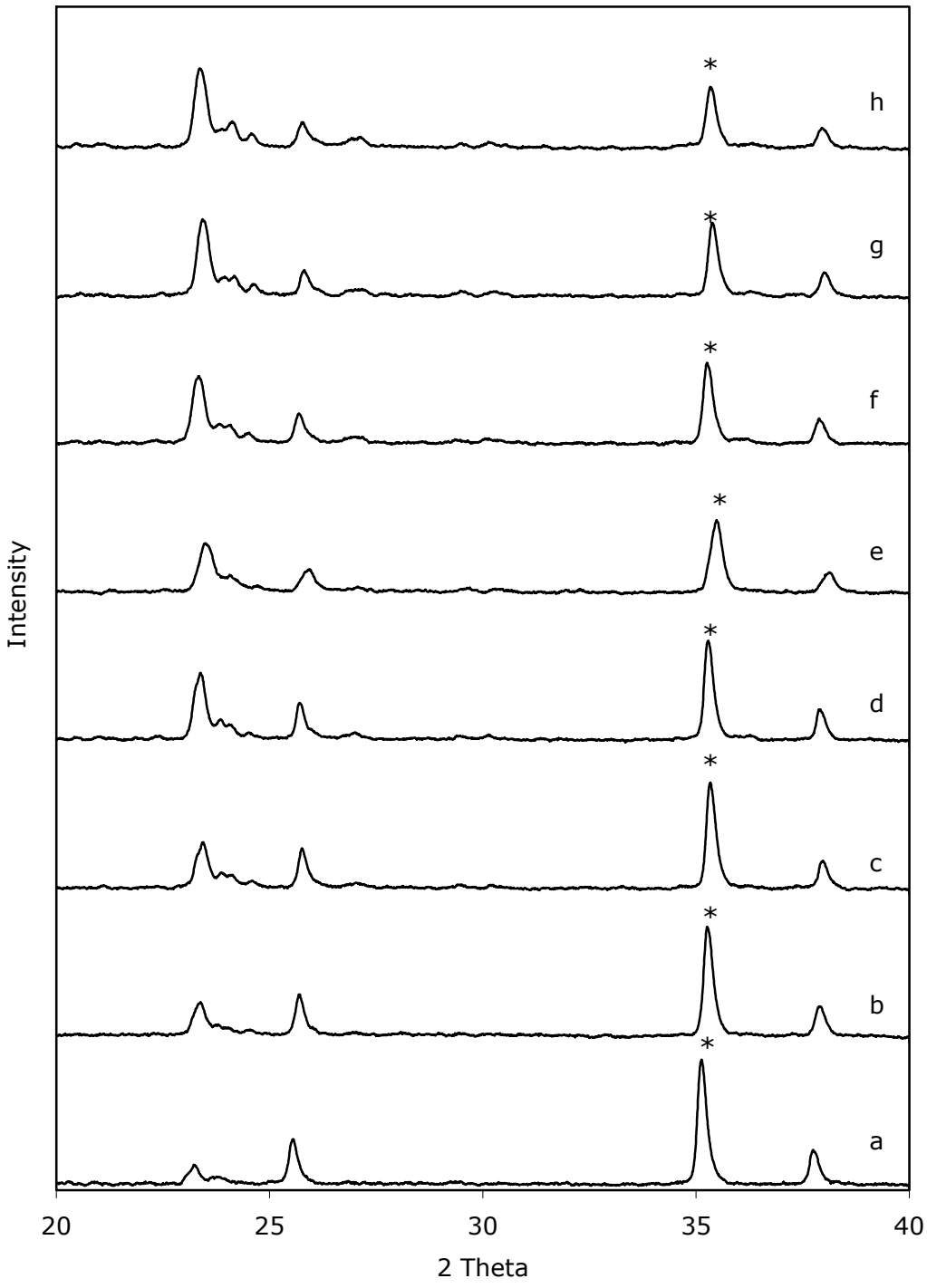

Figure 4.16 XRD patterns of membranes synthesized on supports coated with 0.6 mg/cm^2 of seed at various times of crystallization (a) 0 h (b) 4 h (c) 8 h (d)15 h (e) 20 h (f) 25 h (g) 36 h (h) 47 h (* alumina peak)

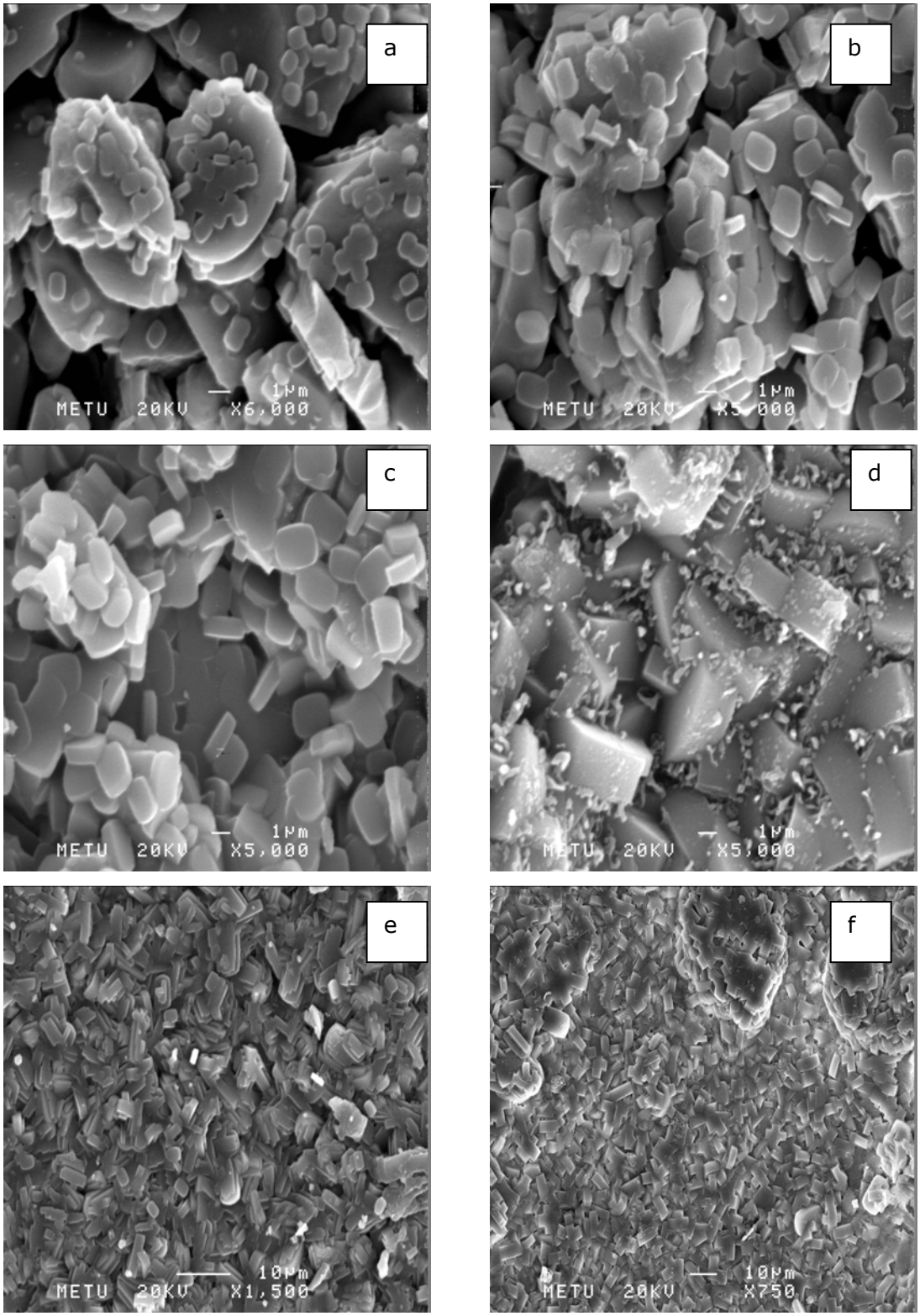

Figure 4.17 Surface SEM images of membranes synthesized in various synthesis time (t) unseeded (a) t:7 h [ED92u] (b) t:10 h [ED93u] (c) t:15 h [ED77u] (d) t:47 h [ED80u] 0.6 mg/cm^2 of seed (e) t:15 h [ED87u] (f) t:47 h [ED90u]

twinned coffin shaped crystals with particle size between 6 μm and 9 μm was formed (Fig 4.17.e). On the other hand, syntheses on bare support in 7 h, 10 h and 15 h showed that MFI crystals were grown on the alumina particles without forming a MFI layer. The MFI crystals were in coffin shape with particle between 0.5 μm and 1 μm after 7 h of synthesis and increased to 2 μm and 3 μm after 10 and 15 hours of crystallization, respectively. There are large voids between the crystals and the surface coverage is very poor. After 47 h of synthesis, continuous MFI layers formed on both bare and seeded supports. The particle size of the crystals forming the MFI layer was between 6 μm and 9 μm.

Cross-section images of membranes synthesized at different synthesis times with 0.6 mg/cm^2 of seed and support coated with 0.6 mg/cm^2 of seed are shown in Figure 4.18. The support with 0.6 mg/cm^2 of seed has a uniform seed layer with thickness of 9 μm. However, after 15 h of synthesis, about 7 μm thick uniform and continuous MFI layer formed on the seeded support. With the increase in synthesis time the MFI layers become denser. Thicknesses of the membranes are 9 μm and 13 μm after 24 and 47 hours of crystallization, respectively. Thus membrane thickness synthesized on seeded support did not change much after 24 h of synthesis.

In contrast, without seeding MFI layer did not form after 15 h of crystallization (Figure 4.19). A non-uniform MFI layer formed after 24 h and its thickness changed between 9 μm and 13 μm. After 47 h of crystallization 10 μm thick continuous and uniform MFI layer was obtained, so that increasing the synthesis time to 47 h resulted in uniform MFI layer without seeding.

Comparing the membranes synthesized on bare and seed coated supports, continuous MFI layer obtained in a shorter synthesis time with seeding and highly intergrown and denser layers formed on seed coated supports. These results were in agreement with results of Lai and Gavalas [43]. They observed that seeding increased reaction rate of continuous ZSM-5 membranes formation and lead to form continuous ZSM-5 layers.

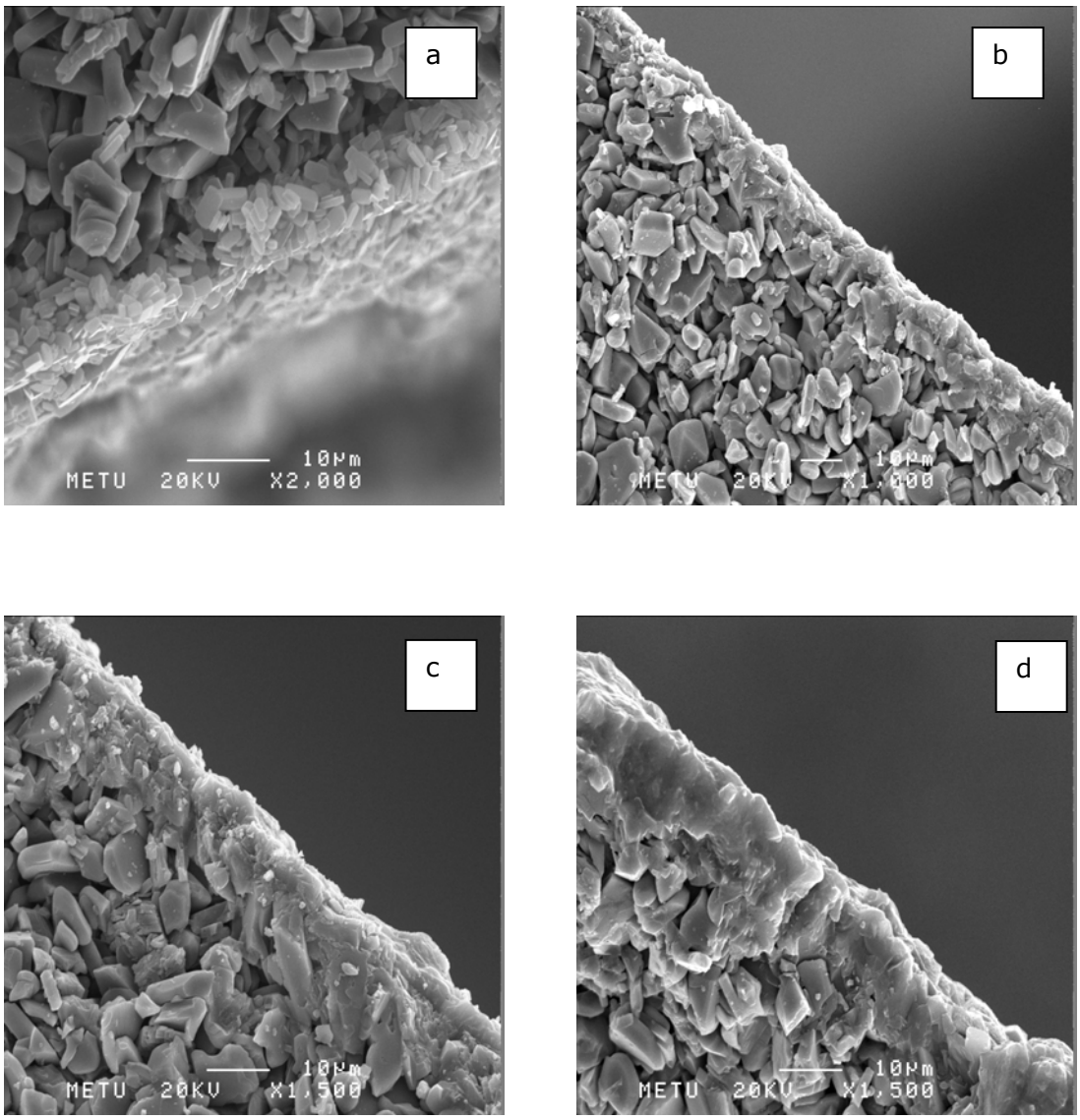

Figure 4.18 Cross-section SEM images of (a) support coated with 0.6 mg/cm^2 of seed (b) membranes synthesized on supports coated with 0.6 mg/cm^2 of seed for 15 h [ED87u] (c) for 24 h [ED89u] (d) for 47 h [ED90u]

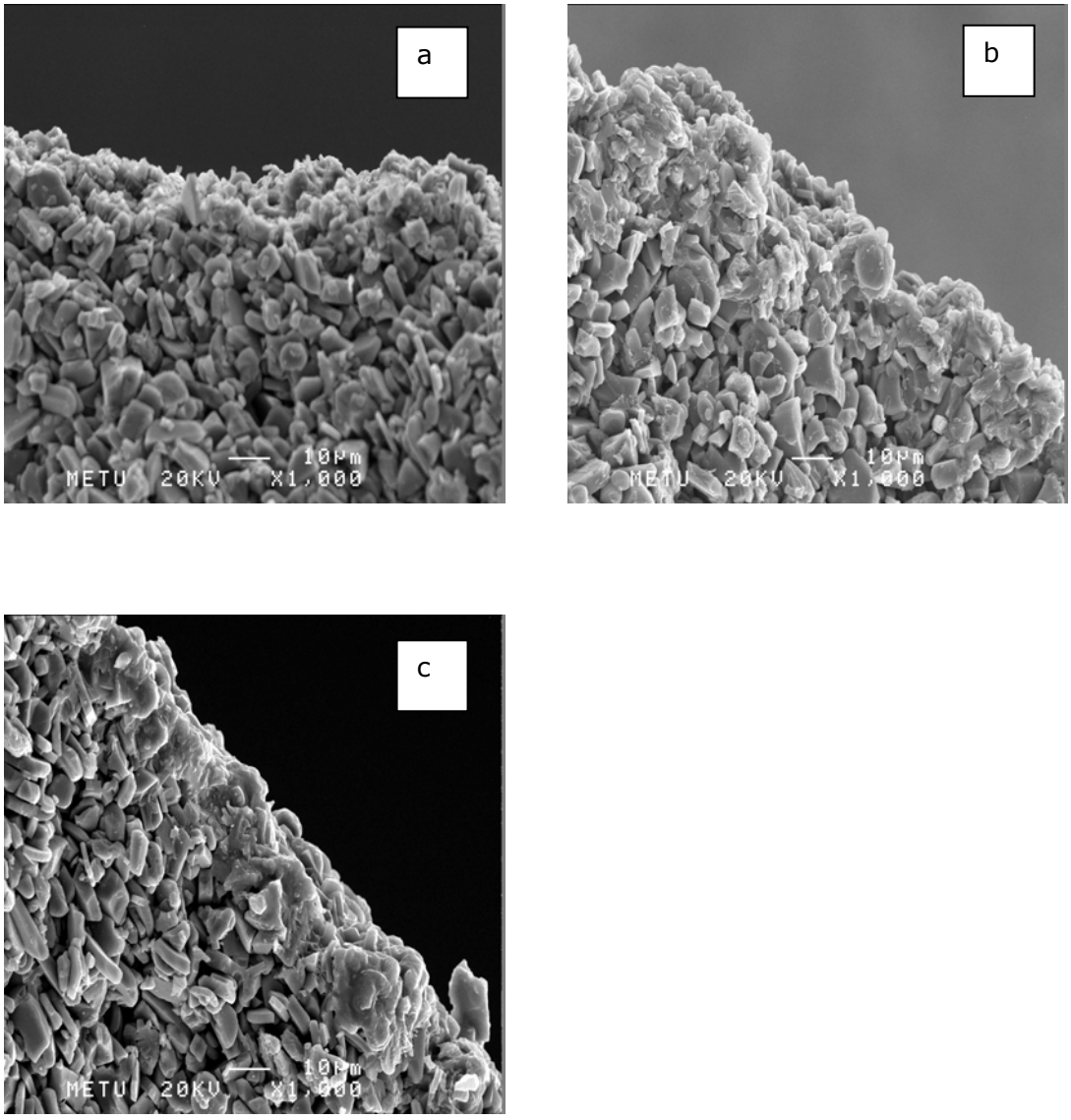

Figure 4.19 Cross-section SEM images of membrane synthesized on bare support (a) for 15 h [ED77u] (b) 24 h [ED79u] (c) for 47 h [ED80u]

The growth of MFI layers was also followed with XRD patterns and the results are shown on Figure 4.20. These membranes were synthesized on bare, 0.6 and 3.5 mg/cm^2 seeded supports at various times of crystallization. In order to collect data for specific time intervals, two set of experiments were performed for each amount of seed and data obtained from different batches are shown on the graph with full and open symbols. Consistent data were obtained from different batches for both unseeded and seeded systems. The growth of MFI layer exhibited typical S-shaped curve in unseeded system indicating the layer growth started with nucleation period and followed by crystal growth [5,56]. When seed crystals are used crystal growth rate increased and a nucleation period is not observed indicating that crystallization starts directly on seed crystals [13,55].

Figure 4.21 shows the N_2 permeances of those membranes before calcination. N_2 permeance before calcination shows the quality of the surface coverage. As the MFI pores are filled with template molecules during hydrothermal synthesis a membrane with continuous coverage and less non-zeolitic pores should be impermeable to N_2 before calcination [10].

Increase of $I_{MFI}/(I_{MFI}+I_{Alumina})$ ratio in unseeded system shows the increase in surface coverage with synthesis time, as in agreement with SEM images, but N_2 permeances, as membranes never become impermeable, indicate that MFI layers are not continuous and contains large non-zeolitic pores. When membranes synthesized on supports with 0.6 mg/cm^2 of seed, up to 20 h of synthesis, increase of $I_{MFI}/(I_{MFI}+I_{Alumina})$ ratio indicates the increase of MFI layer thickness as well as the crystallization of MFI crystals in support pores, on and among the seed crystals, however, those membranes are permeable to N_2 indicating that they are not continuous. After that synthesis time, membranes become impermeable so that they are continuous and compact, without non-zeolitic pores but SEM images show that thickness do not change much, therefore increase of $I_{MFI}/(I_{MFI}+I_{Alumina})$ ratio is likely the result of crystallization in support pores. With 3.5 mg/cm^2 of seed, $I_{MFI}/(I_{MFI}+I_{Alumina})$ ratio increases up to 8 h of synthesis and remains almost constant after that time. However, membranes are permeable up to 24 h of synthesis, then compactness of MFI layers increased with synthesis time. Therefore after 24 h of synthesis membranes have less non-zeolitic pores.

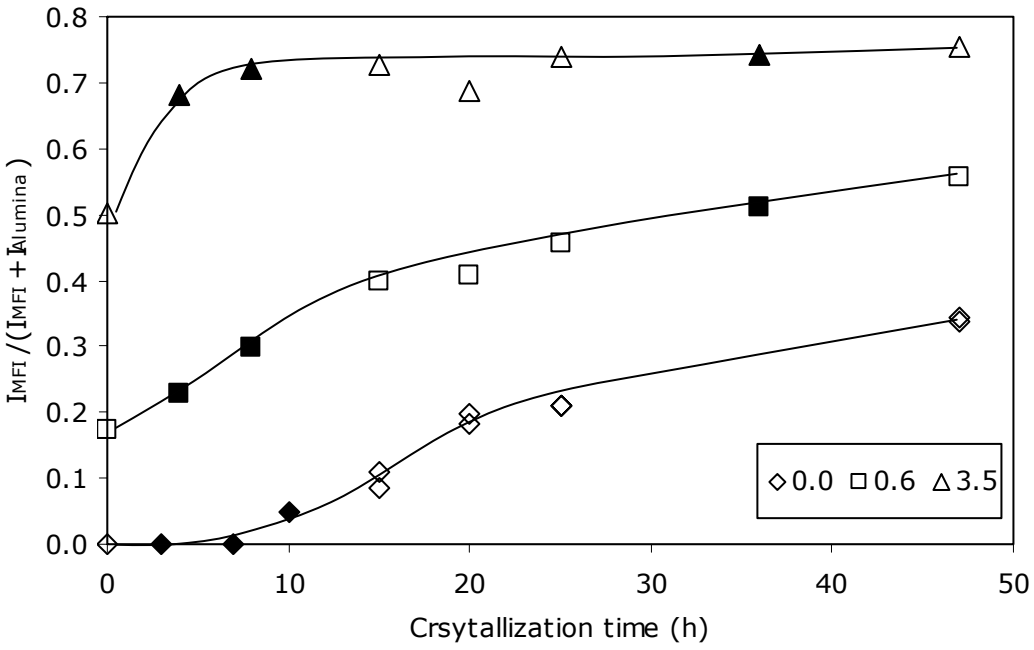

Figure 4.20 Growth of membranes synthesized on variable amount seeded support in various times of crystallization (symbols show amount of seed in mg/cm^2)

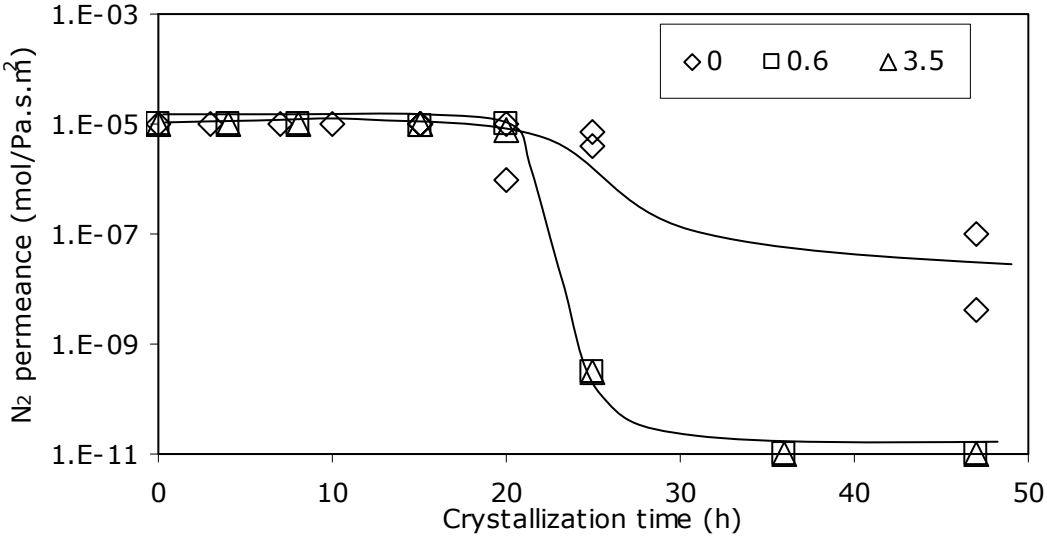

Figure 4.21 N_2 permeance of uncalcined membranes synthesized on variable amount seeded supports in various times of crystallization (symbols show amount of seed in mg/cm^2)

In conclusion, the presence of seed layer increased the growth rate of MFI layer and improved the membrane quality by increasing the intergrowth of the MFI layer with less non-zeolitic pores.

4.4 Single gas permeation through uncalcined membranes

Template molecules can block small non-zeolitic pores as well as MFI pores during synthesis [57]. Therefore N_2 may permeate through only large non-zeolitic pores before calcination. For this reason, N_2 permeances were measured through the membranes before calcination. When N_2 permeance of a membrane is equal to 10^{-10} mol/Pa.s.m^2, N_2 flows so slowly that permeation of 10 ml of gas takes about 47 hours to pass through the membrane. Such a low permeance through non-zeolitic pores is expected to have little effect on the permeances after calcination. Therefore, membranes with N_2 permeance of less than 10^{-10} mol/Pa.s.m^2 were assumed to be impermeable and nearly defect-free.

The percentage of impermeable membranes synthesized on supports coated with different amount of seed is shown in Table 4.4. All membranes were obtained at 130^{o}C after 24 h of synthesis.

Table 4.4 Percentage of impermeable membranes synthesized on variable amount of seed coated supports

# of synthesized membranes	$M_{seed}/A_{support}$ (mg/cm^2)	# of impermeable membranes	% impermeable membranes
2	0.0	0	0
16	0.6	11	69
14	1.0	10	71
9	1.7	7	78

As expected, none of the membranes synthesized on bare supports was impermeable to N_2, SEM images have already shown that there is no continuous MFI layer in these membranes and this may be due to low yield of the

composition used in this study because it probably does not produce enough crystals to form a continuous layer. On the other hand 72% of the membranes synthesized with seeding were impermeable before calcination. These results suggest that membranes prepared with seeding have only few defects. Seeding has strong effect not only on the morphology but also on the gas permeation properties of membranes.

4.5 Effect of amount of seed on membrane quality determined by single gas permeation

Usually N_2 and SF_6 or n-butane and isobutane permeances are used to determine the quality of MFI type membranes [4,5,9,10,16,48,49]. In this study N_2/SF_6 ideal selectivity is selected as quality criterion. Membranes with N_2/SF_6 ideal selectivity of higher than 40 at room temperature are considered to be good quality.

From separation points of view, reproducibility is a substantial problem in the synthesis of zeolite membranes and data reported on the reproducibility are limited in literature [5,26,27]. In this study reproducibility of membrane syntheses is evaluated based on this quality criterion.

Figure 4.22 shows the N_2/SF_6 ideal selectivities versus N_2 permeances of 34 membranes synthesized with different amount of seed on a log-log scale graph. The amount of seed on the support and percentage of membranes satisfying quality criterion are shown in Table 4.5.

Figure 4.22 shows that three of four membranes synthesized on bare support had N_2/SF_6 ideal selectivity of 2, which is below Knudsen selectivity of 2.28. This result indicates that there are defects within the MFI layer. This is also shown by SEM images with no continuous MFI layer on the bare support after hydrothermal synthesis (Section 4.3.1) and high N_2 permeances before calcination. Only one membrane which was synthesized on bare support after 47 h of crystallization had N_2/SF_6 selectivity of 28, which is higher than the Knudsen selectivity, although it was permeable to N_2 before calcination. As a result of

increasing the synthesis time a continuous MFI layer was obtained on bare support (Figure 4.19).

Table 4.5 Membranes which synthesized on supports coated with different amounts of seed, satisfying quality criterion. Synthesis composition: C1, Synthesis temperature: 130°C, Time: 24 h

# impermeable membranes	$M_{seed}/A_{support}$ (mg/cm^2)	% number of membranes satisfied quality criterion
0	0.0	0
10	0.6	60
9	1.0	67
7	1.7	28
2	3.5	_
2	6.9	_

Membranes synthesized with 0.6, 1.0 and 1.7 mg/cm^2 of seed exhibited N_2 permeance between $1x10^{-6}$ and $3x10^{-7}$ (mol/Pa.s.m^2) and showed N_2/SF_6 ideal selectivity between 1 and 282. Those membranes exhibited similar N_2 permeances. The N_2/SF_6 ideal selectivity which is taken as an indication of membrane quality is affected with the amount of seed. About 60% and 67% of the membranes synthesized with 0.6 and 1.0 mg/cm^2 of seed satisfied the quality criterion, respectively (Table 4.5). But this value decreased to 28% (2 of 7 membrane) with 1.7 mg/cm^2 of seed. On the other hand, with the use of 3.5 mg/cm^2 seeded support, one of two membranes satisfied the quality criterion and the other showed selectivity below Knudsen selectivity. Similar results were obtained through membranes synthesized on 6.9 mg/cm^2 of seeded supports.

Decrease in the number of membranes satisfying quality criterion can be the result of membrane morphology. By using low amount of seed crystals, 0.6 and 1.0 mg/cm^2 of seed, compact and thinner membranes were obtained and 12 of

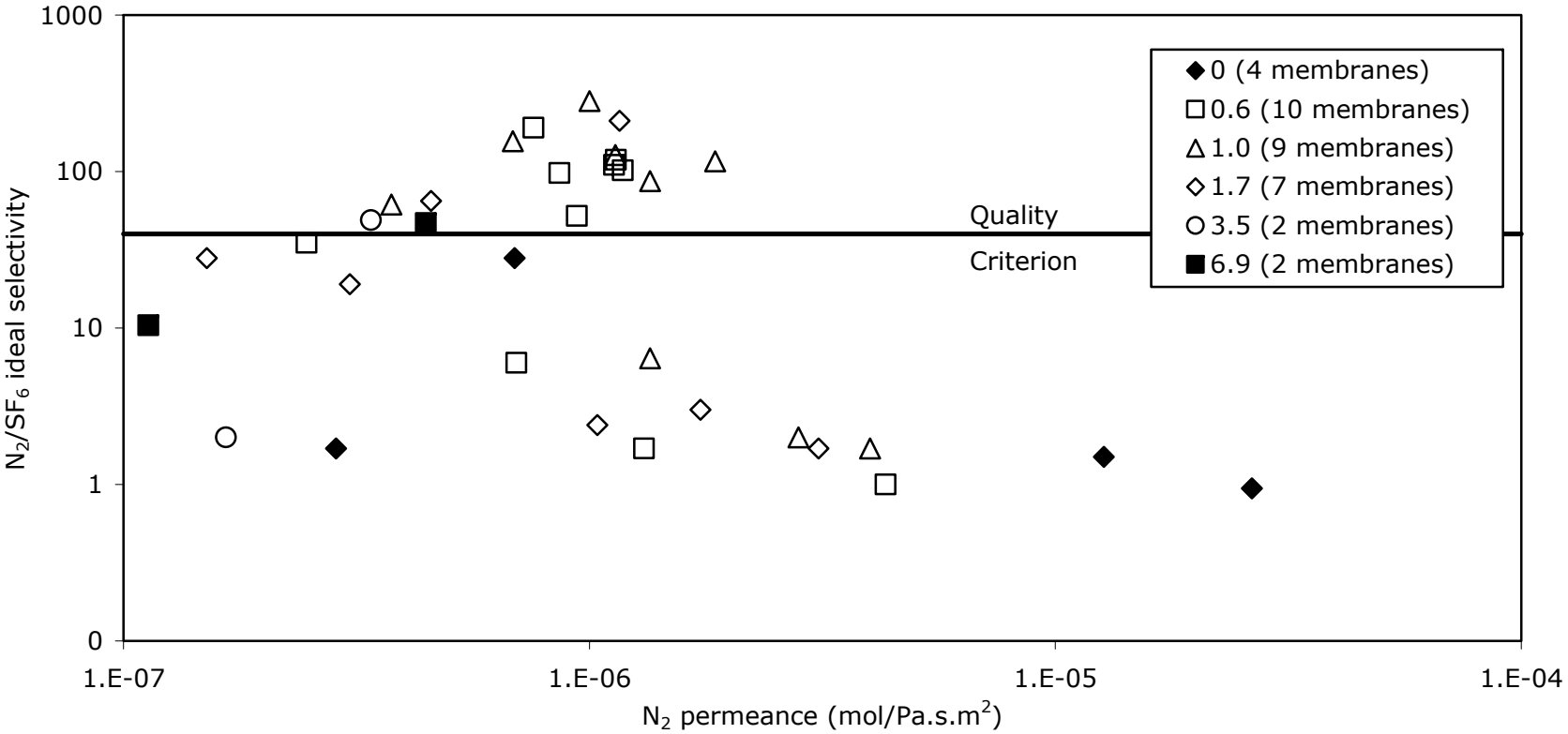

Figure 4.22 Single gas permeances of N_2 and SF_6 through membranes synthesized on variable amount of seed coated supports (symbols show amount of seed in mg/cm^2 and number of membranes)

19 membranes satisfied our quality criterion indicating MFI layers without interzeolitic pores had been synthesized reproducibly. This may be result of appropriate seed layer thickness and good packing of the seed layer obtained by vacuum seeding. However, by increasing the amount of seed to 1.7 mg/cm^2 of seed, a loose intermediate layer was observed by SEM images and only 2 of 7 membranes satisfied the quality criterion. Increasing the seed layer thickness may decrease the packing density of seed layer, therefore big gaps among the seed crystals may form and this may decrease the membrane quality by forming less dense MFI layers including non-zeolitic pores. As Lovolla et al. [18] stated seed layer thickness should have a sufficient thickness to completely cover the support surface but increasing the seed layer thickness may be result in peeling or cracking through seed layer and this may decrease the quality of the membrane. They concluded that thin, closely packed and smooth layer seed crystals enhanced the reproducibility of the membrane synthesis. Consequently increasing amount of seed may have negative impact on the membrane quality.

As a result good quality membranes with less non-zeolitic pores can be obtained with low amount of seed crystals. Increasing the amount of seed lowers the quality of membranes, thus amount of seed affects the quality of membrane.

The N_2 permeances and N_2/SF_6 ideal selectivities of good quality membranes obtained in this study were compared with the literature in Figure 4.23 (see Appendix I). This graph was plotted on a logarithmic scale. Membranes synthesized with and without seeding are shown on the graph by full and open symbols, respectively.

The data taken from literature exhibit a wide distribution such as N_2 permeance changes between $1x10^{-9}$ mol/Pa.s.m^2 and $1x10^{-5}$ mol/Pa.s.m^2 and N_2/SF_6 ideal selectivity values change between 3.7 and 2000. The highest permeance is reported as $1x10^{-5}$ mol/Pa.s.m^2, this was measured from a membrane synthesized on seeded support with a special pore masking method, therefore membranes exhibited high permeances due to thin zeolite layer (500 nm) and open support pores [14]. The N_2 permeances of the other seeded membranes are similar with the membranes synthesized without seeding although the seeded membranes have thin MFI layers. On the other hand the selectivities of

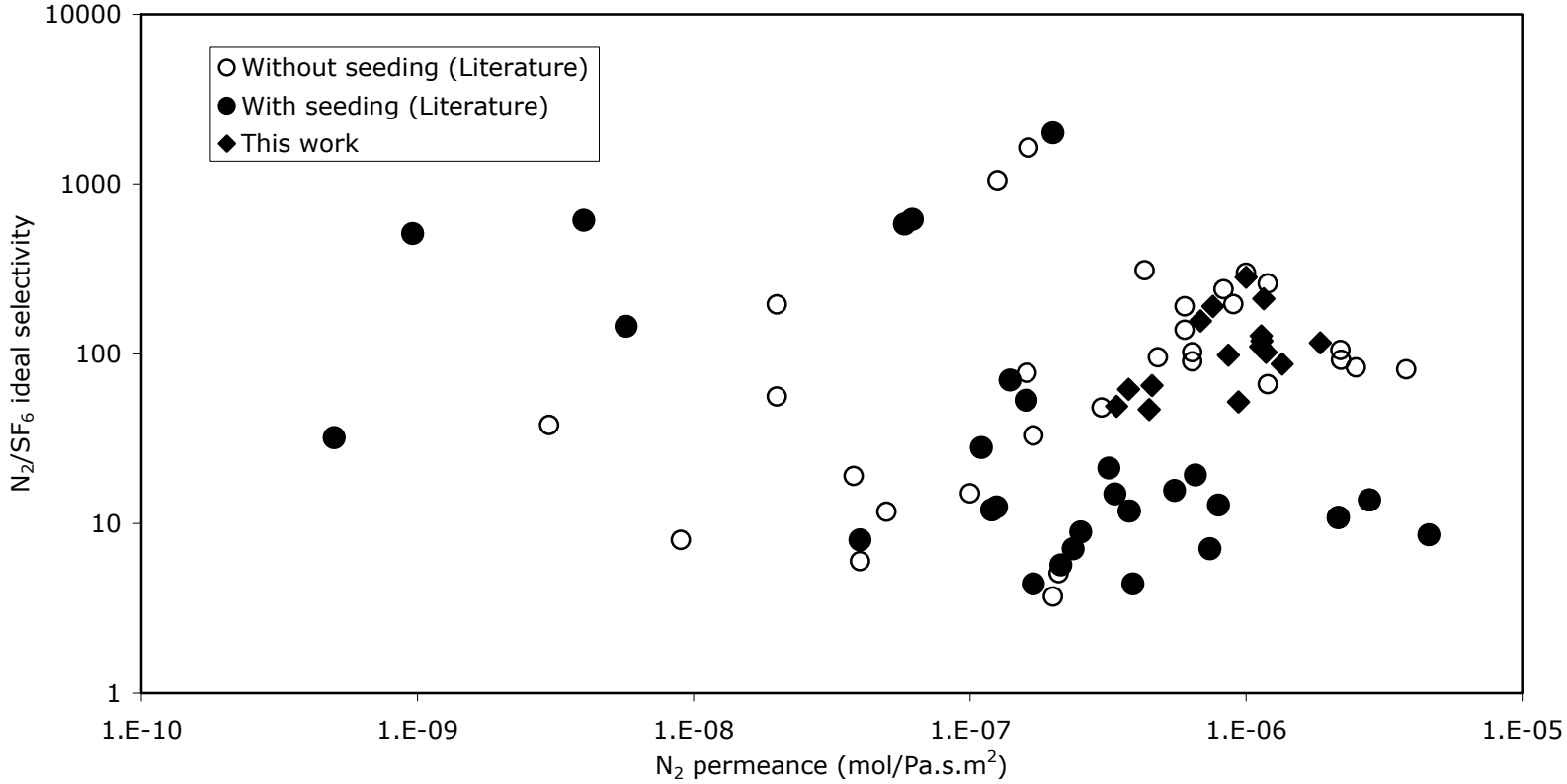

Figure 4.23 Comparison of single gas permeance of good quality membranes with literature

seeded membranes are lower than the unseeded membranes. Low selectivities may caused by thin MFI layers. But those thin layers usually contain large amount of small crystals which means that there are large amounts of grain boundaries. Since grain boundaries act as diffusion barriers, permeances of the thin and thick layers are similar with each other [28,55].

Our membranes which were synthesized by seeding had comparable N_2 permeances and N_2/SF_6 ideal selectivities with the membranes synthesized without seeding. The membranes synthesized in this study composed of larger crystals and had thicker MFI layers compared to membranes synthesized with seeding in literature. Therefore higher selectivities and comparable permeances can be result of the thickness and low amount of grain boundaries. Consequently, good quality membranes having comparable N_2 permeances and N_2/SF_6 ideal selectivities with the unseeded membranes reported in literature obtained by seeding in this study.

The percentage of membranes satisfying quality criterion is compared with literature in Table 4.6. Reported results showed that percentage of MFI membranes satisfying quality criterion is quite low. Van de Graaf et al. [9] used n-butane/isobutane ideal selectivity higher than 10 as a quality criterion and he confirmed that 8 of 12 membranes failed according to their quality criterion without an obvious cause. Noack et al. [17] used H_2/SF_6 ideal selectivity higher than 43 as a quality criterion. They obtained about 70% yield in membrane preparation by varying the synthesis composition and conditions systematically. Based on these data from literature, it can be said that our membrane synthesis procedure yields mostly high quality membranes and also percentage of membranes satisfying quality criterion is comparable with literature.

Table 4.6 Comparison of percentage of membranes satisfying quality criterion with the literature

Reference	Quality Criterion Ideal selectivity	% of membranes satisfying quality criterion
van de Graaf et al. [9]	$n\text{-}C_4H_{10}/i\text{-}C_4H_{10}$ >10	33
Noack et al. [17]	H_2/SF_6>45	70
Kalıpçılar et al [5]	N_2/SF_6>80	30
Li et al. [19]	$H_2/n\text{-}C_4H_{10}$>27	50
This work (0.6)*	N_2/SF_6>40	60
This work (1.0)*	N_2/SF_6>40	67
This work (1.7)*	N_2/SF_6>40	28

* amount of seed in mg/cm^2

4.6 Separation of butane isomers through membranes synthesized on variable amount seeded supports

A mixture of 50/50 n-butane and isobutane was separated by high quality membranes at temperatures 25°C, 50°C, 100°C and 150°C. Single gas permeances of these gases were also measured at the same temperatures. Three membranes (M1, M2, M3) which exhibited N_2/SF_6 ideal selectivities of 119, 87 and 211 were selected for separation of butane isomers (Table 4.7).

Table 4.7 N_2 permeances and N_2/SF_6 ideal selectivities of membranes used for separation of butane isomers. Synthesis composition: C1, Synthesis temperature: 130°C, Time: 24 h

Sample code	$M_{Seed}/A_{support}$ (mg/cm^2)	Membrane thickness (μm)	N_2 permeance ($mol/Pa.s.m^2$)	N_2/SF_6 ideal selectivity
M1	0.6	9	$1.2x10^{-6}$	119
M2	1.0	17	$1.4x10^{-6}$	87
M3	1.7	23	$1.3x10^{-6}$	211

Figure 4.24 and Figure 4.25 show single gas permeances of n-butane and isobutane and n-butane/isobutane ideal selectivity, respectively. The n-butane and isobutane permeances are similar at room temperature, but n-butane permeance increased significantly with temperature while isobutane permeance showed a slight increase. Ideal selectivities which were around 1.5 at room temperature, increased significantly with temperature for both membranes, and passed through a maxima at 100^{o}C for the membrane M3.

Figure 4.26 and Figure 4.27 show steady state permeances and separation selectivities (Unsteady state data is in Appendix L). All membranes exhibited similar permeation behavior, n-butane and isobutane permeances increased with temperature and at each temperature n-butane permeated considerably faster than isobutane. Separation selectivities of membranes M1, M2 and M3 were 14, 5 and 27, respectively at room temperature and passed through maxima around 50^{o}C.

As butane isomers are strongly adsorbing gases their permeation behavior through MFI layers is influenced by diffusion and adsorption in MFI pores. At low temperatures, where adsorption is significant, permeances of both gases are low. At higher temperatures adsorption coverage of n-butane decreases and diffusivity increases therefore permeance increases. On the other hand isobutane permeance increases slightly with temperature.

In mixture separation, the molecule which is adsorbed more strongly hinders the permeance of the other molecule. Thus separation is achieved by pore blocking effect of the strongly adsorbing molecule. For butane isomers, it is reported that n-butane adsorbs about 1.5 times stronger than isobutane so that it blocks the permeance of isobutane [57]. Pore blocking decreases with temperature as adsorption is exothermic and fewer molecules adsorb at higher temperatures. Up to a certain temperature pore blocking decreases slightly while the diffusivity of gases increases therefore maxima in the selectivity is observed. As in agreement with those, our membranes exhibited increase in n-butane permeance with temperature for both single and binary gases, on the other hand increase of isobutane permeance is less compared to n-butane. In mixture separation,

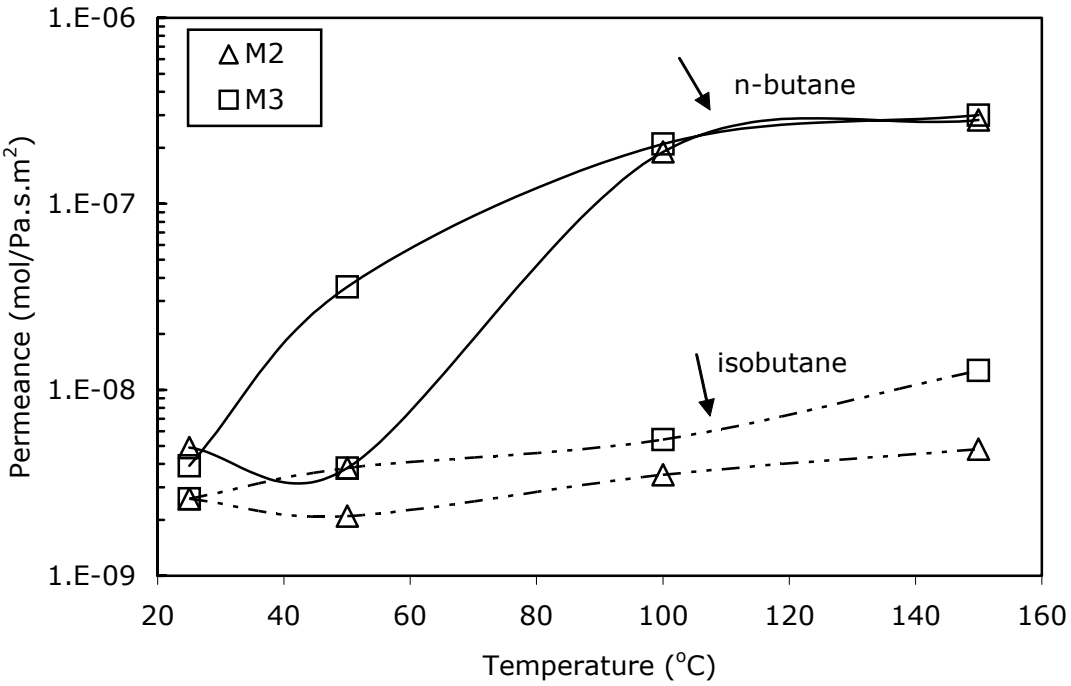

Figure 4.24 Single gas permeances of n-butane and isobutane through membranes M2 and M3 as a function of temperature Solid lines: n-butane permeance Dashed lines: isobutane permeance

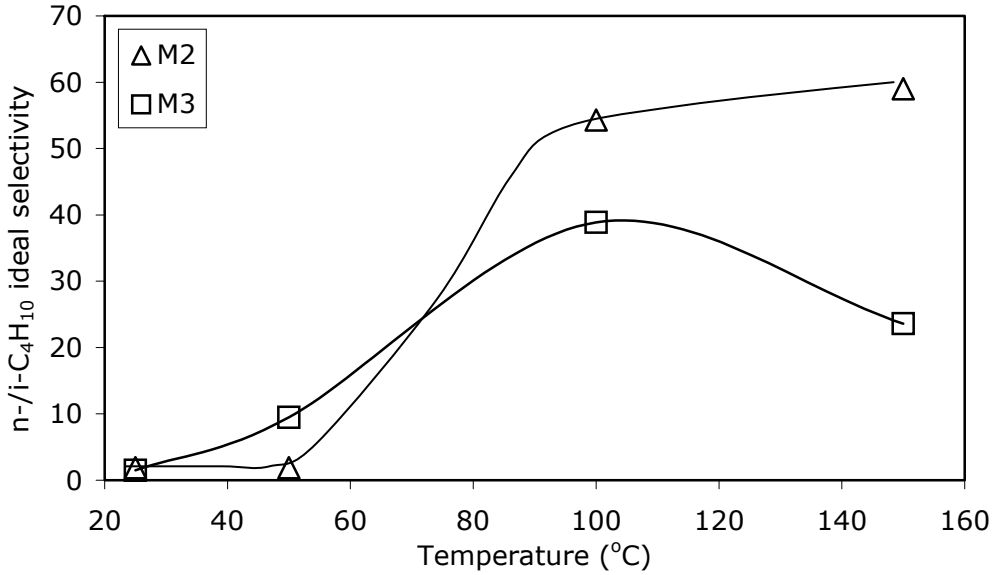

Figure 4.25 n-butane/isobutane ideal selectivities through membranes M2 and M3 as a function of temperature

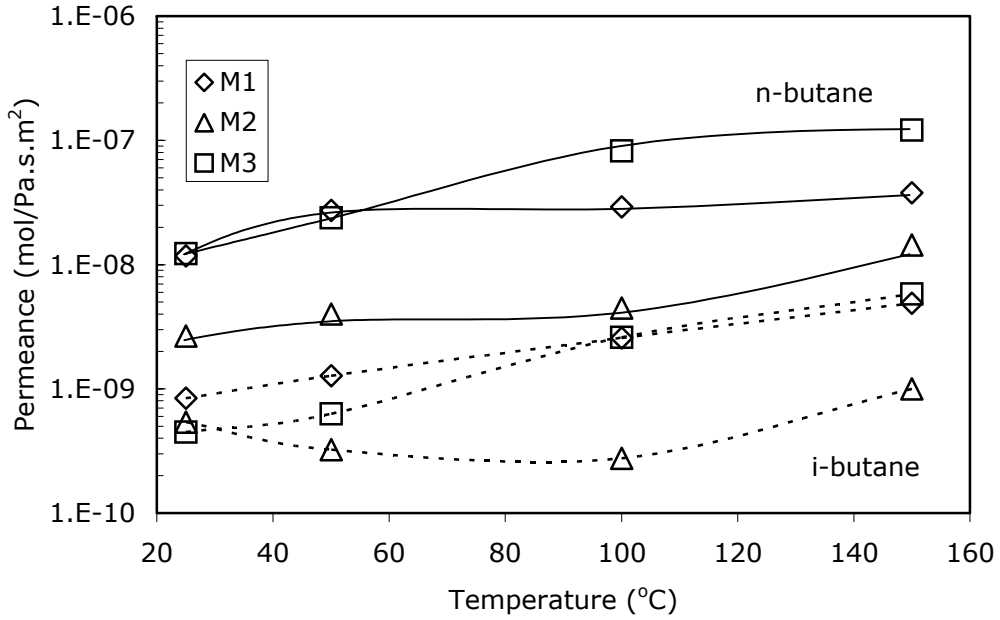

Figure 4.26 Mixture permeances for 50/50 n-butane/isobutane through membranes M1, M2 and M3 as a function of temperature. Solid lines: n-butane permeance, Dashed lines: isobutane permeance

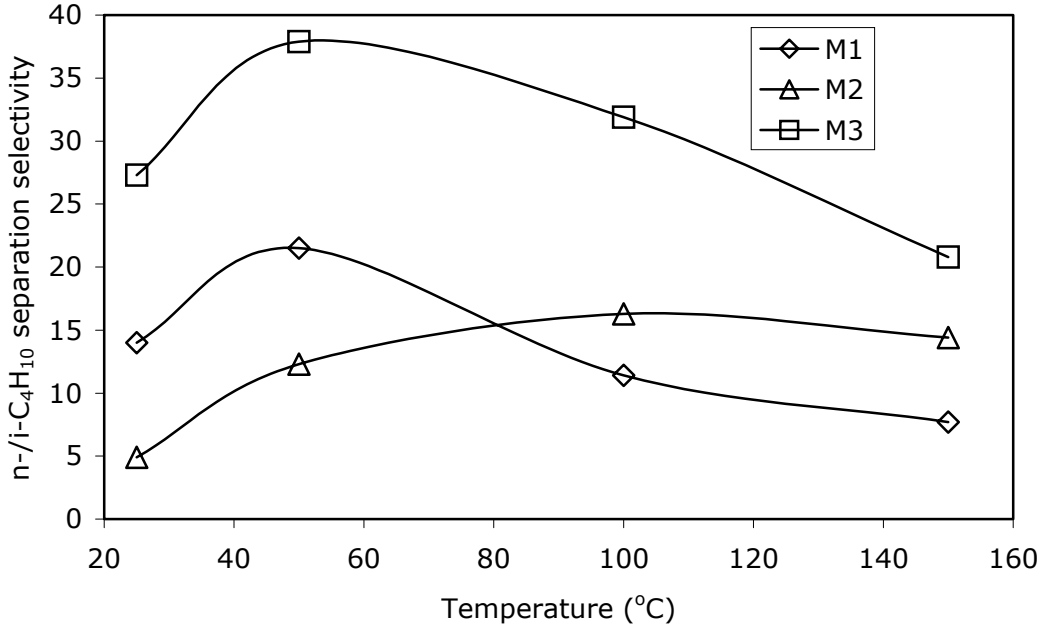

Figure 4.27 Separation selectivites for 50/50 n-butane/isobutane mixture through membranes M1, M2 and M3 as a function of temperature

n-butane permeance is higher than isobutane which can be the result of pore blocking effect of n-butane. For both single and binary gases, selectivities showed maxima, this is probably caused by the slight decrease in adsorption and increase of diffusivities.

Membrane thickness has a pronounced effect on the selectivity when separation is based on adsorption [57]. Table 4.8 shows data form literature and this work for separation of butane isomers. Synthesis temperatures are also given in Table 4.8 because thicker membranes are produced at higher temperatures.

Table 4.8 Separation data for butane isomers from literature and in this work

Reference	Synthesis temp. and seeding	Membr. Thick.	T. (°C)	n-butane Permeance mol/Pa.s.m^2 x10^{-8}	Selec. n-/i-C_4
Hedlund et al. [14]	100°C Seeded	500 nm	25	98.0	9
			160	120.0	3
Gora et al. [18]	120°C	-	30	-	5
	160°C	-	30	-	30
	190°C	-	30	2.75	55
Coronas et al. [10]	180°C No seed	25-30 μm	100	1.0	32
			150	6.0	7
Vroon et al. [16]	120°C No seed	3 μm	25	0.8	52
			200	2.1	11
Gump et al. [58]	170°C No seed	-	25	1.0	15
			160	6.0	10
M1	130°C Seeded	9 μm	25	1.2	14
			150	3.8	8
M2	130°C Seeded	17 μm	25	0.26	5
			150	1.4	14
M3	130°C Seeded	23 μm	25	1.2	27
			150	12	21

- not reported

Thicker membranes exhibit higher selectivities for butane isomers compared to the thin membranes (Table 4.8). For example, Coronas et al. [10] reported that membrane with 30 μm thick exhibited n-butane/isobutane separation selectivity of 32 and 7 at 100^{o}C and 150^{o}C respectively. On the other hand Hedlund et al. [14] reported that 500 nm thick membrane exhibited n-butane/isobutane separation selectivity of 9 and 3 at 25^{o}C and 160^{o}C, respectively. Similarly Gora et al. [18] observed that when the synthesis temperature increased from 120^{o}C to 190^{o}C, thicker membranes were obtained and they exhibited higher n-butane/isobutane separation selectivities. Therefore, it can be concluded that separation behavior of the membranes is influenced by the thickness of the MFI layer.

Membranes tested in this study showed different thicknesses and morphological behavior that can affect gas permeation results. M3 exhibits higher permeances in single and binary systems and higher separation selectivities than M1 and M2. This is probably caused by intermediate layer that exist throughout M3. Intermediate layer was about 17 μm thick and has a loose structure compared to the dense MFI layer on top of it. Adsorption through the thick intermediate layer in addition to dense MFI layer may increase the selectivities. The dense top layer was about 5 μm and it was thinner than M1 and M2 therefore M3 showed higher permeances. M2 had lower permeance and moderate selectivity compared to the other membranes. M2 has 17 μm thick dense MFI layer, therefore thickness and dense structure may decrease permeances. As M1 was nearly two times thinner than the others, it is expected to show high permeance and low selectivity compared to other membranes. In addition to those, all of the membranes separated butane isomers at room and at higher temperatures and this indicates that membranes had continuous coverage with negligible amount of non-zeolitic pores.

CHAPTER 5

CONCLUSIONS

In this study the effect of seeding on MFI membrane morphology and quality was investigated. Membranes were synthesized from a composition yielding small amount of MFI crystals to observe the effect of seeding on membrane morphology clearly.

1. Coating the support surface with seed crystals improved the membrane quality and the reproducibility. On these membranes, MFI layer was continuous and compact. Of the membranes synthesized with seeding were 72% impermeable to N_2; this indicates that those membranes contain few defects. On the other hand, a continuous MFI layer cannot be obtained on bare supports under the same synthesis conditions. None of the membranes synthesized without seeding was impermeable.

2. About 60% of the membranes satisfied the quality criterion if the support is coated with low amount of seed crystals, 0.6 and 1.0 mg/cm^2 of seed. When 1.7 mg/cm^2 of seed is used 28% of the membranes satisfied the quality criterion. Decreasing seed amount increased reproducibility and quality of membranes.

3. Increasing the amount of seed does not increase the membrane thickness but MFI layers with asymmetric structure forms; dense MFI layer on top of a loose seed layer because all seed crystals do not participate into the secondary growth and crystallization occurred only at the solution side of the seed layer where dense MFI layer forms.

4. Vacuum seeding is a reproducible and practical method to prepare uniform and closely packed seed layers with controllable amount of seed crystals and high coverage.

CHAPTER 6

RECOMMENDATIONS

Support material can be changed with one having smaller pore size and smoother surface. By using supports with these properties, seed layers can be prepared with nanosize seed crystals and amount of seed crystals can be lowered therefore thin membranes can be produced.

REFERENCES

[1] Mulder, M., "Basic Principles of Membrane Technology", Kluwer Academic, Second edition, 2000, Dordrecht

[2] van de Graaf, J.M., Kapteijn, F., Moulijn, A.J., "Methodological and operational aspects of permeation measurements on silicalite-1 membranes", Journal of Membrane Science, 144, 1998, p. 87-104

[3] Skoulidas, A.I., Sholl, D.S., "Multiscale models of sweep gas and porous support effects on zeolite membranes", AIChE Journal, 51, 2005, p. 867-877

[4] Kusakabe, K., Yoneshige, S., Murata, A., Morooka, S., "Morphology and gas permeance of ZSM-5-type zeolite membrane formed on a porous α-alumina support", Journal of Membrane Science, 116, 1996, p. 39-46

[5] Kalıpçılar, H., Çulfaz, A., "Role of water content of clear synthesis solutions on the thickness of silicalite layers grown on porous α-alumina supports", Microporous and Mesoporous Materials, 52, 2002, p. 39-54

[6] Dong, J., Wegner, K., Lin, Y.S., "Synthesis of submicron polycrystalline MFI zeolite films on porous ceramic supports", Journal of Membrane Science, 148, 1998, p.233-241

[7] Algieri, C., Bernardo, P., Golemme, G., Barbieri, G., Drioli, E., "Permeation properties of a thin silicalite-1 (MFI) membrane", Journal of Membrane Science, 222, 2003, p. 181-190

[8] Munoz T., Kenneth, J., Balkus, Jr., "Preparation of oriented zeolite UTD-1 membranes via pulsed laser ablation", Journal of the American Chemical Society, 121, 1999, p. 139-146

[9] van de Graaf, J.M., van der Bijl, E., Stol, A., Kapteijn, F., Moulijn, A.J., "Effect of operating conditions and membrane quality on the separation performance of composite silicalite-1 membranes", Industrial and Engineering Chemistry Research, 1998, 37, p. 4071-4083

[10] Coronas, J., Falconer, J.L., Noble, R.D., "Characterization and permeation properties of ZSM-5 tubular membranes", AIChE Journal, 43, 1997, p. 1797-1812

[11] Mabande, G.T.P., Pradhan, G., Schwieger, W., Hanebuth, M., Dittmeyer, R., Selvam, T., Zampieri, A., Baser, H., Herrmann, R., "A study of silicalite-1 and Al-ZSM-5 membrane synthesis on stainless steel supports", Microporous and Mesoporous Materials, 75, 2004, p. 209-220

[12] Bonhomme, F., Welk, E.M., Nenoff, T.M., "CO_2 selectivity and lifetimes of high silica ZSM-5 membranes", Microporous and Mesoporous Materials, 66, 2003, p. 181-188

[13] Lin X., Chen, X., Kita, H., Okamoto, K., "Synthesis of silicalite tubular membranes by in-situ crystallization", AIChE Journal, 49, 2003, p. 237-247

[14] Hedlund, J., Strete, J., Anthonis, M., Bons, A-J., Carstensen, B., Corcoran, N., Cox, D., Deckman, H., De Gijnst, W., de Moor P-P., Lai, F., Mortier, W., Reinoso, J., Peters, J., "High-flux MFI membranes", Microporous and Mesoporous Materials, 52, 2002, p.179-189

[15] Geus, E.R., den Exter, J.M., van Bekkum, H., "Synthesis and characterization of zeolite (MFI) membranes on porous ceramic supports", Journal of Chemical Society-Faraday Transactions, 88, 1992, p. 3101-3109

[16] Vroon, Z.A.E.P., Keizer, K., Burggraaf, A.J., Verweij, H., "Preparation and characterization of thin zeolite MFI membranes on porous supports", Journal of Membrane Science, 144, 1998, p. 65-76

[17] Noack, M., Kölsch, P., Schafer, R., Toussaint, P., Sieber, I., Caro, J., "Preparation of MFI membranes of enlarged area with high reproducibility", Microporous and Mesoporous Materials, 49, 2002, p. 25-37

[18] Gora, L., Nishiyama, N., Jansen, J.C., Kapteijn, F., Teplyakov, V., Maschmeyer,Th., "Highly reproducible high-flux silicalite-1 membranes: optimization of silicalite-1 membrane preparation", Separation and Purification Technology, 22-23, 2002, p. 223-229

[19] Li, Y., Wang, J., Shi, J., Zhang, X., Lu, J., Bao, Z., Yan, D., "Synthesis of ZSM-5 zeolite membranes with large area on porous, tubular alpha-alumina supports", Separation and Purification Technology, 32, 2003, p.397-401.

[20] Gouzinis, A., Tsapatsis, M., "On the preferred orientation and microstructural manipulation of molecular sieve films prepared by secondary growth", Chemistry of Materials, 10, 1998, p. 2497-2504

[21] Lovallo, M.C., Gouzinis, A., Tsapatsis, M., "Synthesis and characterization of oriented membranes prepared by secondary growth", AIChE Journal, 44, 1998, p. 1903-1913

[22] Boudreau, L.C., Kuck, A.J., Tsapatsis, M., "Deposition of oriented zeolite A films: in situ and secondary growth", Journal of Membrane Science, 152, 1999, p. 41-59

[23] Hedlund, J., Mintova, S., Sterte, J., "Controlling the preferred orientation in silicalite-1 films synthesized by seeding", Microporous and Mesoporous Materials, 28, 1999 , p. 185-194

[24] Lovallo, M.C., Tsapatsis, M., "Preferentially oriented submicron silicalite membranes", AIChE Journal, 42, 1996, p. 3020-3029

[25] Lin X., Kita, H., Okamoto, K., "Silicalite membrane preparation, characterization and separation performance", Industrial and Engineering Chemistry Research, 40, 2001, p. 4069-4078

[26] Xomeritakis, G., Gouzinis, A., Nair, S., Okubo, T., He, M., Overney, M.R., Tsapatsis, M., "Growth, microstructure and permeation properties of supported zeolite (MFI) films and membranes prepared by secondary growth", Chemical Engineering Science, 54, 1999, p. 3521-3531

[27] Huang, A., Lin, Y.S., Yang, W., "Synthesis and properties of A-type zeolite membranes by secondary growth method with vacuum seeding", Journal of Membrane Science, 245, 2004, p. 41-51

[28] Caro, J.,Noack, M., Kölsch, P., Schafer, R., "Zeolite membranes-state of their development and perspective", Microporous and Mesoporous Materials, 38, 2000, p. 3-24

[29] Koros, W.J., Ma, Y.H., Shimidzu, T., " Terminology for membranes and membrane processes", Journal of Membrane Science, 120, 1996, p. 149-159

[30] Breck, D.W., " Zeolites molecular sieves, structure, chemistry and use", John Wiley and Sons, Inc., New York, 1971

[31] Li G., Kikuchi, E., Matsukata, M., "The control of phase and orientation in zeolite membranes by secondary growth method", Microporous and Mesoporous Materials, 62, 2003, p. 211-220

[32] Kusakabe, K., Kuroda, T., Murata A., Morooka, S., "Formation of a Y-Type Zeolite Membrane on a Porous α-Alumina Tube for Gas Separation", Ind. Eng. Chem. Res., 1997**,** 36, p. 649-655

[33] Flanigen E.M., Bennett, J.M., Grose, R.W., Cohen, J.P., Patton, R.L., Kirchner, R.M., Smith, J.V., " Silicalite, a new hydrophobic crystalline silica molecular sieve", Nature, 271, 1978, p. 512-516

[34] Tosheva, L., Valtchev, V.P., "Nanozeolites: Synthesis, Crystallization Mechanism, and Applications", Chemistry of Materials, 17, 2005, p. 2494-2513

[35] Persson, A.E., Schoeman, B.J., Sterte, J., Otterstedt, J.E., "The synthesis of discrete colloidal particles of TPA-silicalite-1", Zeolites, 14, 1994, p. 557-567

[36] Sano, T., Kiyozumi, Y., Kawamura, M., Mizukami, F., Takaya, H., Mouri, T., Inaoka, W., Toida, Y., Watanabe, M., Toyoda, K., "Preparation and characterization of ZSM-5 zeolite film", Zeolites, 11, 1991, p. 842-845

[37] Tsikoyiannis, J.G., Haag, W.O., "Synthesis and characterization of a pure zeolitic membrane", Zeolites, 12, 1992, p. 126-130

[38] Sano, T., Kiyozumi, Y., Mizukami, F., Takaya, H.,Mouri, T., Watanabe, M., "Steaming of ZSM-5 zeolite film", Zeolites, 12, 1992, p. 131-134

[39] Kikuchi, E., Yamashita, K., Hiromoto, S., Ueyama, K., Matsukata, M., "Synthesis of zeolitic thin layer by vapor phase transport method: appearance of preferential orientation of MFI zeolite", Microporous Materials, 11, 1997, p. 107-116

[40] Koegler, J.H., van Bekkum, H., Jansen, J.C., "Growth model of oriented crystals of zeolite Si-ZSM-5", Zeolites, 19, 1997, p. 262-269

[41] Lai, R., Yan, Y., Gavalas, G.R., "Growth of ZSM-5 films on alumina other surfaces", Microporous and Mesoporous Materials, 37, 2000, p. 9-19

[42] Vilaseca, M., Mateo, E., Palacio, L., Pradanos, P.,Hernandez, A., Paniagua, A., Coronas, J., Santamarıa, J., "AFM characterization of the growth of MFI-type zeolite films on alumina substrates", Microporous and Mesoporous Materials, 71, 2004, p. 33–37

[43] Lai, R., Gavalas, R.G., "Surface Seeding in ZSM-5 Membrane Preparation", Industrial and Engineering Chemistry Research, 37, 1998, p. 4275-4283

[44] Au, T.Y.L., Mui, Y.W., Lau, S.Z., Ariso, C.L., Yeung, K.L., "Engineering the shape of zeolite crystal grain in MFI membranes and their effects on the gas permeation properties", Microporous and Mesoporous Materials, 203, 2001, p. 203-216

[45] Hedlund, J., Noack, M., Kölsch, P., Creaser, D., Caro, J., Sterte, J., "ZSM-5 membranes synthesized without organic templates using a seeding technique", Journal of Membrane Science, 159, 1999, p. 263-273

[46] Xu, X., Yang, W., Liu, J., Lin, L., "Synthesis and perfection evaluation of NaA zeolite membrane", Separation and Purification Technology, 25, 2001, p. 475–485

[47] Au, L.T.Y., Yeung, K.L., "An investigation of the relationship between microstructure and permeation properties of ZSM-5 membranes" , Journal of Membrane Science, 194, 2001, p. 33-55

[48] Kusakabe, K., Murata, A., Kuroda, T., Morooka, S., "Preparation of MFI-type zeolite membranes and their use in separating n-butane and i-butane", Journal of Chemical Engineering of Japan, 30, 1997, p. 72-78

[49] Bernal, M.P., Xomeritakis, G., Tsapatsis, M., "Tubular MFI membranes made by secondary (seeded) growth", Catalysis Today, 67, 2001, p. 101-107

[50] Tuan, V.A., Falconer, J.L., Noble, R.D., "Alkali-Free ZSM-5 Membranes: Preparation Conditions and Separation Performance", Industrial and Engineering Chemistry Research, 38, 1999, p. 3635-3646

[51] Algieri, C., Golemme,G., Kallus, S., Ramsay, J.D.F., "Preparation of thin supported MFI membranes by in-situ nucleation and secondary growth", Microporous and Mesoporous Materials, 47, 2001, p. 127-134

[52] Lee, G.S., Lee, Y-J., Yoon, K.B., "Layer by layer assembly of zeolite crytsals on glass with polyelectrolytes as ionic linkers", Journal of the American Chemical Society, 123, 2001, p. 9769-9779

[53] Robson, H., (ed.), "Verified syntheses of zeolitic materials" Microporous and Mesoporous Materials, 22, 1998, p. 626-627

[54] Li, G., Kikuchi, E., Matsukata, M., "ZSM-5 zeolite membranes prepared from a clear template-free solution", Microporous and Mesoporous Materials, 60, 2003, p. 225–235

[55] Wong, C.W., Au, L.T.K., Ariso, C.T., Yeung, K.L., "Effects of synthesis parameters on the zeolite membrane growth", Journal of Membrane Science, 191, 2001, p. 143-163

[56] Valtchev, V., Mintova, S., Konstantinov, L., "Influence of metal substrate properties on the kinetics of zeolite film formation", Zeolites, 15, 1995, p. 679-683

[57] Bakker, W.J.W., van den Brooke, J.L.P., Moulijn, J.A., "Temperature dependence of one-component permeation through a silicalite-1 membrane", AIChE Journal, 43, 1997, p. 2203-2214

[58] Gump, C.J., Lin, X., Falconer, J.L., Noble, R.D., "Experimental configuration and adsorption effects on the permeation of C_4 isomers through ZSM-5 zeolite membranes", Journal of Membrane Science, 173, 2000, p. 35-52

[59] Szostak, R., "Handbook of molecular sieves", Van Nostrand Reinhold, New York, 1984

APPENDIX A

A sample calculation for a batch composition

A sample calculation for amounts of reagents to prepare 100 g synthesis solution for a molar batch composition of $9.80SiO_2$:TPAOH:$0.025Na_2O$: $0.019Al_2O_3$:$602.27H_2O$:$39.16C_2H_5OH$ is given below. TEOS (Acros Organics, 98% in water), TPAOH (Acros Organics, 25% in water), $NaAlO_2$ (44% Na_2O, 55% Al_2O_3, 1% H_2O, Riedel de Haen) and distilled water were the raw materials.

Amount of TEOS solution;

Molecular weight of TEOS=208.3 g/mol

$$M_{(TEOS\ soln)_{required}} = 9.8\ \text{mole}\ SiO_2 \left(\frac{1\,\text{mole TEOS}}{1\ \text{mole}\ SiO_2}\right)\left(\frac{208.3\,\text{g/mole}}{1\,\text{mole TEOS}}\right)\left(\frac{100\,\text{g TEOS soln}}{98\,\text{g TEOS}}\right)$$

$$= 2083\ \text{g}$$

$$M_{H_2O\ \text{in TEOS soln}} = 2083\ \text{g}\left(\frac{2\,\text{g}\ H_2O}{100\,\text{g TEOS}}\right)$$

$$= 41.66\,\text{g}$$

Amount of TPAOH solution;

Molecular weight of TPAOH=203.4 g/mol

$$M_{(TPAOH\ soln)\,required} = 1\,\text{mole TPAOH}\left(\frac{203.4\,\text{g/mole}}{1\,\text{mole TPAOH}}\right)\left(\frac{100\,\text{g TPAOH soln.}}{25\,\text{g TPAOH}}\right)$$

$$= 813.4\,\text{g}$$

$$M_{H_2O\ in\ TPAOH\ soln} = 813.4\ g\ TPAOH_{soln}\left(\frac{75\ g\ H_2O}{100\ g\ TPAOH_{soln}}\right)$$

$$= 610.2\ g$$

Amount of $NaAlO_2$;

$$M_{(NaAlO_2)required} = 0.025\ mole\ Na_2O\left(\frac{61.99\ g/mole}{1\ mole\ Na_2O}\right)\left(\frac{100\ g\ NaAlO_2}{44\ g\ Na_2O}\right)$$

$$= 3.52\ g$$

$$M_{H_2O\ in\ NaAlO_2} = 3.52\ g\ NaAlO_2\left(\frac{1\ g\ H_2O}{100\ g\ NaAlO_2}\right)$$

$$= 0.035\ g$$

Amount of H_2O;

$$M_{H_2O\ added} = M_{H_2O\ required} - M_{H_2O\ with\ (TEOS + TPAOH + NaAlO_2)}$$

$$M_{(H_2O)\ required} = 602.27\ mole\ H_2O\left(\frac{18.016\ g/mole}{1\ mole\ H_2O}\right)$$

$$M_{H_2O\ required} = 10850.5\ g$$

$$M_{H_2O\ added} = 10850.5 - (41.66 + 610.20 + 0.035)$$

$$= 10198.6\ g$$

Amounts of reagents were calculated as;

TEOS = 2083 g
TPAOH = 813.4 g
$NaAlO_2$ = 3.52 g
H_2O = 10198.6 g
Weight of batch = 13098.52 g

For 100 g batch preparation the amounts of reactants;

$$M_{TEOS\ soln} = 2083\ g\ TEOS_{soln}\left(\frac{100\ g\ batch}{13098.52\ g\ batch}\right) = 15.90\ g$$

$$M_{TPAOH\,soln} = 813.4\,g\,TPAOH_{soln}\left(\frac{100\,g\,batch}{13098.52\,g\,batch}\right) = 6.21\,g$$

$$M_{NaAlO_2} = 3.52\ g\,NaAlO_2\left(\frac{100\,g\,batch}{13098.52\,g\,batch}\right) = 0.03\,g$$

$$M_{H_2O} = 10198.6\ g\ H_2O\left(\frac{100\,g\,batch}{13098.52\,g\,batch}\right) = 77.86\,g$$

Table A.1 Amounts of reagents for 100 g batch preparation

Composition	TEOS	TPAOH	$NaAlO_2$	NaOH	H_2O
C1	15.90 g	6.21 g	0.03 g	-	77.86 g
C2	35.97 g	16.86 g	-	0.86 g	47.03 g

where

C1: $9.8SiO_2$:TPAOH:$0.025NaOH$:$0.019Al_2O_3$:$602.27H_2O$:$39.16C_2H_5OH$

C2: TPAOH:$8.17SiO_2$:$0.08Na_2O$:$162.09H_2O$:$32.68C_2H_5OH$

Calculation of maximum yield:

Molar batch composition:

TPAOH:$9.80SiO_2$:$0.025Na_2O$:$0.019Al_2O_3$:$602.27H_2O$: $39.16C_2H_5OH$

Amount of reagents to prepare 100 g batch is shown in Table A.1. In 100 g basis solution;

$$n_{SiO_2} = 15.90\,g\,TEOS\left(\frac{1\,mole}{208.3\,g}\right)\left(\frac{1\,mole\,SiO_2}{1\,mole\,TEOS}\right)$$
$$= 0.076\,mole\,SiO_2$$

$$M_{SiO_2} = 0.076\,mole\,SiO_2\left(\frac{60.088\,g}{1\,mole\,SiO_2}\right)$$
$$= 4.59\,g\,SiO_2$$

In one unit cell of MFI, there exist 96 moles of SiO_2 and 4 moles of TPA.

$$M_{TPAOH} = 0.076\,\text{mole}\,SiO_2\left(\frac{4\,\text{mole TPAOH}}{96\,\text{mole}\,SiO_2}\right)\left(\frac{203.4\,\text{g}}{1\,\text{mole TPAOH}}\right)$$
$$= 0.65\,\text{g TPAOH}$$

From 100 grams of synthesis solution, the maximum yield that can be achieved is,

$M_{ZSM\text{-}5}$ = 4.59 g SiO_2 + 0.65 g TPAOH

= 5.24 g ZSM-5

So, the maximum yield is 5.24%.

APPENDIX B

A sample calculation for the single gas permeance and selectivity

Constant pressure variable volume method was used through gas permeation experiments. The pressure at the feed side was kept constant at 1.9 bar absolute while the permeate side was at atmospheric pressure. The volume change per unit area was measured through a bubble flow meter for every 15 min. Table B.1 includes the data required for single gas permeance calculation.

Table B.1 Single gas permeation experimental data for membrane ED74

Experimental gases	N_2	SF_6
Volume change	0.005 L	0.0005 L
Time interval	11.3 s	208 s
Room temperature	290 K	290 K
Effective membrane area (m^2)	2.43×10^{-4}	2.43×10^{-4}
Transmembrane pressure difference	1.011×10^5 Pa	1.036×10^5 Pa

Volumetric flow rate calculated as;

$$\dot{\upsilon} = \Delta V / \Delta t$$

$$\dot{\upsilon} = 5\,L / 11.3\,s$$

$$= 4.4 \times 10^{-04}\,L/s$$

Assuming the permeating gas to be ideal, molar flow rate was calculated as;

$$\dot{n} = \frac{P.\dot{\upsilon}}{R.T}$$

$$\dot{n} = \frac{(9.12 \times 10^4\ Pa)(4.4 \times 10^{-4}\ L/s)}{(8314.34\ L\,Pa/mol\,K)(290\,K)}$$

$$\dot{n} = 1.66 \times 10^{-5}\ \text{mol/s}$$

Permeance through the membrane can be calculated as;

$$\underline{P} = \frac{\dot{n}}{\Delta P.A}$$

$$\underline{P} = \frac{1.66 \times 10^{-5}\ \text{mol/s}}{\left(1.011 \times 10^{5}\ \text{Pa}\right)\left(2.43 \times 10^{-4}\ \text{m}^2\right)}$$

$$\underline{P}_{N_2} = 6.77 \times 10^{-7}\ \text{mol/Pa.s.m}^2$$

SF_6 permeance was calculated as;

$$\underline{P}_{SF_6} = 4.03 \times 10^{-9}\ \text{mol/Pa.s.m}^2$$

Ideal selectivity is defined as the ratio of the permeance of two single gases.

$$\alpha_{ij} = \underline{P}_i / \underline{P}_j$$

$$\alpha_{N_2/SF_6} = 188$$

APPENDIX C

Calibration of mass flow controllers

For the adjustment of feed composition, MFC's were calibrated using n-butane and isobutane gases at room temperature. Calibration was performed by measuring the flow rate of gas stream by a soap bubble flow meter to calibrate MFC reading on LCD display. Figures C.1 and C.2 show the calibration curves of MFC's for n-butane and isobutane gases, respectively.

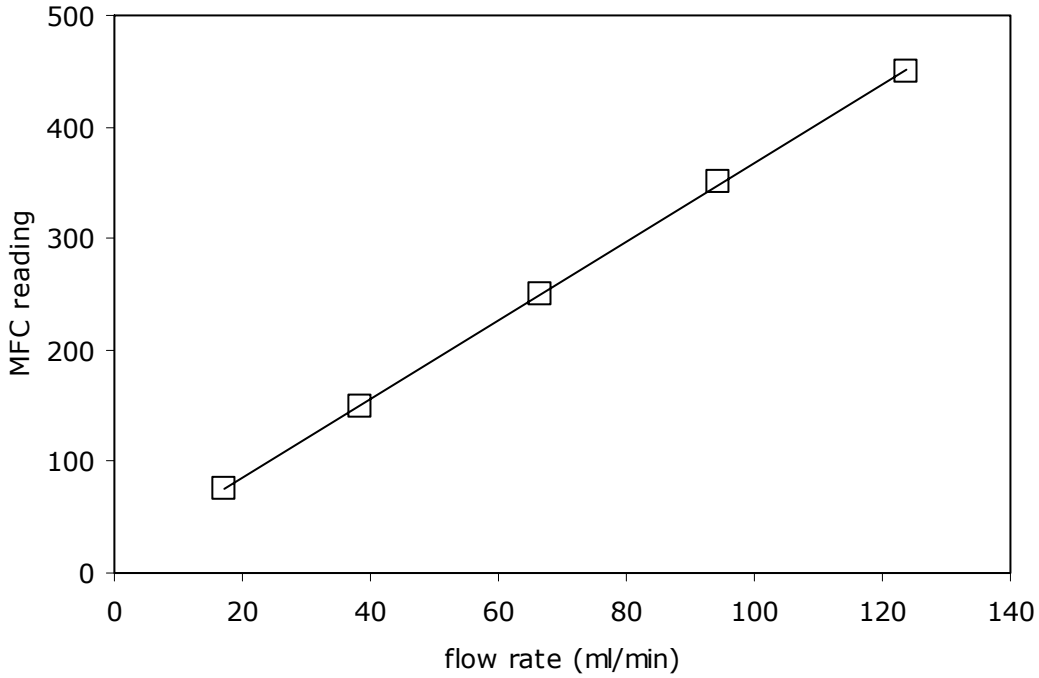

Figure C.1 Calibration plot of MFC for n-butane

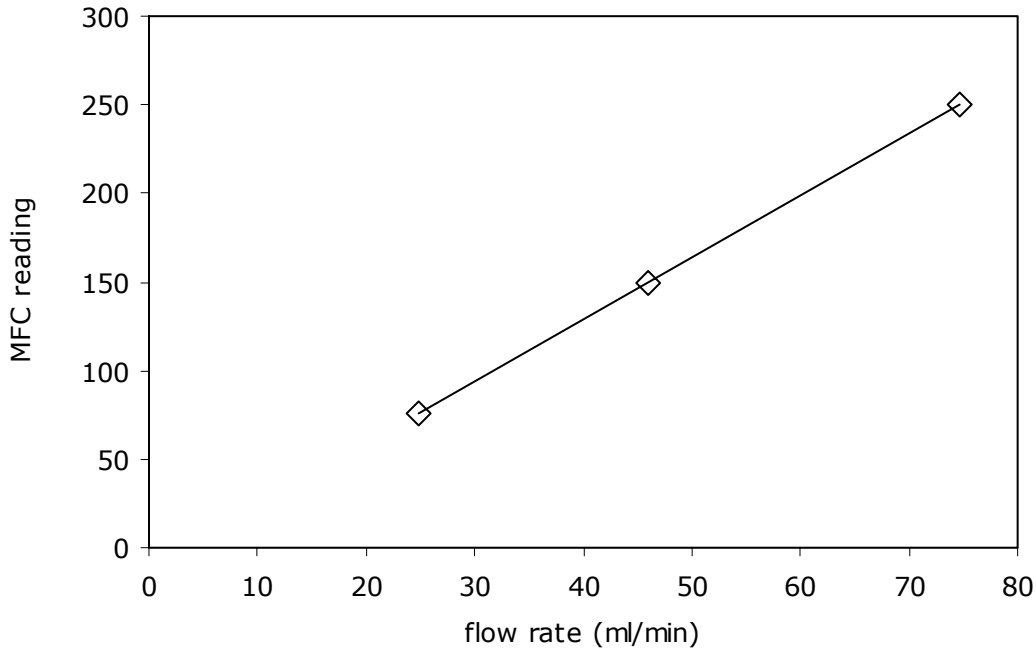

Figure C.2 Calibration plot of MFC for isobutane

APPENDIX D

A sample calculation for the determination of permeances and selectivites of binary gas mixtures

D.1 Calibration of GC outputs and sample calculation for the determination of gas compositions

Sample GC output can be seen on Figure D.1. First peak (retention time is 0.436 min) corresponds to isobutane and the second peak (retention time is 0.481 min) corresponds to n-butane.

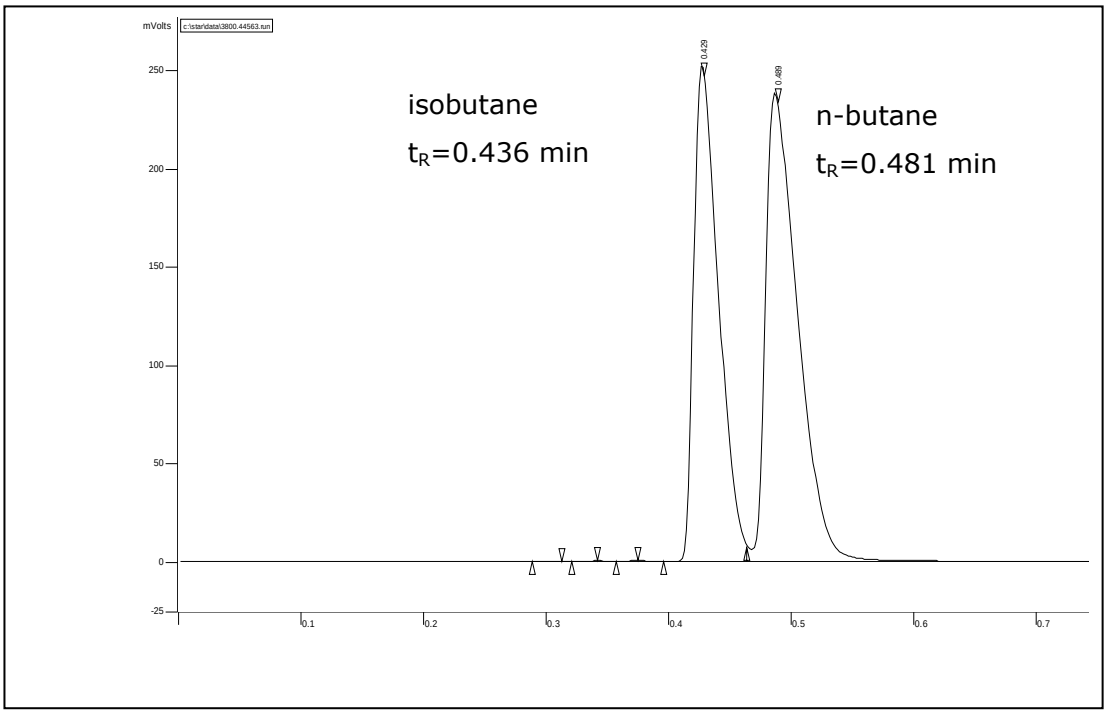

Figure D.1 Sample GC output for feed stream

As mentioned in the experimental section, for the analysis of gas composition, gas chromatograph was calibrated for n-butane and isobutane gas mixtures. Compositions of gas mixtures were adjusted by MFC's. Gas mixtures were fed to GC and the area under the peak for each single gas which is taken from the integrator denotes the composition of gas mixture that was fed to GC. By using calibration curve the composition of feed and permeate streams were determined. Retentate stream could not be analyzed by GC for this reason its composition is calculated through mass balance around the system. Calibration curves for n-butane and isobutane are shown in Figures D2 and D3, respectively.

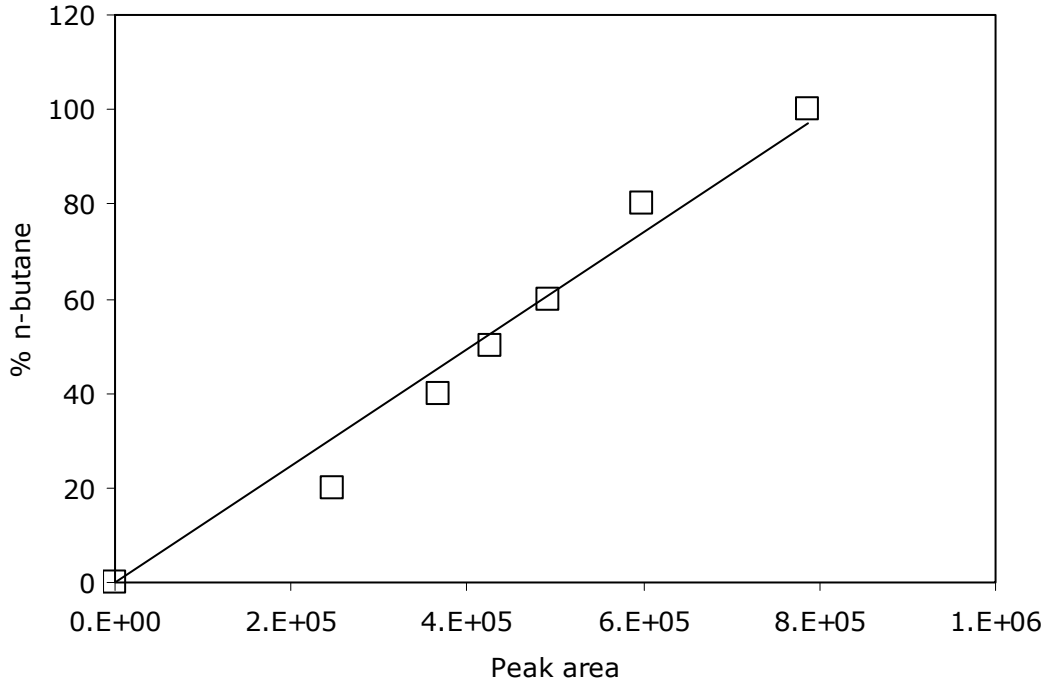

Figure D.2 Calibration plot of n-butane for GC analysis

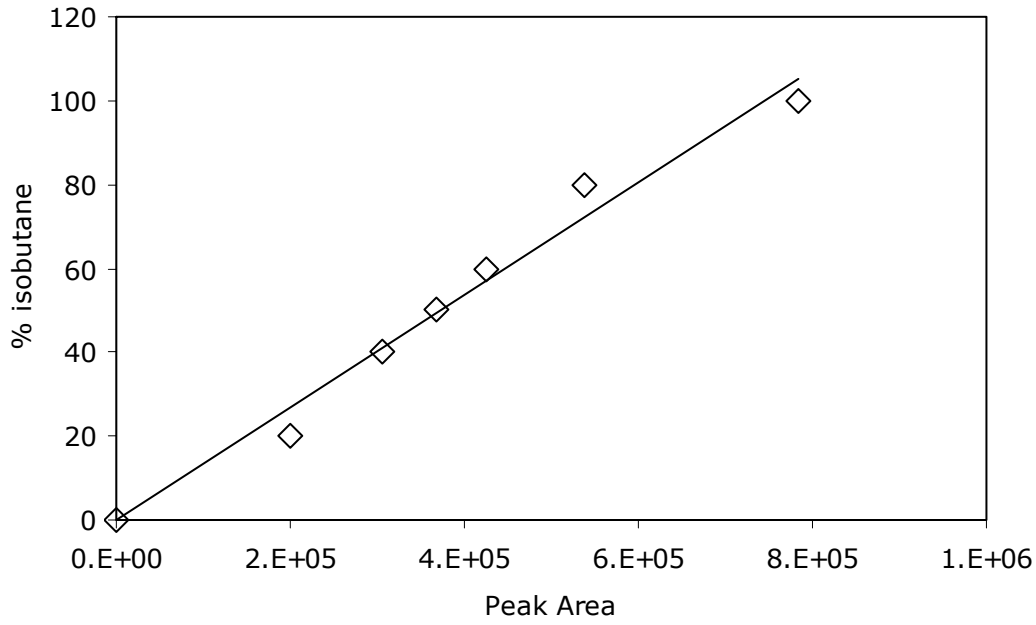

Figure D.3 Calibration plot of isobutane for GC analysis

Results of calibration curves ;

$$\%\, n-C_4H_{10} = (1.23\times10^{-4})x(\text{area of } n-C_4H_{10})$$

$$\%\, i-C_4H_{10} = (1.34\times10^{-4})x(\text{area of } i-C_4H_{10})$$

The composition of gas mixtures in permeate and feed side were calculated by using results of calibration as follows,

$$\%\, n-C_4H_{10} = \left[\frac{(1.23\times10^{-4})(\text{area of } n-C_4H_{10})}{(1.23\times10^{-4})(\text{area of } n-C_4H_{10})+(1.34\times10^{-4})(\text{area of } i-C_4H_{10})}\right]x100$$

$$\%\, i-C_4H_{10} = \left[\frac{(1.34\times10^{-4})(\text{area of } i-C_4H_{10})}{(1.23\times10^{-4})(\text{area of } n-C_4H_{10})+(1.34\times10^{-4})(\text{area of } i-C_4H_{10})}\right]x100$$

Sample calculation of permeate composition through membrane ED98 is as follows;

$$\%\, n-C_4H_{10} = \left[\frac{\left(1.23\times10^{-4}\right)(625710)}{\left(1.23\times10^{-4}\right)(625701)+\left(1.34\times10^{-4}\right)(137434)}\right] x\,100$$

$$= 80.69\,\%$$

$$\%\ i-C_4H_{10} = \left[\frac{\left(1.23\times10^{-4}\right)(137434)}{\left(1.23\times10^{-4}\right)(625701)+\left(1.34\times10^{-4}\right)(137464)}\right] x\,100$$

$$= 19.31\,\%$$

Composition of retentate side was calculated by mass balance;

mass balance for n-C_4H_{10} and i-C_4H_{10};

$$(\dot{\upsilon}_{FEED})(X^{FEED}_{n-C_4H_{10}}) = (\dot{\upsilon}_{PER})(X^{PER}_{n-C_4H_{10}}) + (\dot{\upsilon}_{RET})(X^{RET}_{n-C_4H_{10}})$$

$$(\dot{\upsilon}_{FEED})(X^{FEED}_{i-C_4H_{10}}) = (\dot{\upsilon}_{PER})(X^{PER}_{i-C_4H_{10}}) + (\dot{\upsilon}_{RET})(X^{RET}_{i-C_4H_{10}})$$

$$(47.07\,ml/min)(0.5156) = (0.8069)(0.05\,ml/min) + (47.02\,ml/min)(X^{RET}_{n-C_4H_{10}})$$

$$X^{RET}_{n-C4H10} = 0.5153$$

$$(47.07\,ml/min)(0.4844) = (0.1930)(0.05\,ml/min) + (47.02\,ml/min)(X^{RET}_{n-C_4H_{10}})$$

$$X^{RET}_{i-C4H10} = 0.4847$$

D.2 Sample calculation of permeance and binary gas mixture selectivity

Table D.1 Feed, permeate and retentate compositions of ED98

Composition	Flow rate (l/s)	Pressure (Pa) $x10^{-5}$	Mole Fractions (Y)		Partial Pressures $x\ 10^4$ (Pa)	
			n-C_4	i-C_4	n-C_4	i-C_4
Feed	$7.85x10^{-4}$	1.93	0.5156	0.4844	9.93	9.33
Permeate	$8.33x10^{-7}$	91.2	0.8069	0.1931	7.36	1.76
Retentate	$7.84x10^{-4}$	1.93	0.5153	0.4847	9.92	9.33

For each component transmembrane log-mean pressure difference was calculated with the following the equation;

$$\Delta P_{\log-\text{mean}} = \frac{\left(P_i^F - P_i^P\right) - \left(P_i^R - P_i^P\right)}{\ln\left[\left(P_i^F - P_i^P\right) / \left(P_i^R - P_i^P\right)\right]}$$

Log-mean pressure difference of n-C_4H_{10}

$$\left[\Delta P_{\log-\text{mean}}\right]_{n-C_4H_{10}} = \frac{\left[(9.93-7.36)-(9.92-7.36)\right]x\,10^4}{\ln\left[(9.93-7.36)x\,10^4 \,/\, (9.92-7.36)x\,10^4\right]}$$

$$\left[\Delta P_{\log-\text{mean}}\right]_{n-C_4H_{10}} = 2.56\times10^4 \text{ Pa}$$

Similarly log-mean transmembrane pressure difference of isobutane is calculated as;

$$\left[\Delta P_{\log-\text{mean}}\right]_{i-C_4H_{10}} = 7.57\times10^4 \text{ Pa}$$

Permeance of each component was calculated with the following equation;

$$\underline{P}_i = \left[\left(\frac{\Delta \upsilon}{\Delta t}\right)\frac{P_{atm}.y_i}{R.T}\right]\frac{1}{A}\frac{1}{\Delta P_{\log - mean}}$$

where A is the effective membrane area for permeation ($2.43x10^{-4}$ m^2), T is the room temperature, R is the ideal gas constant, ($\Delta v/\Delta t$) is the flow rate of permeate and y_i is the mol fraction of i in permeate.

$$\underline{P}_{n-C_4H_{10}} = \left[\left(8.33\times10^{-7}\ L/s\right)\frac{9.12x10^4\ (Pa).0.8069}{(297K).(8314.34\ L.Pa/mol.K)}\right]$$
$$\left(\frac{1}{2.43\times10^{-4}\ m^2}\right)\left(\frac{1}{2.56\times10^4\ Pa}\right)$$

$$\underline{P}_{n-C_4H_{10}} = 3.99\times10^{-9}\ mol/m^2.s.Pa$$

$$\underline{P}_{i-C_4H_{10}} = 3.23\times10^{-10}\ mol/m^2.s.Pa$$

Separation selectivity is the ratio of the permeances of these gases;

$$\alpha_{ij} = \underline{P}_i / \underline{P}_j$$

$$\alpha_{n-C_4H_{10}/i-C_4H_{10}} = 12.3$$

APPENDIX E

Mercury porosimeter results

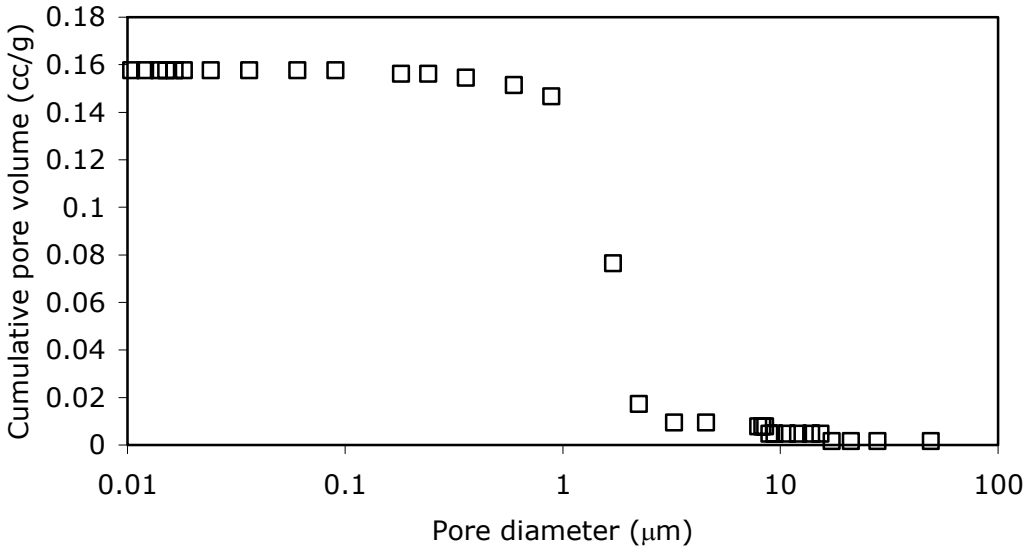

Figure E.1 Pore size distribution of alumina disc with pore volume

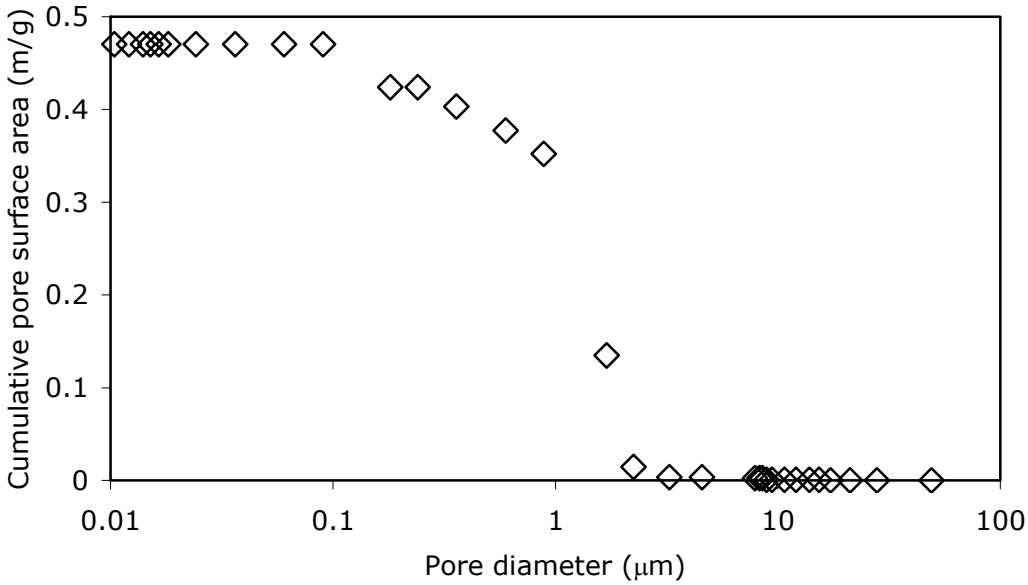

Figure E.2 Pore size distribution of alumina disc with surface area

APPENDIX F

List of samples synthesized in powder form

Table F.1 Synthesis conditions and crystallization results of samples synthesized in powder form

Code	Batch code	Aging (h)	T. (°C)	t. (h)	% Crys.	% yield	Size	Aspect ratio
ED1	C1	24	130	46	45		4-6	2-2.5
ED3	C1	24	130	46	88	48	4-6	2-2.5
ED6	C2	45	91	24	80	90	0.25-0.35	
ED7	C1	24	130	24	89	23	1-5	1.6-2.2
ED8	C1	24	130	46	100	60	3-7	2
ED9	C1	24	130	24		29	2-4	2-2.5
ED10	C1	24	130	24		31	2-4	2-2.5
ED11	C1	24	120	24		15	1-4	2
ED12	C1	24	120	24		-	2-5	2-2.5
ED13	C1	24	130	24		26	1-4	2-2.5
ED14	C1	24	130	24		27	2-4	2-2.5
ED15	C1	24	120	24		39	2-4	2
ED16	C1	24	120	24		28	1-4	2
ED17	C1	24	130	24		21	3-5	2-2.5
ED18	C2	45	91	24	91	40		
ED19	C2	45	91	14.5		5		
ED20	C2	45	91	19.5		18		

C1. $TPAOH:9.8SiO_2:0.025NaOH:0.019Al_2O_3:602.27H_2O:39.16C_2H_5OH$

C2. $TPAOH:8.17SiO_2:0.08Na_2O:162.09H_2O:32.68C_2H_5OH$

APPENDIX G

List of membranes

G.1 Gas permeation results

Table G.1 Single gas permeation and XRD analysis results of membranes

Code	t (h)	Seed (mg/cm^2)	Thick. XRD (μm)	N_2 permeance (before calcination)	Permeance ($mol/Pa.s.m^2$) $x10^{-7}$		Ideal Selec.
					N_2	SF_6	N_2/ SF_6
ED23	24	0.0	3.8		264	280.000	1
ED44	24	4.0			8.70	0.082	106
ED45	24	1.0			11.4	0.089	127
ED46a	24	0.0	8.1		127.00	85.000	2
ED47a	24	0.0			2.86	1.680	2
ED48u	24	1.0	15.9		40.00	24.000	2
ED50a	24	3.5			3.40	0.070	49
ED50u	24	3.5	32.0		1.66	1.980	1
ED51u	24	3.5	28.4				
ED52a	24	6.9			4.46	0.095	47
ED52u	24	6.9	42.7		1.13	0.109	10
ED53u	24	6.9	38.9				
ED66a	24	0.6	12.1	$2x10^{-6}$			
ED66u	24	0.6			11.30	0.102	110
ED67a	24	0.6		$9x10^{-11}$	43.20	36.000	1
ED67u	24	0.6			2.47	0.070	35
ED68a	24	1.0		$5x10^{-6}$			
ED69a	24	1.0	20.8	$1x10^{-7}$			

Code	t (h)	Seed (mg/cm^2)	Thick. XRD (μm)	N_2 permeance (before calcination)	Permeance ($mol/Pa.s.m^2$) $x10^{-7}$		Ideal Selec.
					N_2	SF_6	N_2/ SF_6
ED69u	24	1.0			13.50	2.100	6
ED70a	24	1.7	27.0		3.06	0.163	19
ED70u	24	1.7		$<1x10^{-11}$	4.57	0.070	65
ED71a	24	1.7			10.40	4.400	2
ED71u	24	1.7		$3x10^{-6}$			
ED73a	24	0.6	14.8	$4x10^{-10}$	6.97	1.240	6
ED73u	24	0.6		$4x10^{-10}$	13.10	7.540	2
ED74a	24	0.6		$4x10^{-10}$	7.58	0.040	190
ED74u	24	0.6		$<1x10^{-11}$	8.63	0.088	98
ED75u	24	1.0	21.8	$4x10^{-08}$	6.85	0.040	156
ED76u	24	1.0		$2x10^{-10}$	10.00	0.036	282
ED77a	15	0.0	1.6	$1x10^{-04}$			
ED77u	15	0.0	1.1	$1x10^{-04}$			
ED78a	20	0.0	4.1	$1x10^{-06}$			
ED78u	20	0.0	3.6	$1x10^{-05}$			
ED79a	25	0.0	4.5	$7x10^{-07}$			
ED79u	25	0.0	4.5	$4x10^{-07}$			
ED80a	47	0.0	9.7	$4x10^{-09}$	6.91	0.250	28
ED80u	47	0.0	9.9	$1x10^{-07}$			
ED83a	15	3.5	32.7	$1x10^{-05}$			
ED83u	15	3.5		$1x10^{-10}$			
ED84a	20	3.5	29.8	$8x10^{-06}$			

Code	t (h)	Seed (mg/cm^2)	Thick. XRD (μm)	N_2 permeance (before calcination)	Permeance ($mol/Pa.s.m^2$) $x10^{-7}$		Ideal Selec.
					N_2	SF_6	N_2/ SF_6
ED84u	20	3.5		$<1x10^{-11}$			
ED85a	25	3.5		$6x10^{-06}$			
ED85u	25	3.5	33.6	$3x10^{-10}$	9.98	0.204	49
ED86a	47	3.5		$<1x10^{-11}$			
ED86u	47	3.5	34.6	$<1x10^{-11}$	2.98	0.031	97
ED87a	15	0.6		$7x10^{-06}$			
ED87u	15	0.6	12.5	$9x10^{-06}$			
ED88a	20	0.6		$1x10^{-06}$			
ED88u	20	0.6	13.0	$1x10^{-05}$			
ED89a	25	0.6		$<1x10^{-11}$	11.8	0.116	102
ED89u	25	0.6	15.5	$3x10^{-10}$	9.4	0.181	52
ED90a	47	0.6		$3x10^{-08}$			
ED90u	47	0.6	21.5	$<1x10^{-11}$	6.09	0.100	61
ED91a	3	0.0					
ED91u	3	0.0	0.0	$1x10^{-04}$			
ED92a	7	0.0		$1x10^{-04}$			
ED92u	7	0.0	0.0	$1x10^{-04}$			
ED93a	10	0.0		$1x10^{-04}$			
ED93u	10	0.0	0.5	$1x10^{-04}$			
ED94a	72	0.0		$1x10^{-08}$			
ED94u	72	0.0	11.9	$4x10^{-08}$			
ED95a	24	0.6	14.7	$1x10^{-07}$			
ED95u	24	0.6		$1x10^{-05}$			
ED96a	24	0.6		$<1x10^{-11}$	11.4	0.096	119

Code	t (h)	Seed (mg/cm^2)	Thick. XRD (μm)	N_2 permeance (before calcination)	Permeance ($mol/Pa.s.m^2$) $x10^{-7}$		Ideal Selec. N_2/SF_6
					N_2	SF_6	
ED96u	24	0.6	14.7	$1x10^{-05}$			
ED97a	24	1.0	18.0	$7x10^{-06}$			
ED97u	24	1.0		$<1x10^{-11}$	18.60	0.160	116
ED98a	24	1.0	15.1	$<1x10^{-11}$	>100		
ED98u	24	1.0		$<1x10^{-11}$	13.50	0.155	87
ED99a	24	1.7	17.6	$<1x10^{-11}$	31.00	18.235	1.7
ED100u	24	1.7	17.8	$<1x10^{-11}$	1.51	0.054	28
ED101a	24	1.7	18.8	$<1x10^{-11}$	>100		
ED102a	24	1.7		$<1x10^{-11}$	11.60	0.055	211
ED102u	24	1.7	16.9	$<1x10^{-11}$	17.30	5.767	3
ED103a	24	0.6	14.5	$<1x10^{-11}$			
ED104u	24	0.6	11.0	$>1x10^{-05}$			
ED105u	24	1.0	16.3	$<1x10^{-11}$			
ED106a	24	1.0	17.3	$<1x10^{-11}$	3.76	0.061	62
ED106u	24	1.0		$4x10^{-10}$	28.10	28.100	1
ED107u	4	0.6	5.2	$1x10^{-05}$			
ED108u	4	3.5	36.5	$1x10^{-05}$			
ED109u	8	0.6	7.9	$1x10^{-05}$			
ED110u	8	3.5	32.3	$2x10^{-08}$			
ED111u	36	0.6	18.6	$<1x10^{-11}$			
ED112u	36	3.5	33.6	$<1x10^{-11}$			

Table G.2 Permeation results of butane isomers

Code	T (^oC)	Single gas permeance (mol/Pa.s.m^2) x10^{-08}		Ideal Selectivity	Binary gas permeance (mol/Pa.s.m^2) x10^{-08}		Separation Selectivity
		n-C_4	i-C_4	n-C_4/i-C_4	n-C_4	i-C_4	n-C_4/i-C_4
ED96a (M1)	RT				1.18	0.0843	14
	50				2.74	0.127	22
	100				2.92	0.257	11
	150				3.79	0.490	8
ED98u (M2)	RT	0.49	0.26	2	0.265	0.0539	5
	50	0.38	0.21	2	0.399	0.0323	12
	100	19.0	0.35	54	0.449	0.0275	16
	150	28	0.48	59	1.44	0.100	14
ED102a (M3)	RT	0.39	0.26	2	1.23	0.0449	27
	50	3.6	0.38	10	2.39	0.063	38
	100	21	0.54	39	8.25	0.259	32
	150	30	1.3	23	12.1	0.582	21

RT room temperature

G.2 SEM images of the synthesized membranes

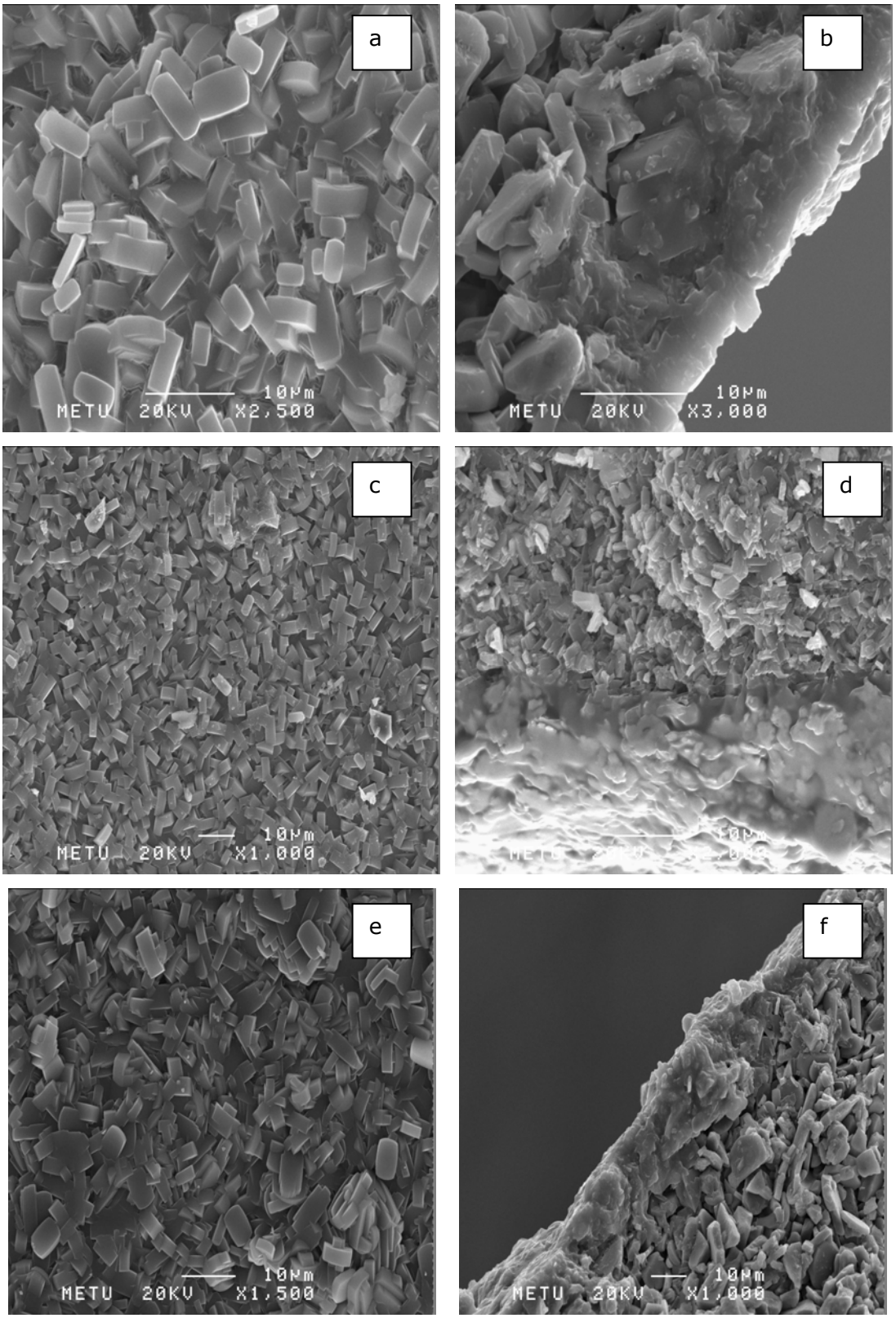

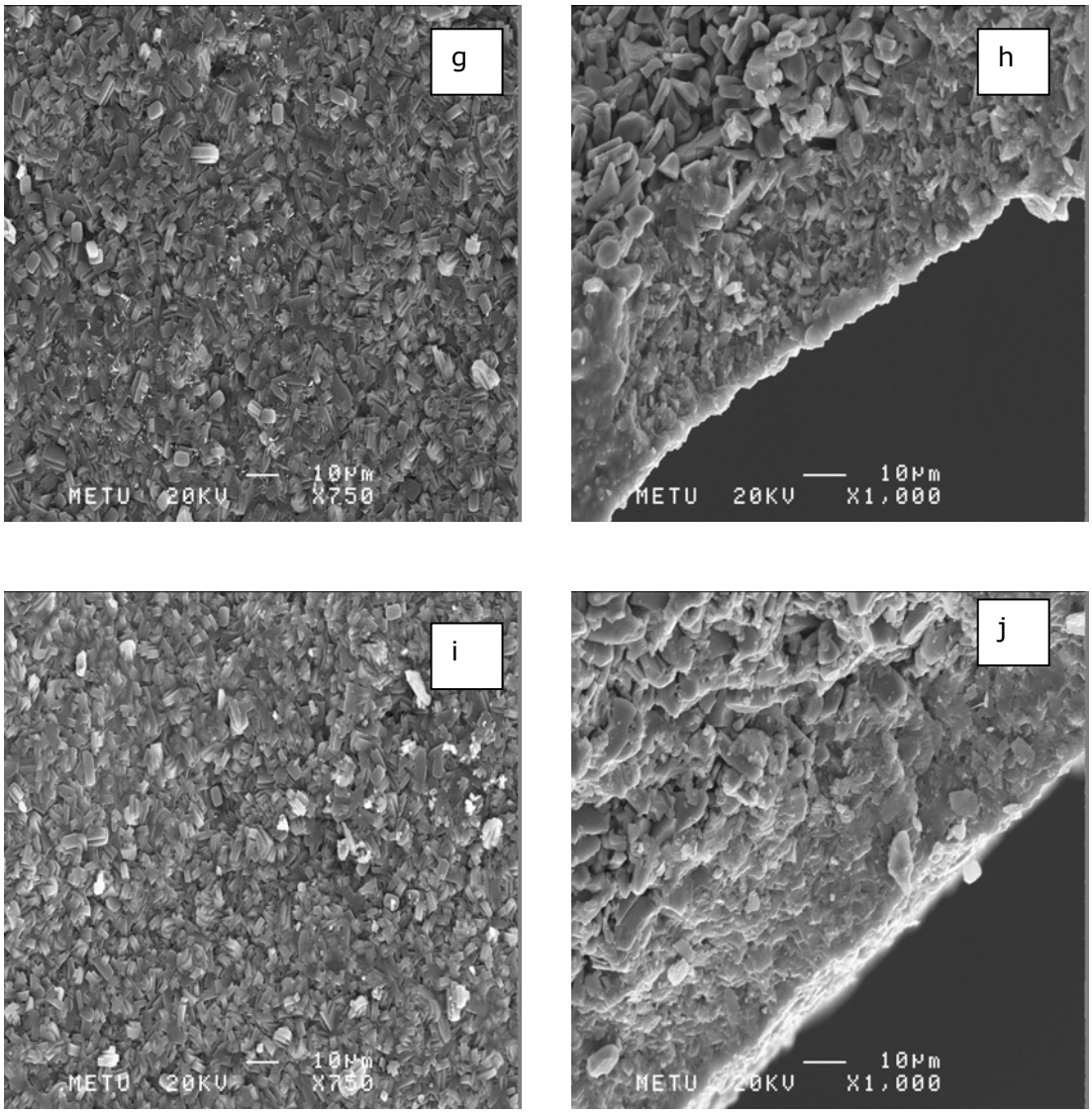

Figure G.1 SEM surface and cross-section images of membranes (a,b) ED49a (c,d) ED52a (e,f) ED74u (g,h) ED85a (i,j) ED85u

G.3 XRD results of the synthesized membranes

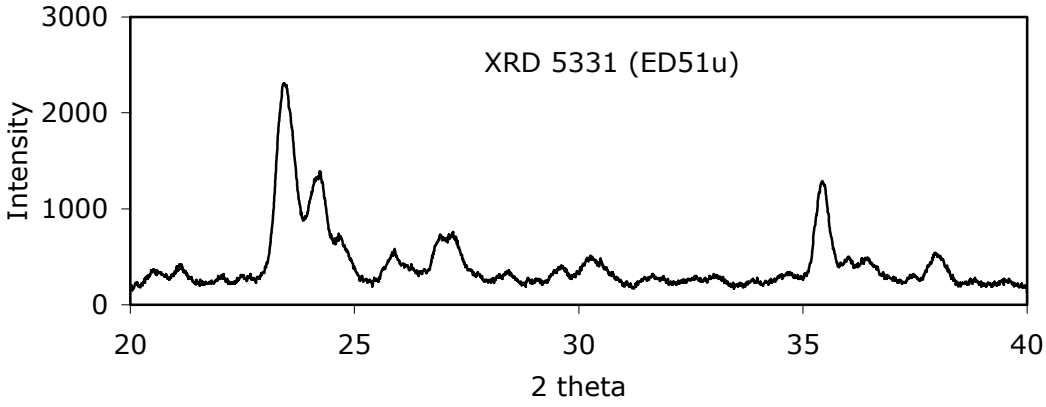

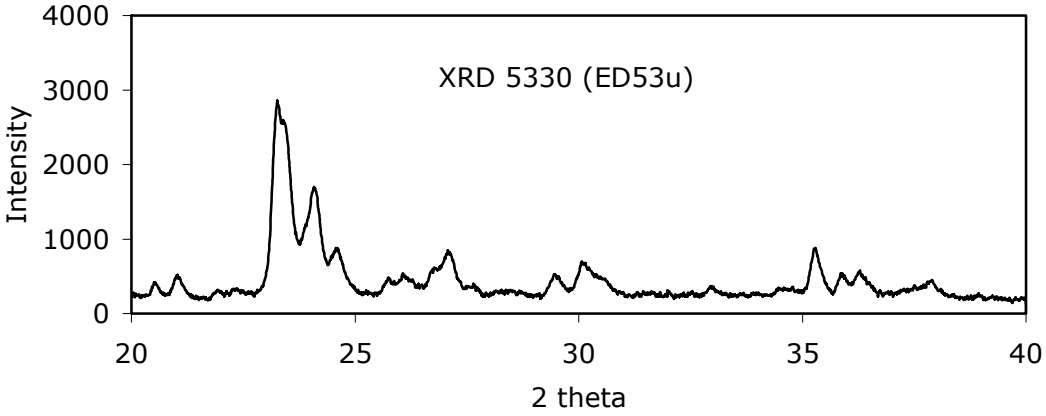

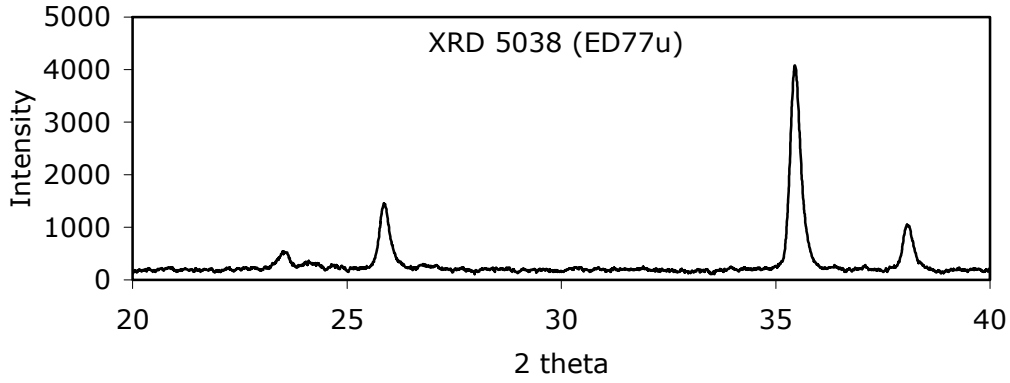

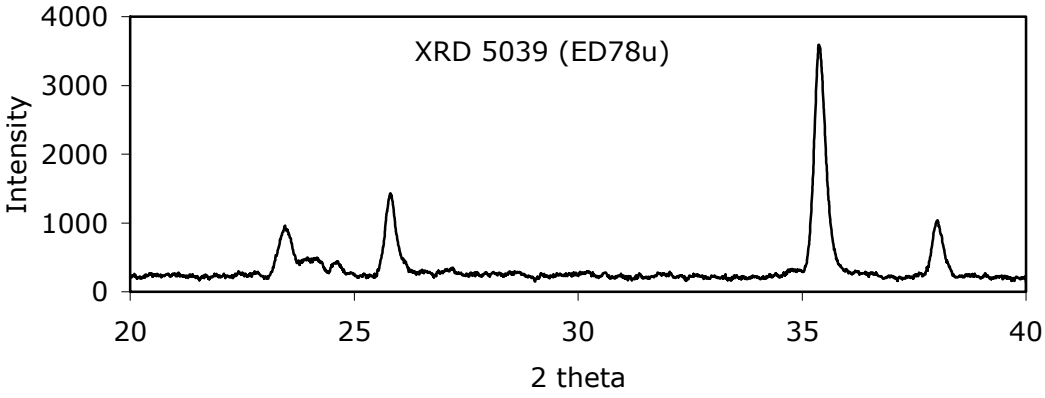
XRD 5039 (ED78u)
Intensity
4000
3000
2000
1000
0
20
25
30
35
40
2 theta

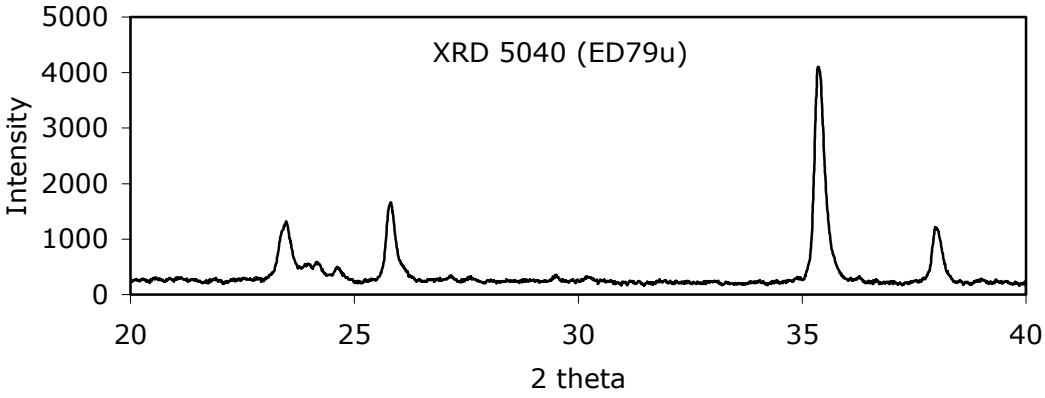
XRD 5040 (ED79u)
Intensity
5000
4000
3000
2000
1000
0
20
25
30
35
40
2 theta

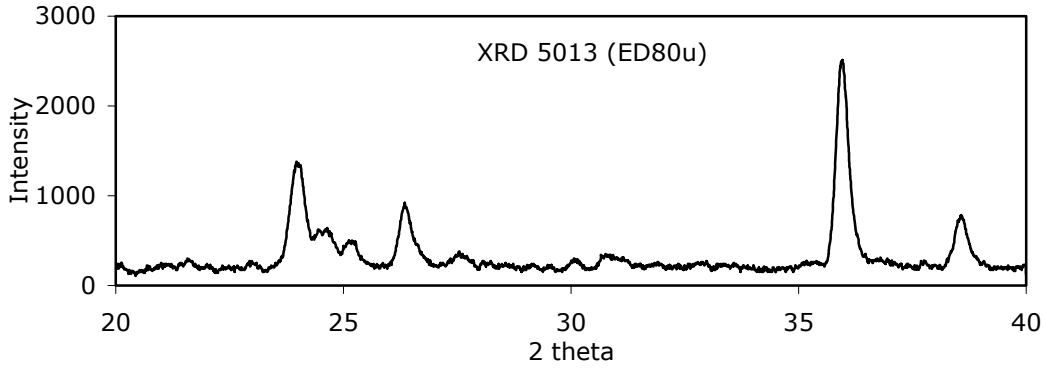
XRD 5013 (ED80u)
Intensity
3000
2000
1000
0
20
25
30
35
40
2 theta

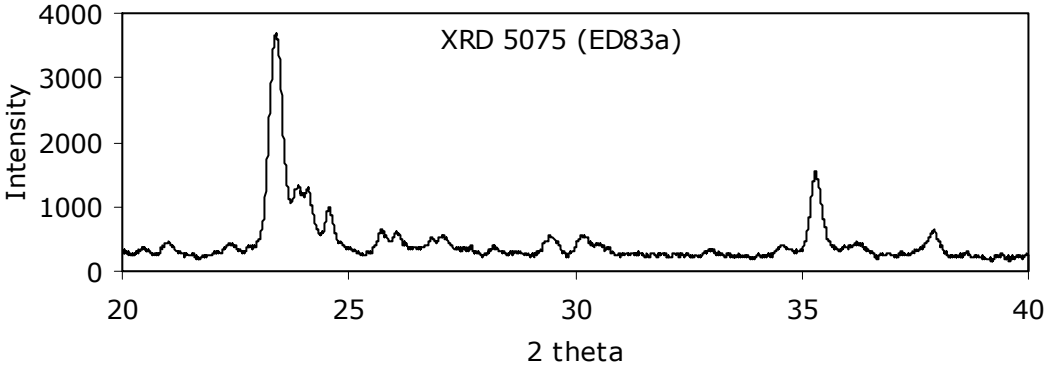
XRD 5075 (ED83a)
Intensity
4000
3000
2000
1000
0
20
25
30
35
40
2 theta

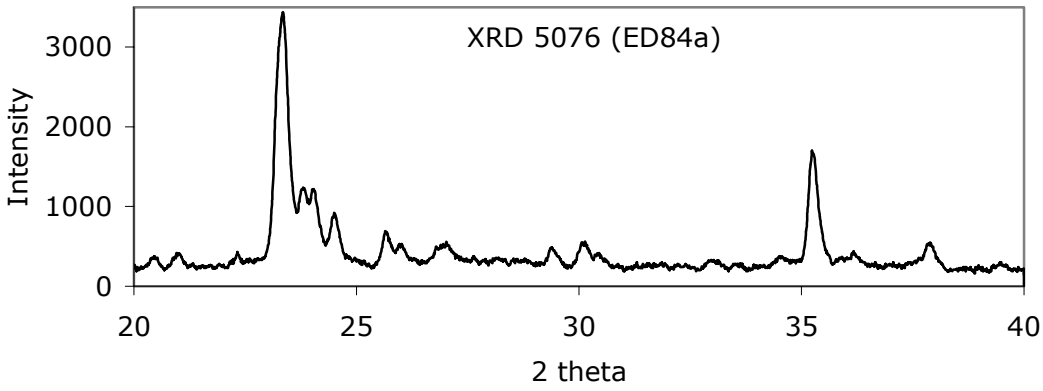
XRD 5076 (ED84a)
Intensity
3000
2000
1000
0
20
25
30
35
40
2 theta

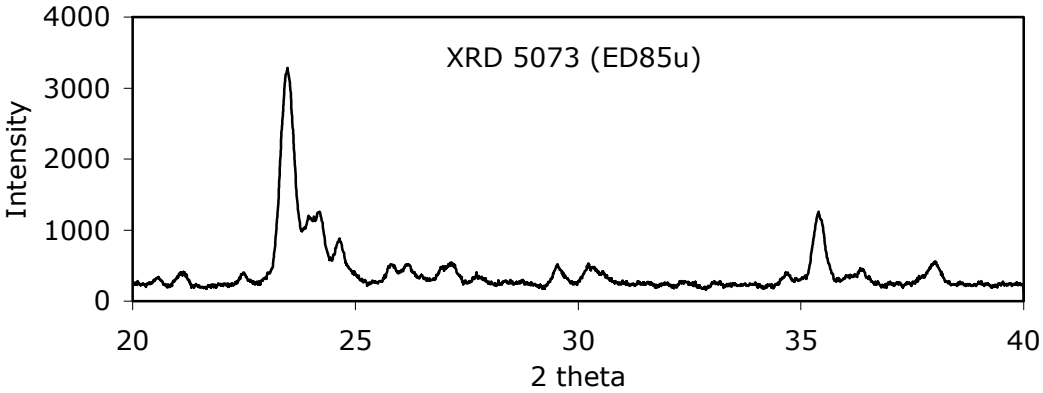
XRD 5073 (ED85u)
Intensity
4000
3000
2000
1000
0
20
25
30
35
40
2 theta

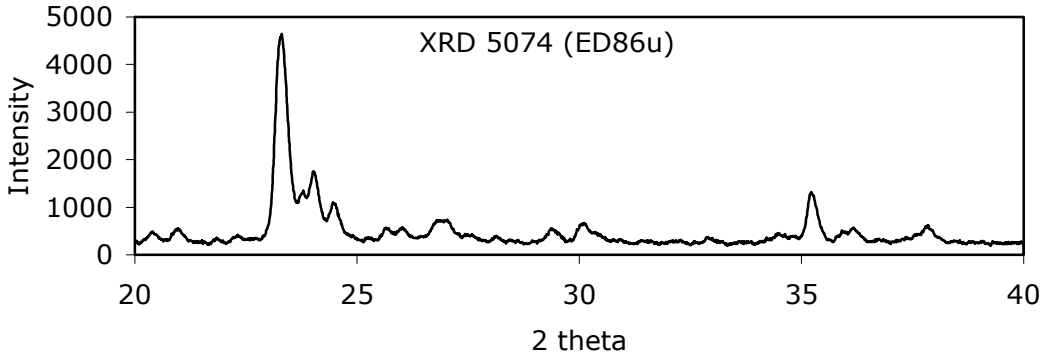
XRD 5074 (ED86u)
Intensity
5000
4000
3000
2000
1000
0
20
25
30
35
40
2 theta

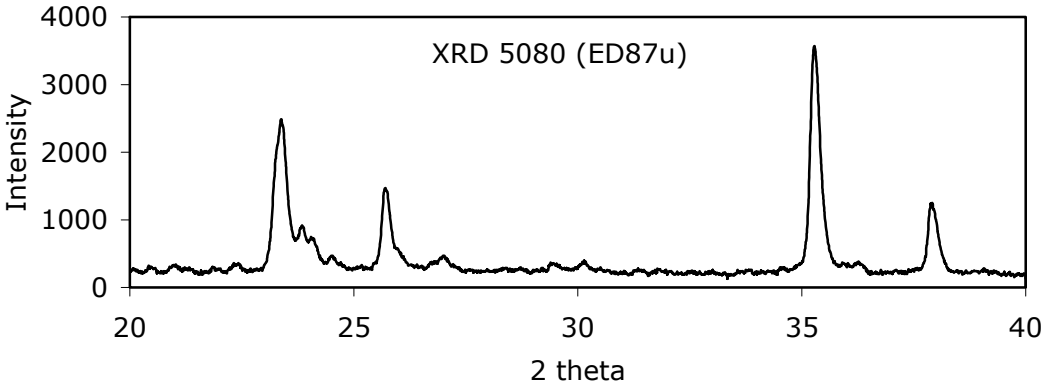
XRD 5080 (ED87u)
Intensity
4000
3000
2000
1000
0
20
25
30
35
40
2 theta

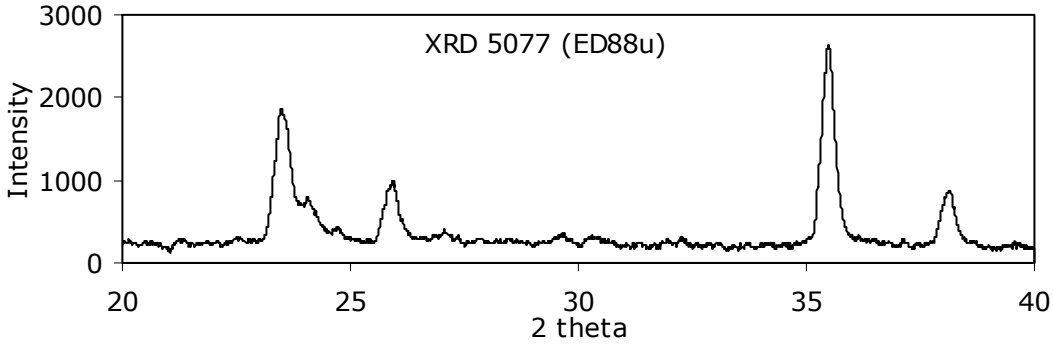
XRD 5077 (ED88u)
Intensity
3000
2000
1000
0
20
25
30
35
40
2 theta

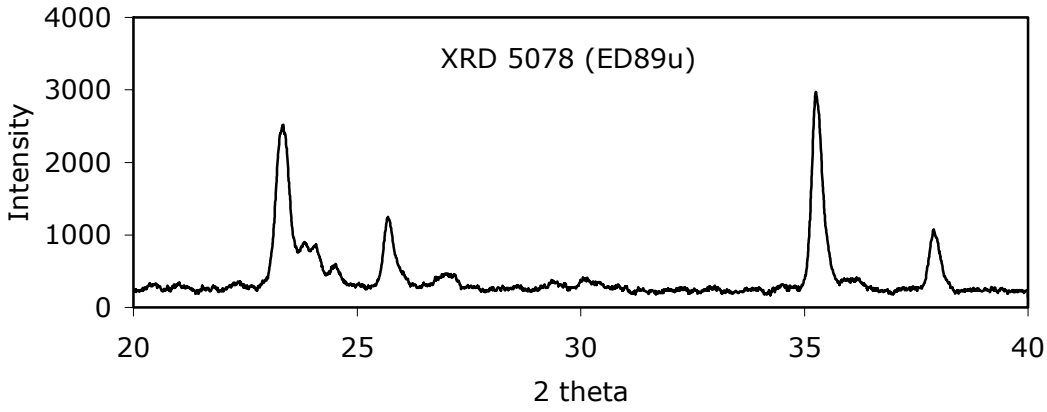
XRD 5078 (ED89u)
Intensity
4000
3000
2000
1000
0
20
25
30
35
40
2 theta

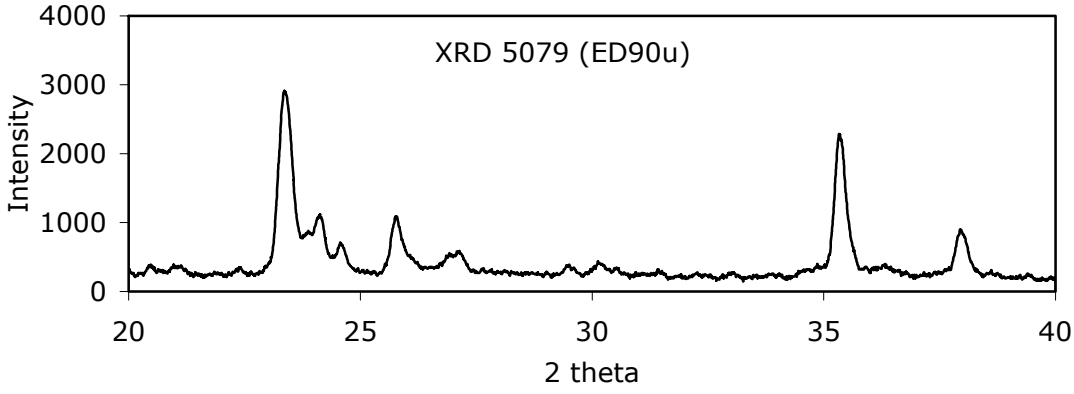
XRD 5079 (ED90u)
Intensity
4000
3000
2000
1000
0
20
25
30
35
40
2 theta

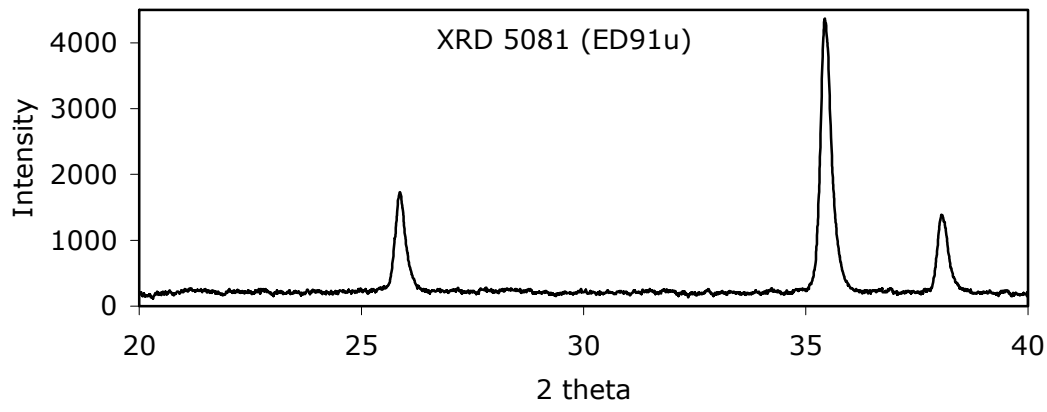
XRD 5081 (ED91u)
Intensity
4000
3000
2000
1000
0
20
25
30
35
40
2 theta

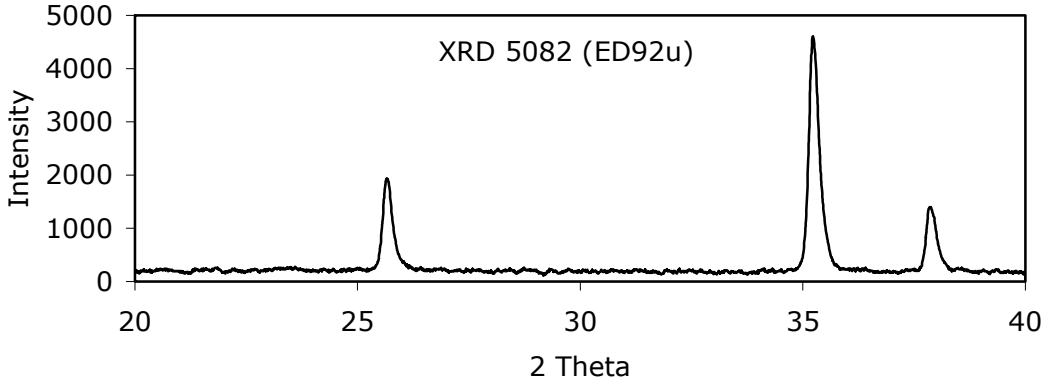
XRD 5082 (ED92u)
Intensity
5000
4000
3000
2000
1000
0
20
25
30
35
40
2 Theta

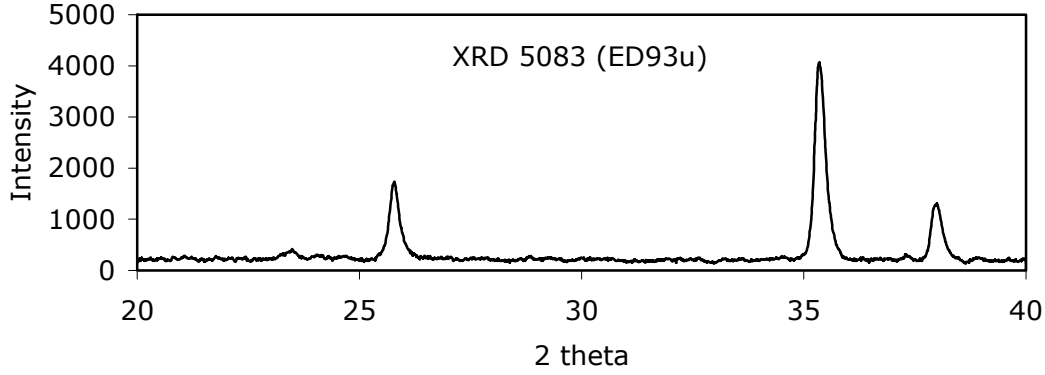
XRD 5083 (ED93u)
Intensity
5000
4000
3000
2000
1000
0
20
25
30
35
40
2 theta

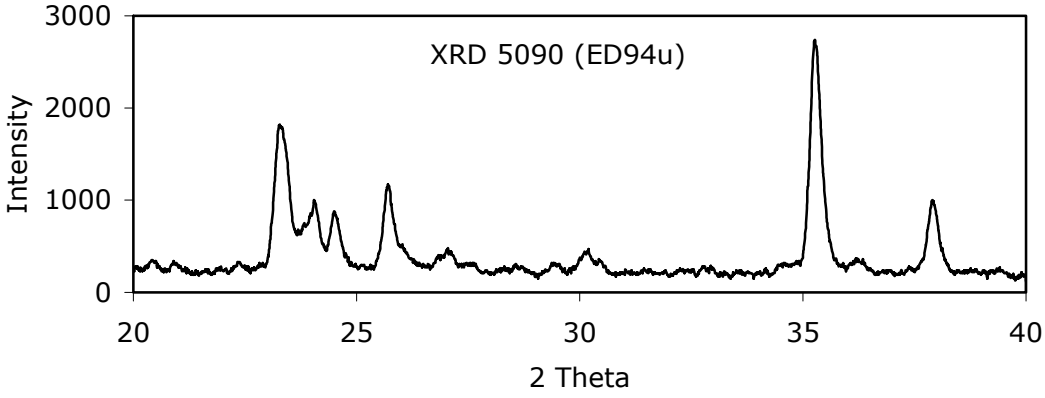
XRD 5090 (ED94u)
Intensity
3000
2000
1000
0
20
25
30
35
40
2 Theta

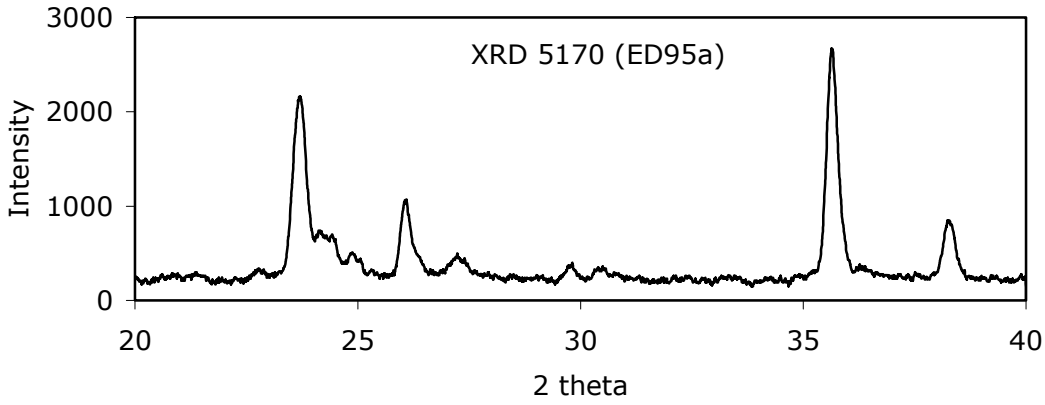
XRD 5170 (ED95a)
Intensity
3000
2000
1000
0
20
25
30
35
40
2 theta

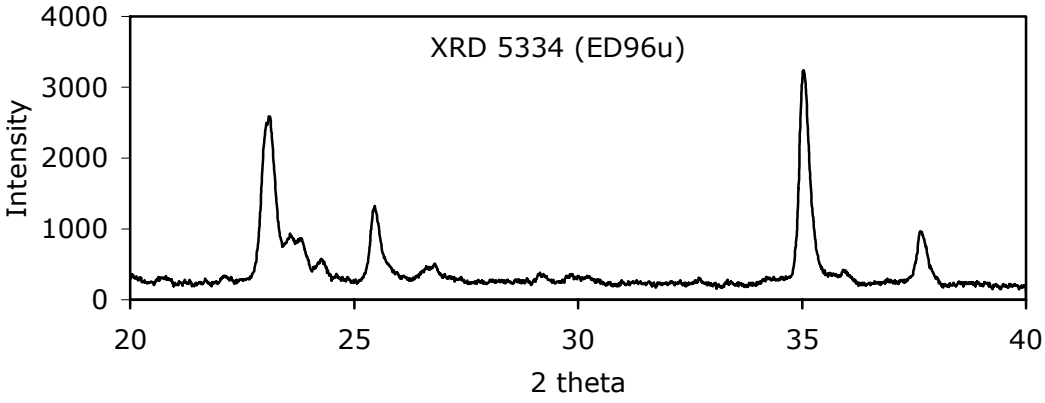
XRD 5334 (ED96u)
Intensity
4000
3000
2000
1000
0
20
25
30
35
40
2 theta

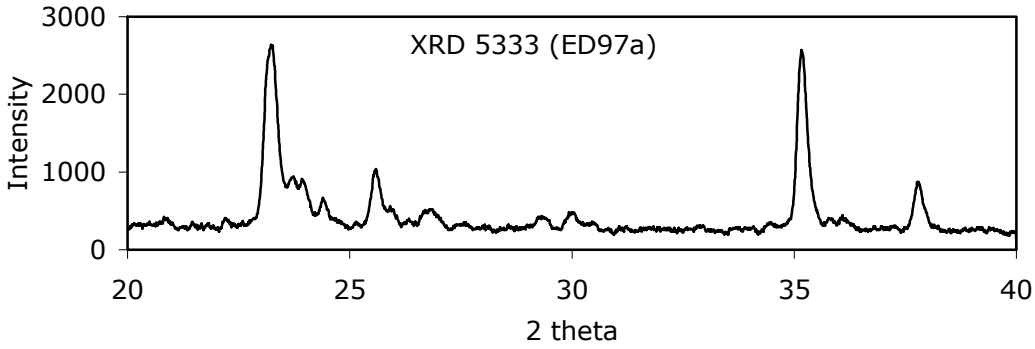
XRD 5333 (ED97a)
Intensity
3000
2000
1000
0
20
25
30
35
40
2 theta

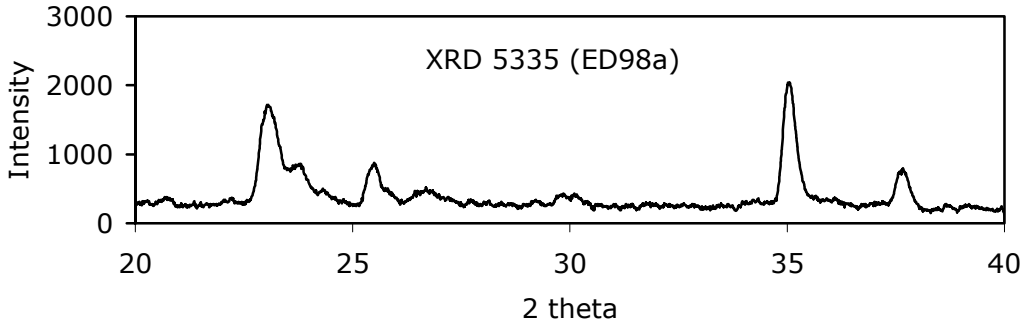
XRD 5335 (ED98a)
Intensity
3000
2000
1000
0
20
25
30
35
40
2 theta

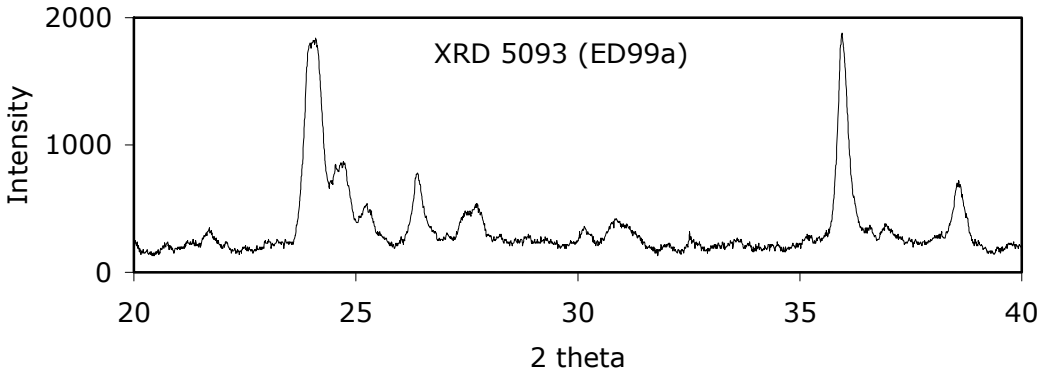
XRD 5093 (ED99a)
Intensity
2000
1000
0
20
25
30
35
40
2 theta

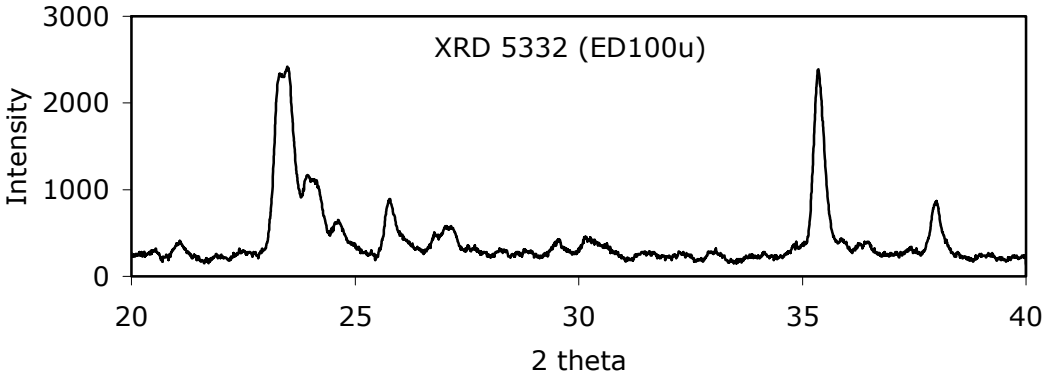
XRD 5332 (ED100u)
Intensity
3000
2000
1000
0
20
25
30
35
40
2 theta

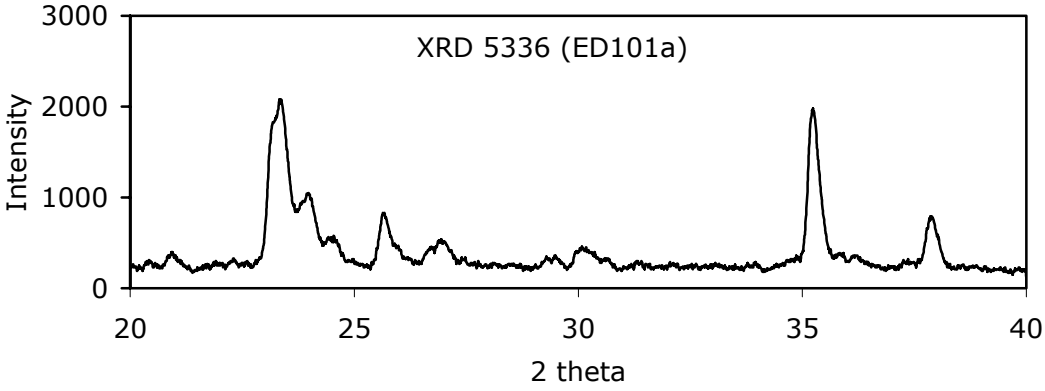
XRD 5336 (ED101a)
Intensity
3000
2000
1000
0
20
25
30
35
40
2 theta

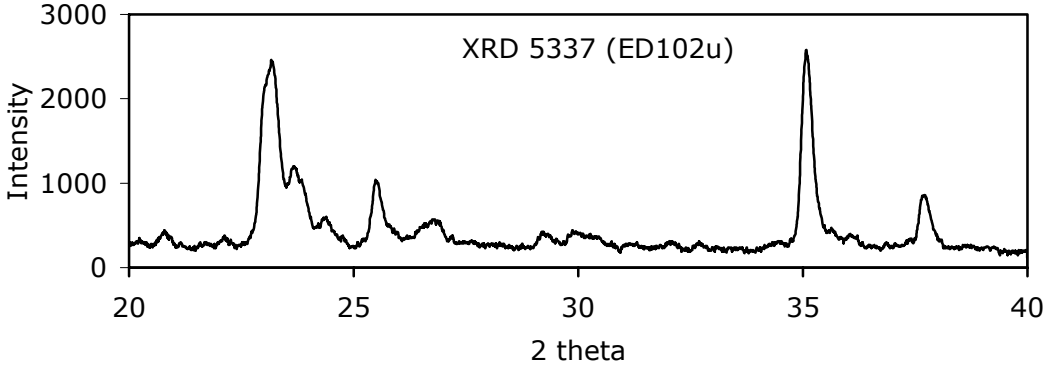
XRD 5337 (ED102u)
Intensity
3000
2000
1000
0
20
25
30
35
40
2 theta

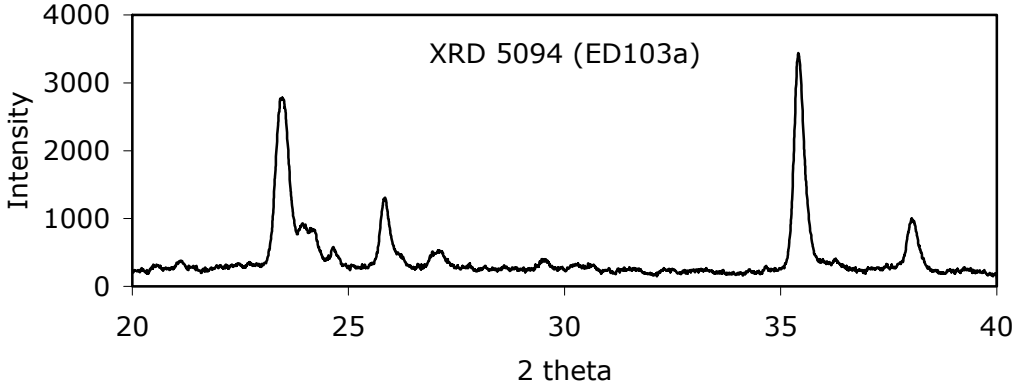
XRD 5094 (ED103a)
Intensity
4000
3000
2000
1000
0
20
25
30
35
40
2 theta

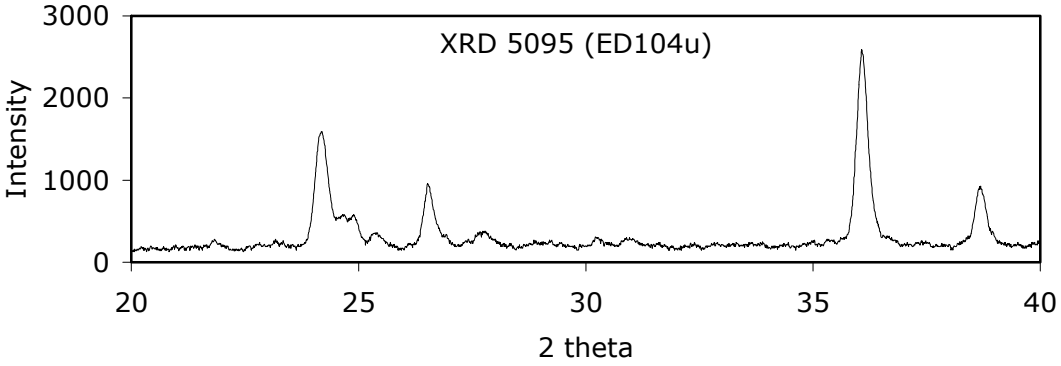
XRD 5095 (ED104u)
Intensity
3000
2000
1000
0
20
25
30
35
40
2 theta

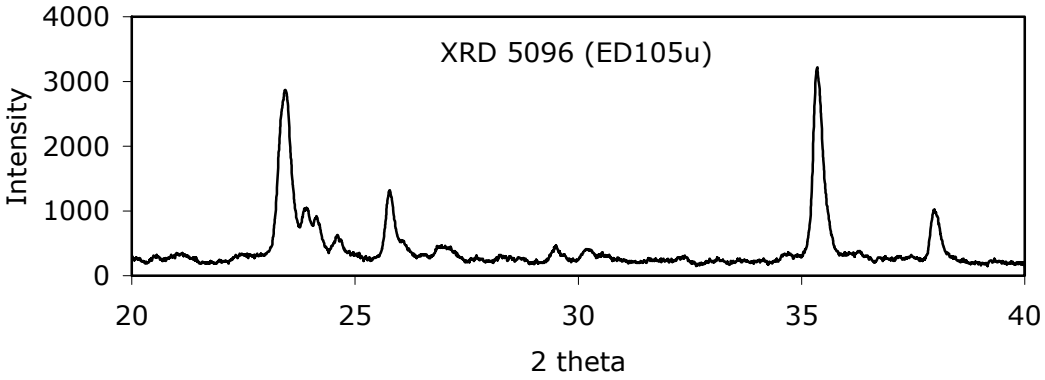
XRD 5096 (ED105u)
Intensity
4000
3000
2000
1000
0
20
25
30
35
40
2 theta

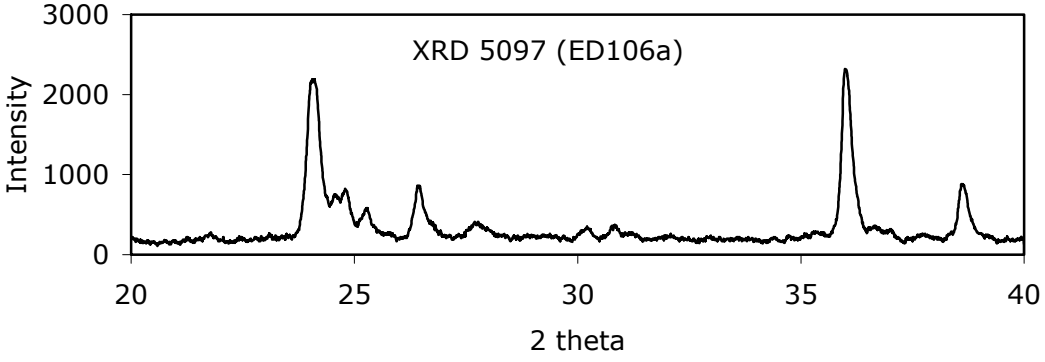
XRD 5097 (ED106a)
Intensity
3000
2000
1000
0
20
25
30
35
40
2 theta

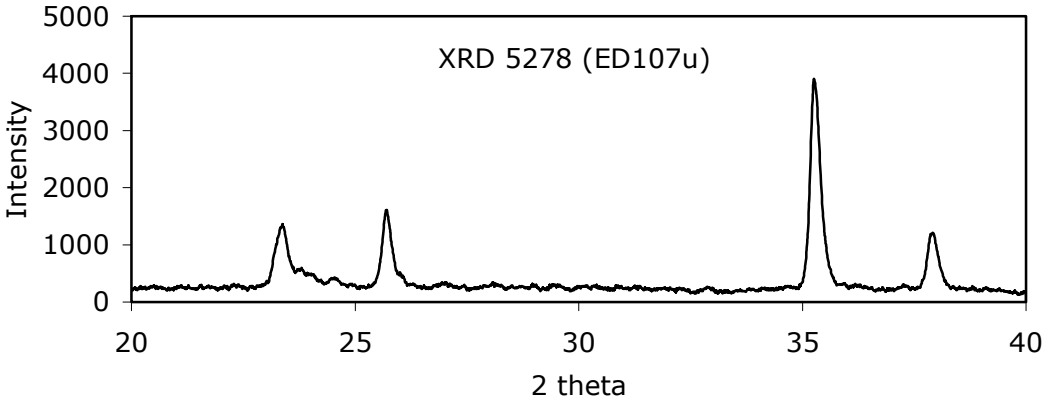
XRD 5278 (ED107u)
Intensity
5000
4000
3000
2000
1000
0
20
25
30
35
40
2 theta

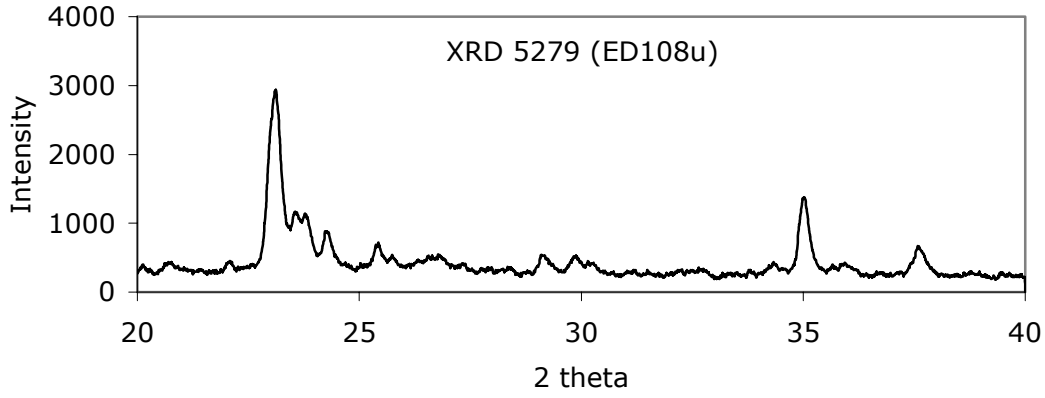
XRD 5279 (ED108u)
Intensity
4000
3000
2000
1000
0
20
25
30
35
40
2 theta

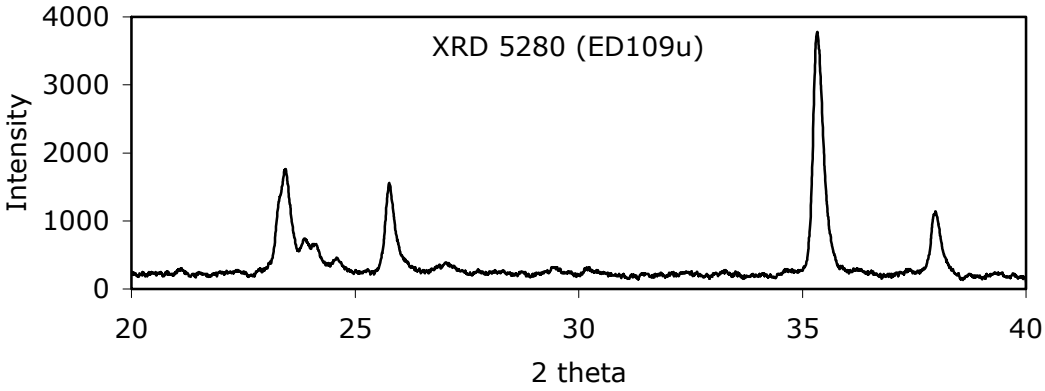
XRD 5280 (ED109u)
Intensity
4000
3000
2000
1000
0
20
25
30
35
40
2 theta

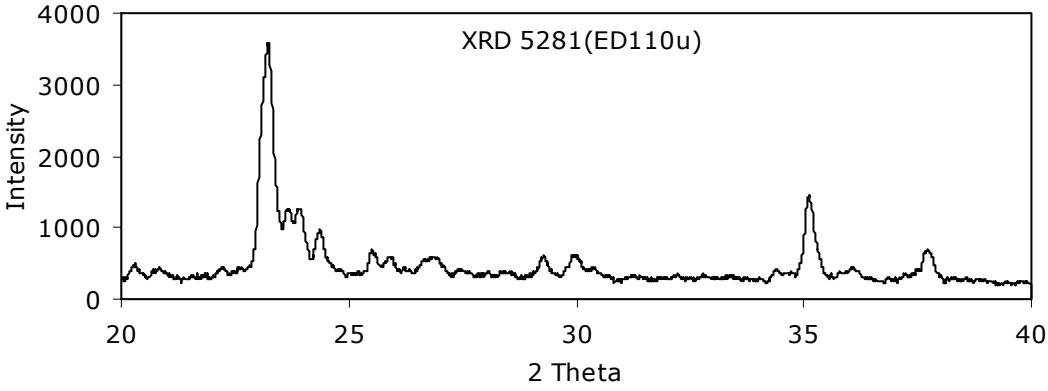
XRD 5281(ED110u)
Intensity
4000
3000
2000
1000
0
20
25
30
35
40
2 Theta

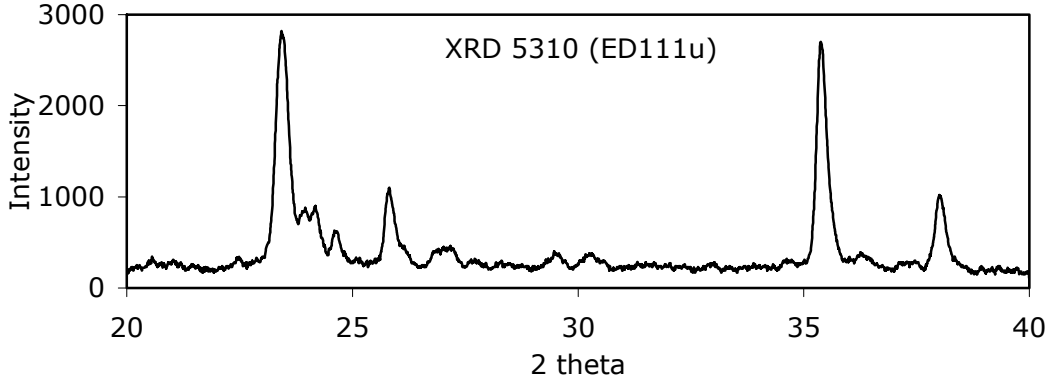
XRD 5310 (ED111u)
Intensity
3000
2000
1000
0
20
25
30
35
40
2 theta

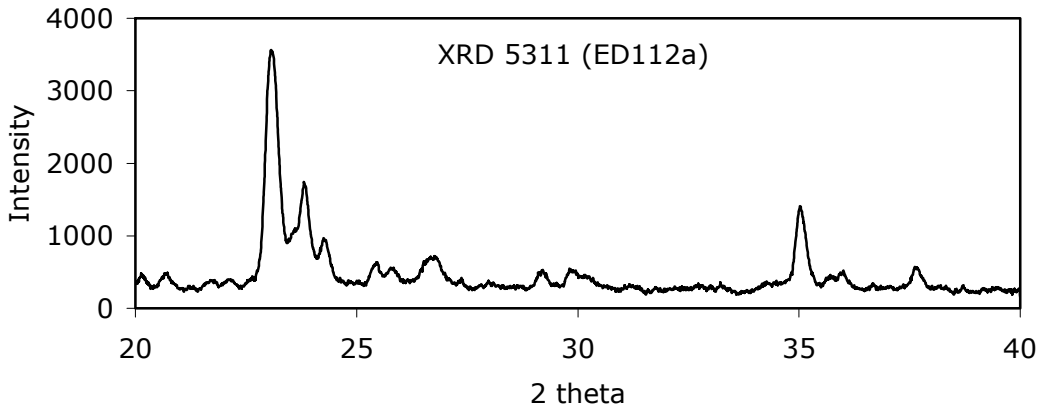

Figure G.2 XRD patterns of synthesized membranes (XRD file number and membrane codes are shown on the figures)

G.4 XRD patterns of seed coated alumina supports

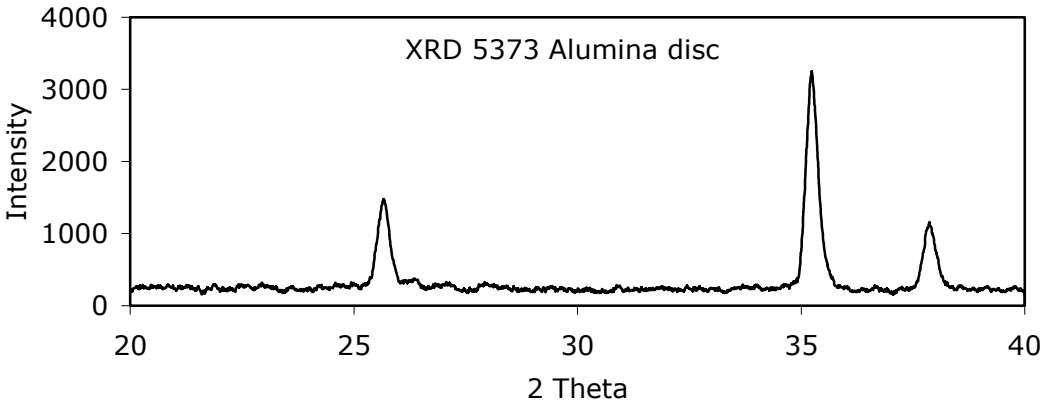

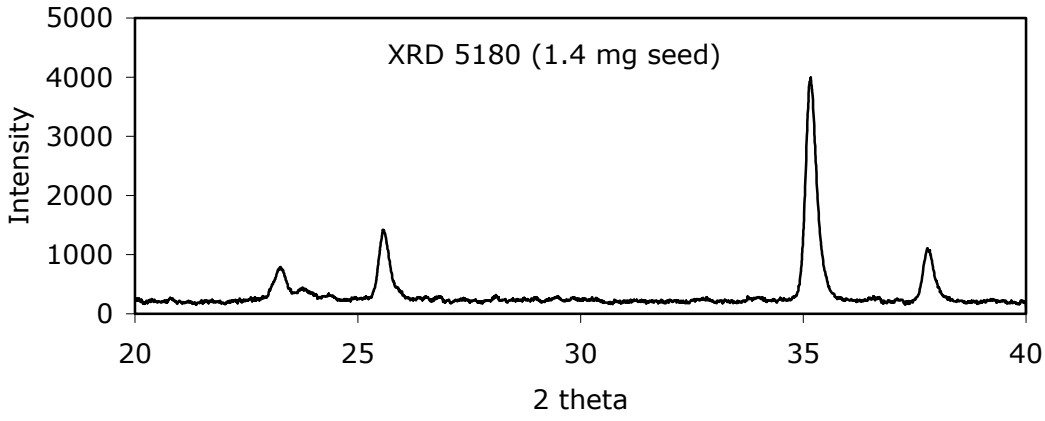

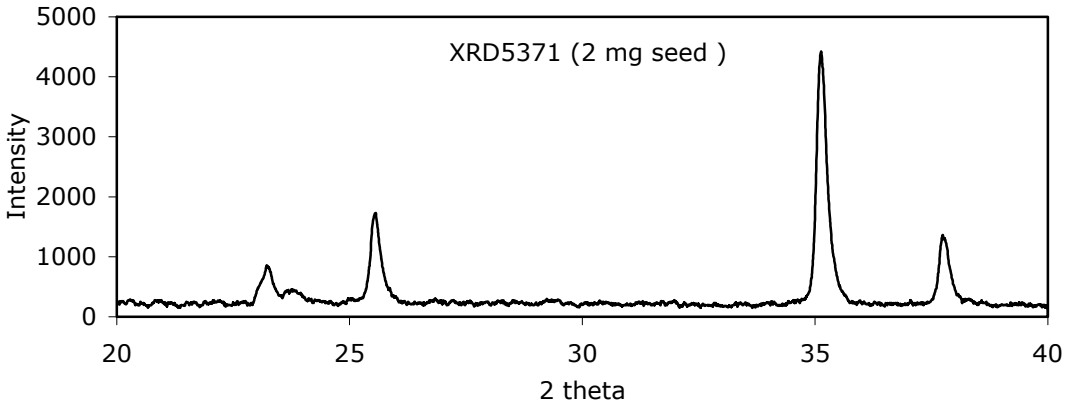
XRD5371 (2 mg seed)
Intensity
5000
4000
3000
2000
1000
0
20
25
30
35
40
2 theta

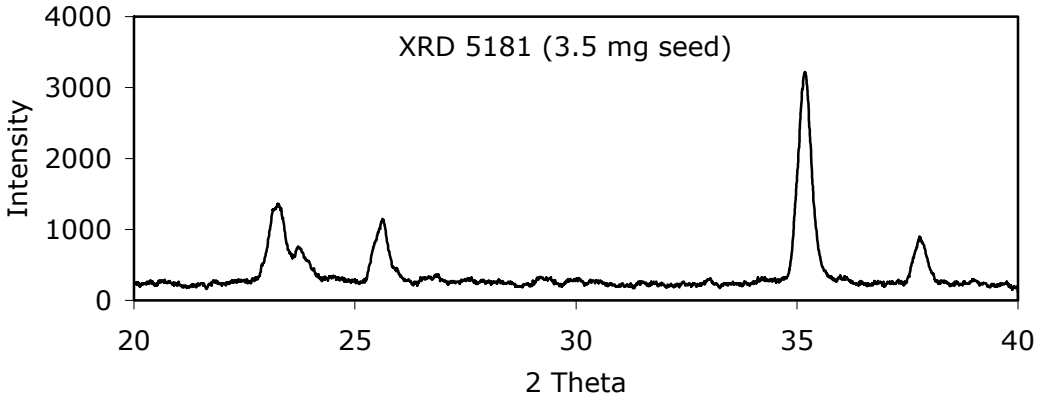
XRD 5181 (3.5 mg seed)
Intensity
4000
3000
2000
1000
0
20
25
30
35
40
2 Theta

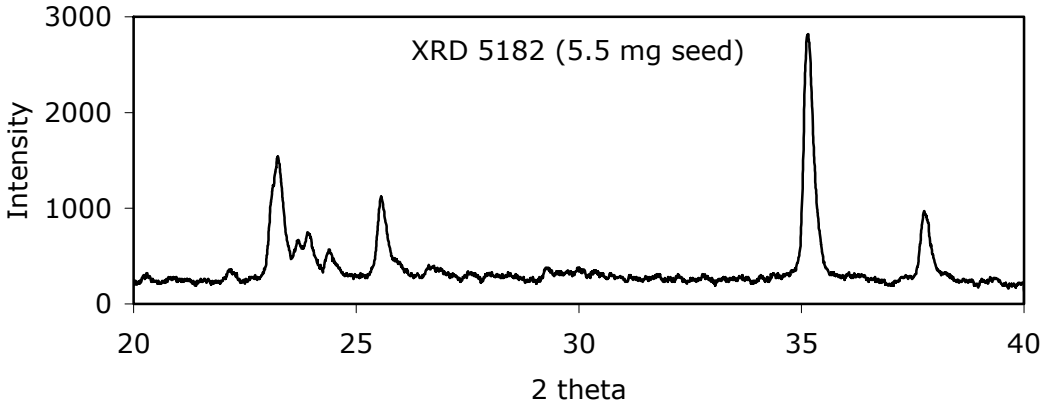
XRD 5182 (5.5 mg seed)
Intensity
3000
2000
1000
0
20
25
30
35
40
2 theta

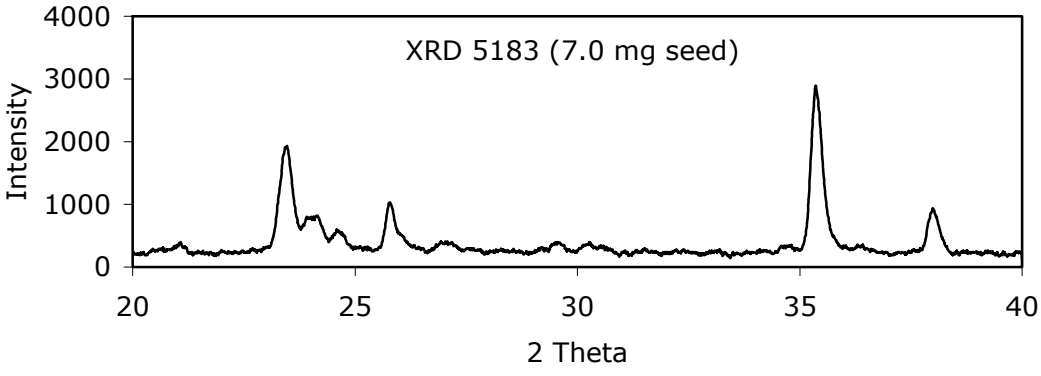
XRD 5183 (7.0 mg seed)
Intensity
4000
3000
2000
1000
0
20
25
30
35
40
2 Theta

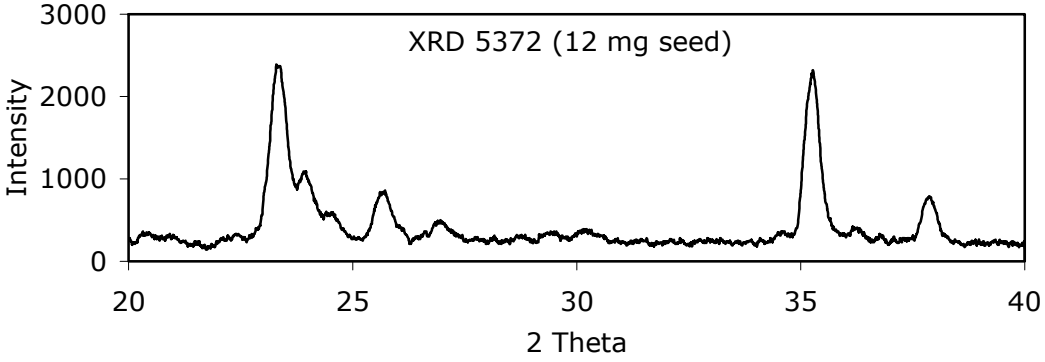
XRD 5372 (12 mg seed)
Intensity
3000
2000
1000
0
20
25
30
35
40
2 Theta

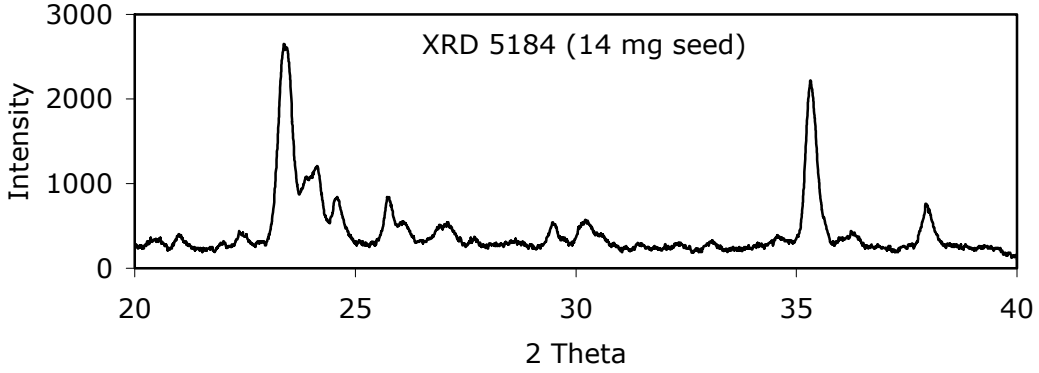
XRD 5184 (14 mg seed)
Intensity
3000
2000
1000
0
20
25
30
35
40
2 Theta

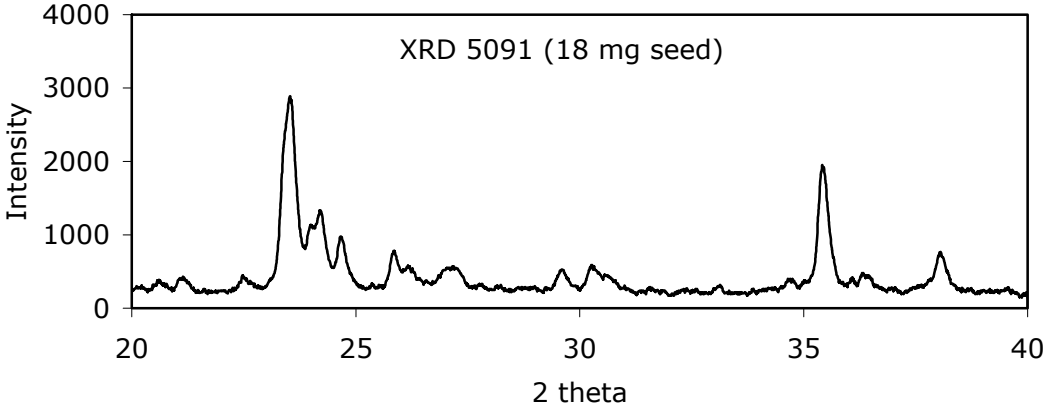
XRD 5091 (18 mg seed)
Intensity
4000
3000
2000
1000
0
20
25
30
35
40
2 theta

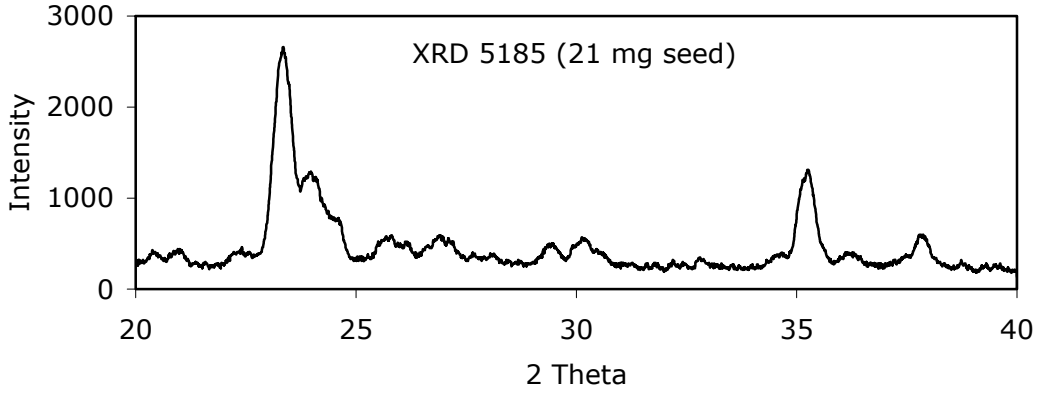
XRD 5185 (21 mg seed)
Intensity
3000
2000
1000
0
20
25
30
35
40
2 Theta

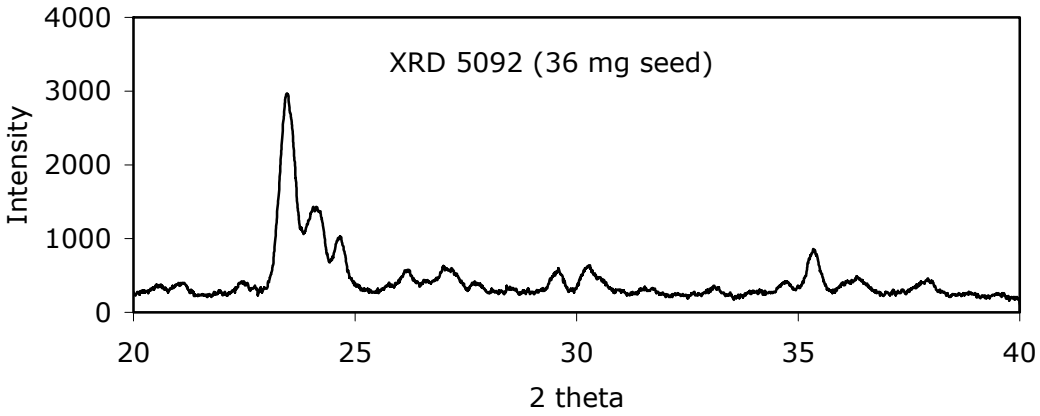

Figure G.3 XRD patterns of seed coated alumina supports (XRD file number and amounts of seed are shown on the figures)

APPENDIX H

Vacuum seeding results

Table H.1 Weight gain of the supports after seeding

Amount of seed in suspension (mg) [Ws]	Support Code	$W_{bare\ support}$ (g)	$W_{seeded\ support}$ (g)	Weight Gain (mg) [Wg]	$\lvert Ws - Wg \rvert$ (mg)
2.0	ED66a	0.9046	0.9064	1.8	0.2
	ED66u	0.9876	0.9892	1.6	0.4
	ED67a	0.9265	0.9280	1.5	0.5
	ED67u	0.8710	0.8730	2	0
	ED73a	0.9260	0.9278	1.8	0.2
	ED73u	0.9210	0.9226	1.6	0.4
	ED74a	0.9314	0.9336	2.2	0.2
	ED74u	0.9471	0.9494	2.3	0.3
	ED87a	0.9684	0.9698	1.4	0.6
	ED87u	0.9720	0.9737	1.7	0.3
	ED88a	0.9428	0.9443	1.5	0.5
	ED88u	0.9248	0.9271	2.3	0.3
	ED89a	0.9081	0.9096	1.5	0.5
	ED89u	0.9827	0.9842	1.5	0.5
	ED90a	0.9205	0.9223	1.8	0.2
	ED90u	0.9515	0.9524	0.9*	1.1*
	ED95a	0.8863	0.8890	2.7*	0.7*
	ED95u	0.8934	0.8947	1.3	0.7
	ED96a	0.9253	0.9271	1.8	0.2
	ED96u	0.8866	0.8882	1.6	0.4
2.0				<1.7>	<0.4>

Amount of seed in suspension (mg) [Ws]	Support Code	$W_{bare\ support}$ (g)	$W_{seeded\ support}$ (g)	Weight Gain (mg) [Wg]	$\lvert Ws - Wg \rvert$ (mg)
3.5	ED48a	0.881	0.886	5.0*	1.5*
	ED48u	0.891	0.895	3.5	0
	ED49a	0.878	0.883	4.6*	1.1*
	ED49u	0.898	0.903	4.7*	1.2*
	ED68a	0.918	0.922	3.3	0.2
	ED68u	0.908	0.911	2.8*	0.7*
	ED69a	0.910	0.914	3.6	0.1
	ED69u	0.918	0.922	3.9	0.4
	ED75a	0.920	0.924	3.5	0
	ED75u	0.937	0.941	3.5	0
	ED76a	0.921	0.925	3.8	0.3
	ED76u	0.928	0.932	3.6	0.1
	ED97a	0.892	0.895	2.8*	0.7*
	ED97u	0.898	0.902	3.6	0.1
	ED98a	0.893	0.896	3.4	0.1
	ED98u	0.877	0.880	3	0.5
3.5				<3.5>	<0.2>
6	ED70a	0.907	0.912	5.4	0.6
	ED70u	0.999	1.005	5.9	0.1
	ED71a	0.915	0.921	5.7	0.3
	ED71u	0.913	0.917	4.6*	1.4*
	ED99a	0.919	0.925	6.5	0.5
	ED99u	0.914	0.920	5.3	0.7
	ED100a	0.891	0.896	5.3	0.7
	ED100u	0.895	0.902	7.0*	1.0*
	ED101a	0.915	0.921	5.3	0.7
	ED101u	0.901	0.907	6.2	0.2
	ED102a	0.898	0.903	5.3	0.7
	ED102u	0.865	0.872	6.1	0.1
6				<5.7>	<0.5>

Amount of seed in suspension (mg) [Ws]	Support Code	$W_{bare\ support}$ (g)	$W_{seeded\ support}$ (g)	Weight Gain (mg) [Wg]	$\lvert Ws - Wg \rvert$ (mg)
12	ED50a	0.901	0.914	13.2*	1.2*
	ED50u	0.902	0.914	12.3	0.3
	ED51a	0.914	0.926	11.7	0.3
	D1	0.888	0.900	12.0	0.0
	ED51u	0.913	0.925	12.4	0.4
	ED54a	0.869	0.880	11.0	1.0
	ED54u	0.857	0.869	12.0	0.0
	ED55a	0.905	0.917	11.5	0.5
	ED55u	0.904	0.916	11.7	0.3
	ED56a	0.910	0.922	11.8	0.2
	ED56u	0.894	0.912	18.2	6.2*
	ED57a	0.902	0.914	11.6	0.4
	ED57u	0.915	0.926	11.2	0.8
	ED83a	0.893	0.903	9.9*	2.1*
	ED84a	0.898	0.910	11.9	0.1
	ED84u	0.912	0.925	12.5	0.5
	ED85a	0.917	0.929	11.7	0.3
	ED85u	0.914	0.926	11.9	0.1
	ED86a	0.757	0.765	7.5	4.5*
	ED86u	0.866	0.878	11.4	0.6
12				<11.8>	<0.4>
24	D2	0.910	0.934	24.2	0.2
	ED52a	0.903	0.927	24.0	0.0
	ED52u	0.921	0.946	24.7	0.7
	ED53a	0.903	0.927	23.8	0.2
	ED53u	0.905	0.929	23.5	0.5
24				<24.0>	<0.4>

* not included in calculations

APPENDIX I

Gas permeation data from literature

Table I.1 N_2 permeance and N_2/SF_6 ideal selectivity data taken from literature

Reference	N_2 permeance (mol/Pa.s.m^2)	Ideal selectivity N_2/ SF_6
Coronas, J., Falconer, J.L., Noble, R.D., "Characterization and permeation properties of ZSM-5 tubular membranes", AIChE Journal, 43, 1997, p. 1797-1812	$6.00x10^{-07}$	138
	$1.00x10^{-06}$	299
	$9.00x10^{-07}$	196
	$6.00x10^{-07}$	190
	$1.20x10^{-06}$	259
	$1.20x10^{-06}$	66
	$1.00x10^{-07}$	15
	$4.00x10^{-08}$	6
Kalıpçılar, H., Çulfaz, A., "Role of water content of clear synthesis solutions on the thickness of silicalite layers grown on porous a-alumina supports", Microporous and Mesoporous Materials, 52, 2002, p. 39-54	$9.00x10^{-09}$	8
	$3.00x10^{-09}$	38
	$1.63x10^{-07}$	1630
	$1.61x10^{-07}$	77
	$1.26x10^{-07}$	1050
	$2.00x10^{-08}$	195
Lassinanti M., Jareman, F., Hedlund, J., Creaser, D., Sterte, J., "Preparation and evaluation of thin ZSM-5 membranes synthesized in the absence of organic template molecules", Catalysis today, 67, 2001, p 109-119	$3.90x10^{-07}$	4.4
	$1.70x10^{-07}$	4.4
	$2.00x10^{-07}$	2000
	$1.20x10^{-07}$	12
	$6.20x10^{-08}$	620
	$1.20x10^{-07}$	12
	$5.80x10^{-08}$	580
Bonhomme, F., Welk, M.E., Nenoff, T.M., "CO2 selectivity and lifetimes of high silica ZSM-5 membranes", Microporous and mesoporous materials, 66, 2003, p. 181-188	$1.10x10^{-07}$	28
	$1.40x10^{-07}$	70
	$1.60x10^{-07}$	53

Reference	N_2 permeance (mol/Pa.s.m^2)	Ideal selectivity N_2/ SF_6
Hedlund, J., Sterte, J., Anthonis, M., Bons, Anton-Jans, Crastensen, B., Corcoran, N., Cox, D., Deckman, H., De Gijnst, W., de Moor, P., Lai, F., McHenry, J., Mortier, W., Reinoso, J., Peters, J., "High-flux MFI membranes", Microporous and Mesoporous Materials, 52, 2002, p. 179-189	$1.29x10^{-05}$	10
Tuan, V.A., Falconer, J.L., Noble, R.D., "Alkali-Free ZSM-5 Membranes: Preparation Conditions and Separation Performance", Industrial and Engineering Chemistry Research, 38, 1999, p. 3635-3646	$2.00x10^{-08}$	56
Nomura, M., Yamaguchi, T., Nakao, S., "Transport phenomena through intercrystalline and intracrystalline pathways of silicalite zeolite membranes", Journal of membrane science, 187, 2001, p. 203-212	$2.00x10^{-07}$	3.7
	$5.00x10^{-08}$	11.7
Gump, C.J., Lin, X., Falconer, J.L., Noble, R.D., "Experimental configuration and adsorption effects on the permeation of C4 isomers through ZSM-5 zeolite membranes", Journal of Membrane Science, 173, 2000, p.35-52	$8.30x10^{-07}$	240
	$4.30x10^{-07}$	310
	$3.80x10^{-08}$	19
Algieri, C., Bernardo, P., Golemme, G., Barbieri, G., Drioli, E., "Permeation properties of a thin silicalite-1 (MFI) membrane", Journal of Membrane Science, 222, 2003, p. 181-190	$4.60x10^{-06}$	8.56
Flanders, C.L., Tuan, V.A., Noble, R.D., Falconer, J.L., "Separation of C6 isomers by vapor permeation and pervaporation through ZSM-5 membranes", Journal of membrane science, 176, 2000, p. 43-53	$3.00x10^{-07}$	48
Arruebo, M., Coronas, J., Menéndez, M., Santamaría, J., "Separation of hydrocarbons from natural gas using silicalite membranes", Separation and Purification Technology, 25, 2001, p. 275-286	$6.56x10^{-07}$	19.3
	$5.51x10^{-07}$	15.6
	$7.96x10^{-07}$	12.8
	$2.52x10^{-07}$	8.9
	$3.35x10^{-07}$	14.9
	$2.14x10^{-07}$	5.7
	$2.37x10^{-07}$	7.1
	$7.41x10^{-07}$	7.1
	$3.19x10^{-07}$	21.2
Piera, E., Brenninkmeijer, C.A.M., Santamaría, J., Coronas, J., "Separation of traces of CO from air using MFI-type zeolite membranes", Journal of membrane science, 201, 2002, p. 229-232	$2.10x10^{-07}$	5.1
	$1.70x10^{-07}$	33
	$4.80x10^{-07}$	95

Reference	N_2 permeance (mol/Pa.s.m^2)	Ideal selectivity N_2/ SF_6
Li, G., Kikuchi, E., Matsukata, M., "ZSM-5 zeolite membranes prepared from a clear template-free solution", Microporous and Mesoporous Materials, 60, 2003, p. 225–235	$1.25x10^{-07}$	12,5
	$4.00x10^{-08}$	8
Funke, H.H., Frender, K.R., Green, K.M., Wilwerding, J.L., Sweitzer, B.A., Falconer, J.L., Noble, R.D., "Influence of adsorbed molecules on the permeation properties of silicalite membranes", Journal of membrane science, 129, 1997, p. 77-82	$2.20x10^{-06}$	105
	$2.50x10^{-06}$	83
	$3.80x10^{-06}$	81
	$2.21x10^{-06}$	92
	$6.39x10^{-07}$	90
	$6.40x10^{-07}$	102
Algieri, C., Golemme,G., Kallus, S., Ramsay, J.D.F., "Preparation of thin supported MFI membranes by in-situ nucleation and secondary growth", Microporous and Mesoporous Materials, 47, 2001, p. 127-134	$3.78x10^{-07}$	12
	$2.16x10^{-06}$	11
	$2.80x10^{-06}$	14
	$3.78x10^{-07}$	11.8
	$2.16x10^{-06}$	10.8
	$2.80x10^{-06}$	13.7
Lai, R., Gavalas, G.R., "Surface seeding in ZSM-5 membrane preparation", Industrial and Engineering Chemistry Research, 37, 1998, p. 4275-4283	$4.00x10^{-09}$	611
	$5.70x10^{-09}$	145
	$5.00x10^{-10}$	32
	$9.60x10^{-10}$	510

APPENDIX L

Results of binary mixture permeation with ED98u

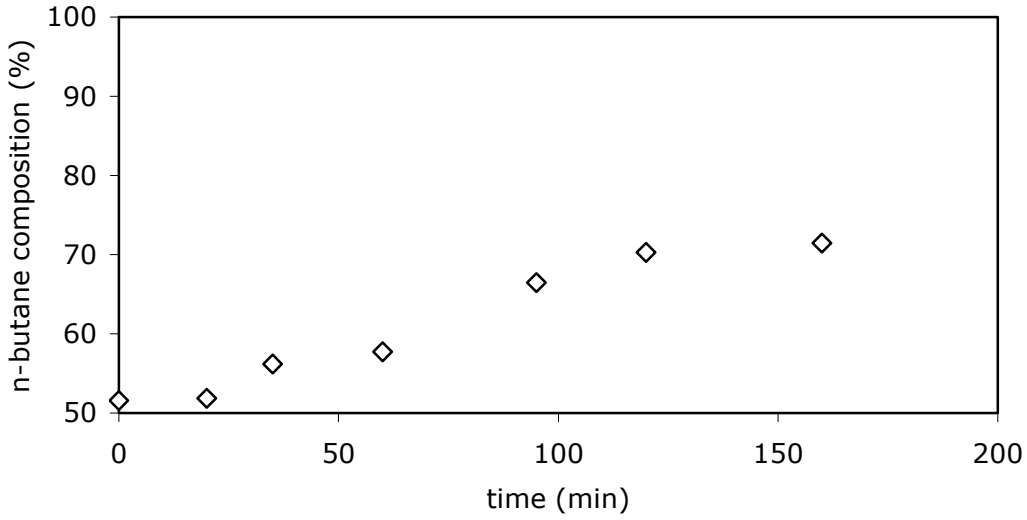

Figure L.1 Change of n-butane composition with time at room temperature

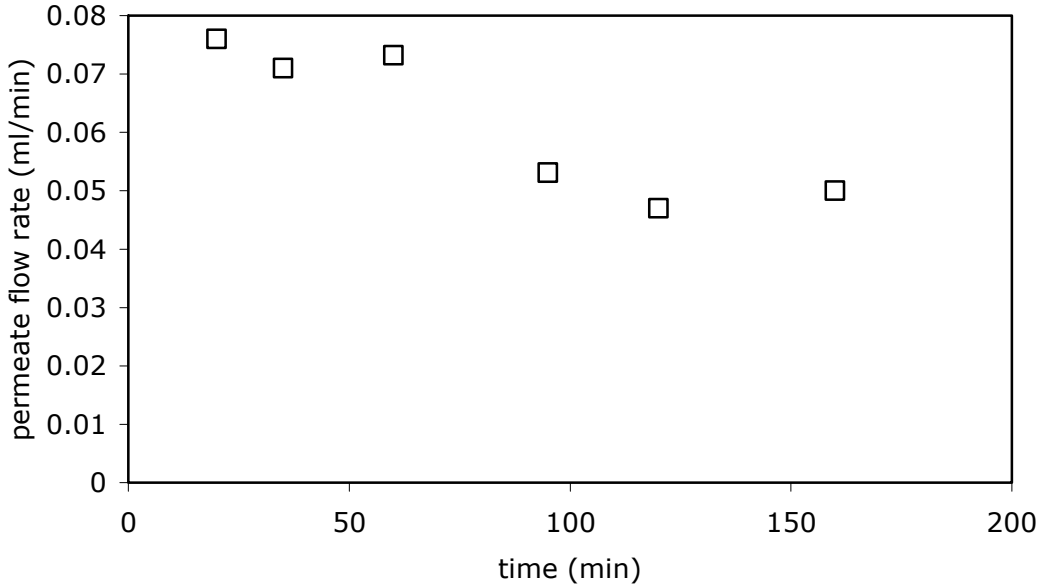

Figure L.2 Change of permeate flow rate with time at room temperature

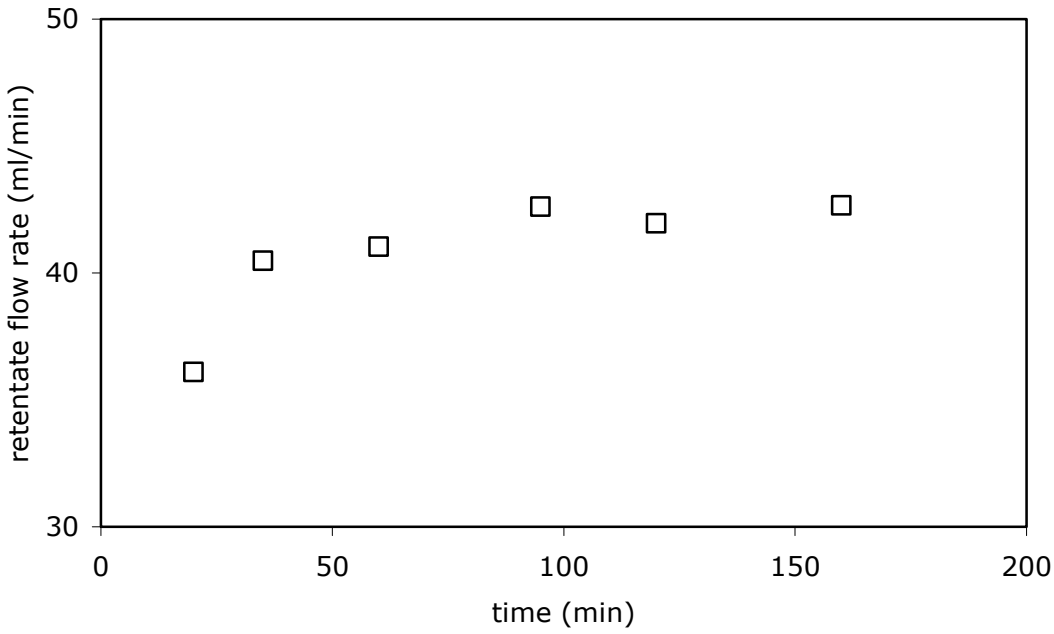

Figure L.3 Change of retentate flow rate with time at room temperature

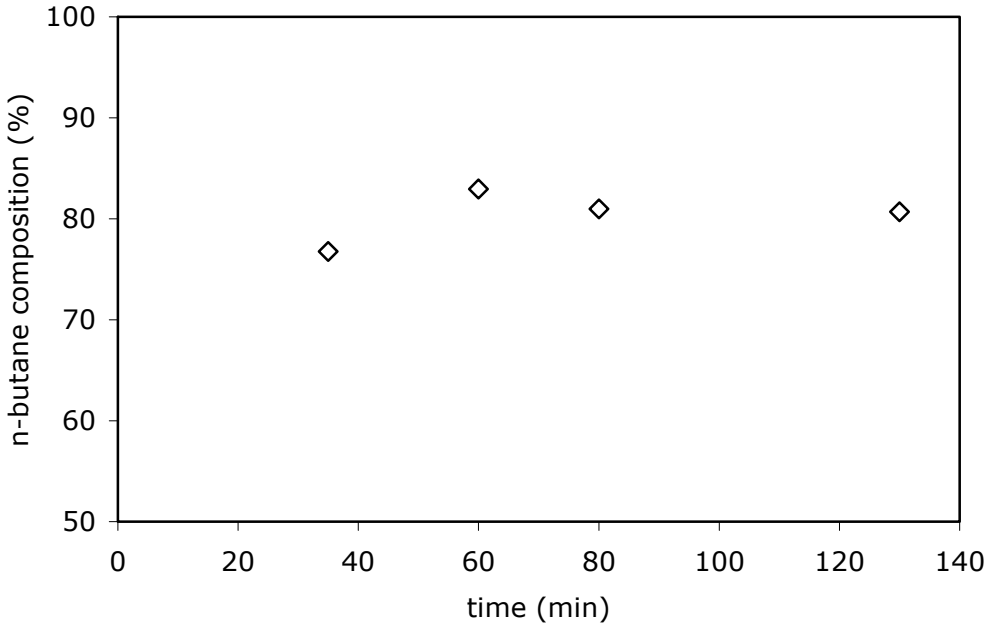

Figure L.4 Change of n-butane composition with time at 50°C

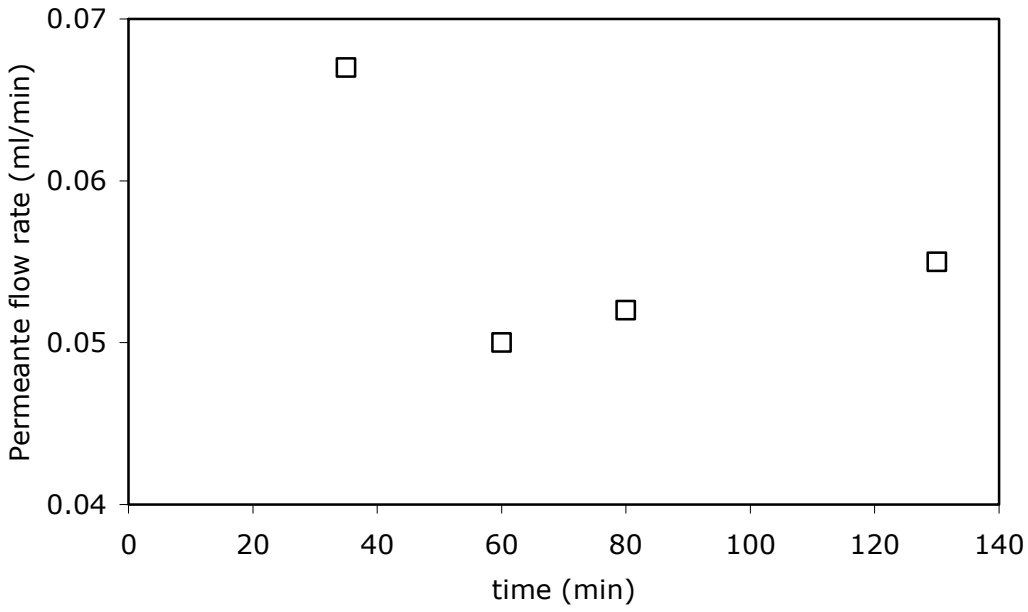

Figure L.5 Change of permeate flow rate with time at 50°C

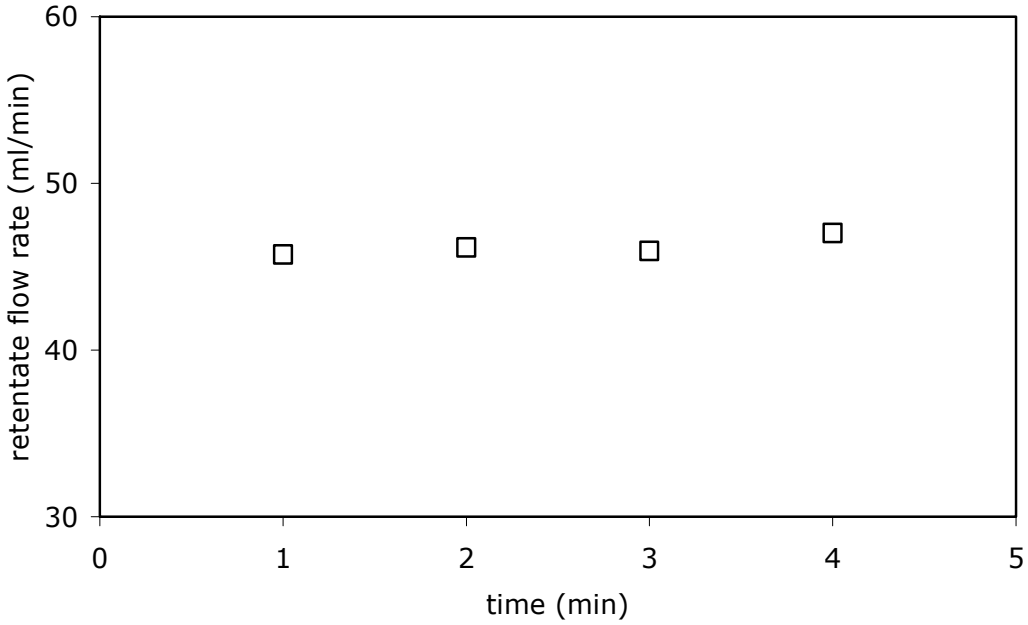

Figure L.6 Change of retentate flow rate with time at 50°C

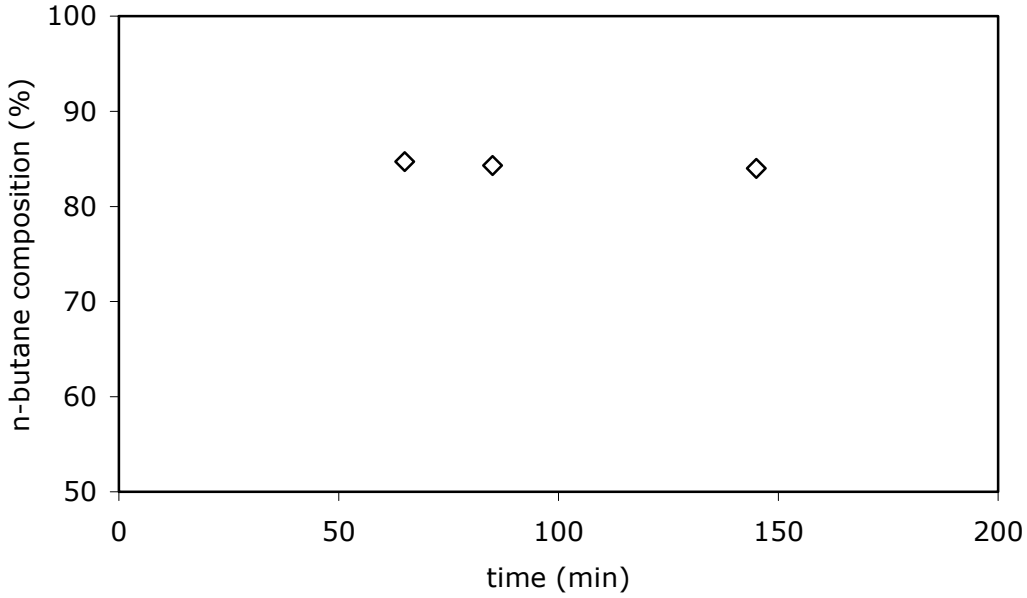

Figure L.7 Change of n-butane composition with time at 100°C

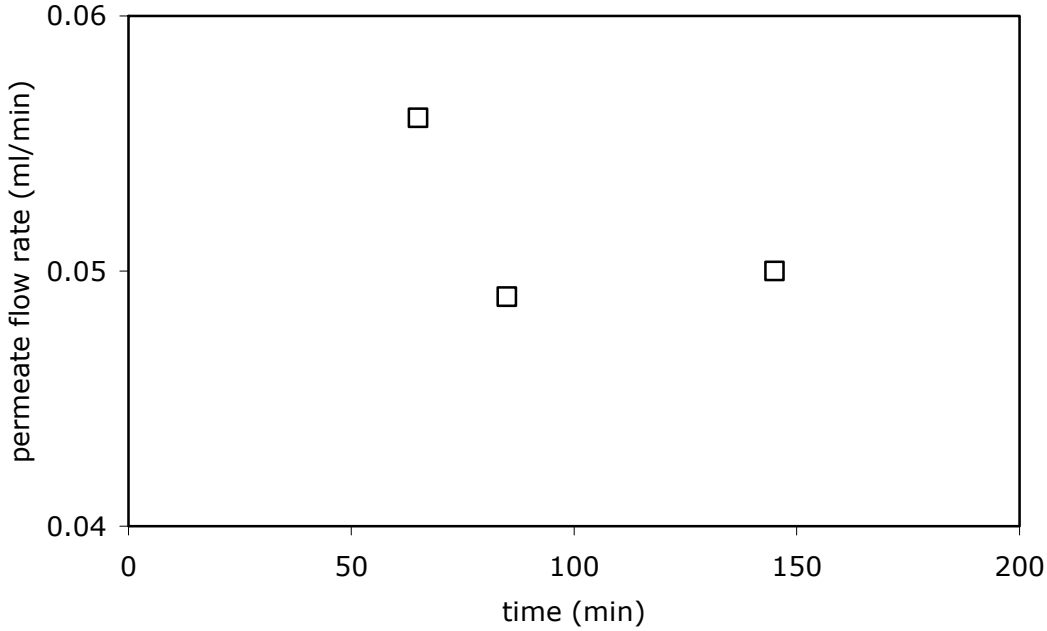

Figure L.8 Change of permeate flow rate with time at 100°C

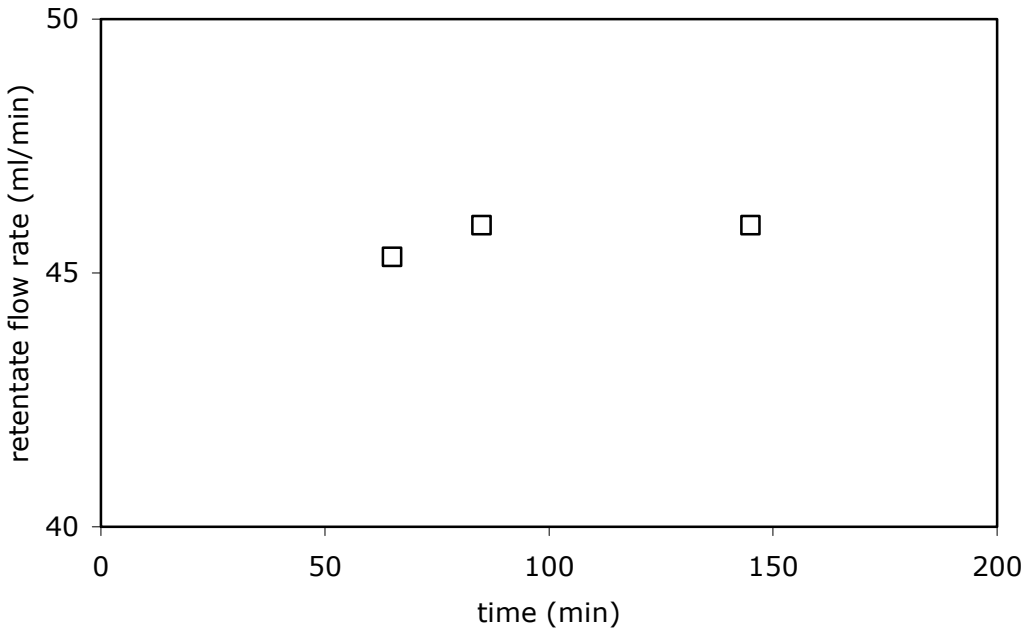

Figure L.9 Change of retentate flow rate with time at 100°C

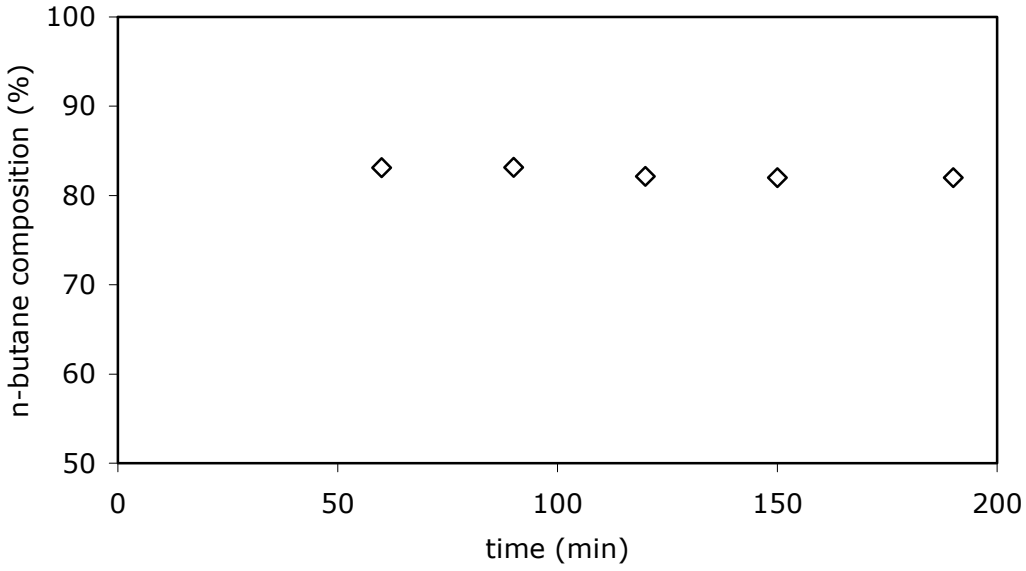

Figure L.10 Change of n-butane composition with time at 150°C

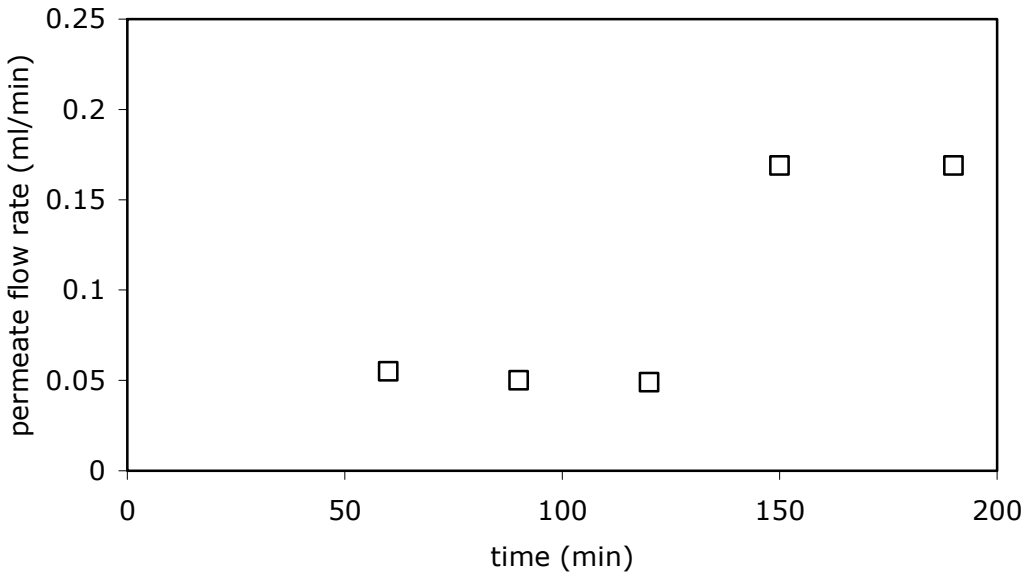

Figure L.11 Change of permeate flow rate with time at 150°C

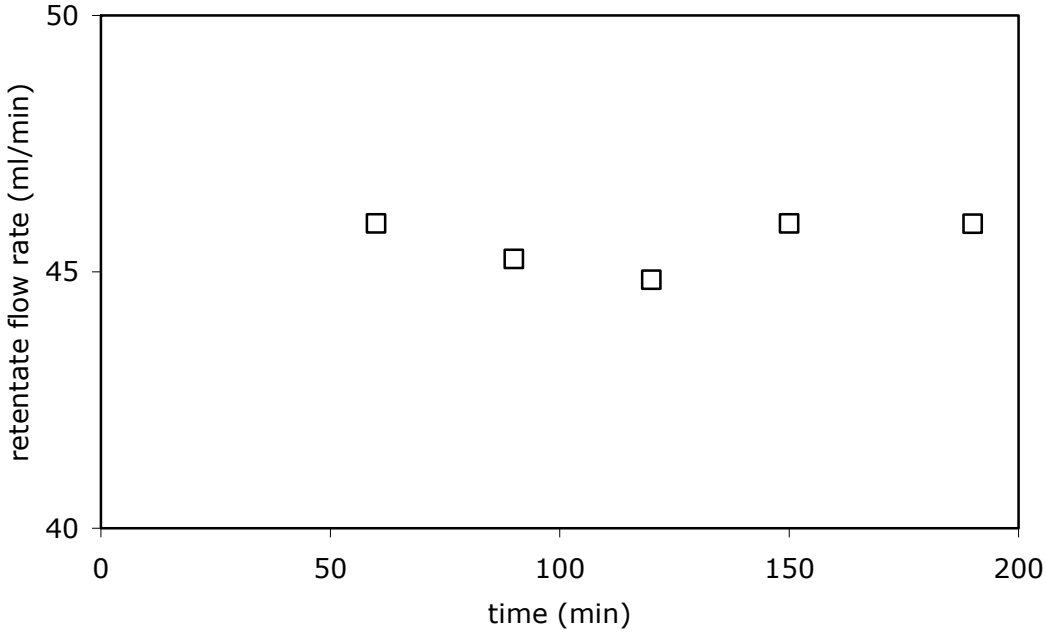

Figure L.12 Change of retentate flow rate with time at 150°C